

The Dynamics of the Global Monsoon: Connecting Theory and Observations

Ruth Geen^{1,1}, Simona Bordoni^{2,2}, David S. Battisti^{3,3}, and Katrina L. Hui^{4,4}

¹University of Exeter

²University of Trento

³University of Washington

⁴California Institute of Technology

November 30, 2022

Abstract

Earth's tropical and subtropical rainbands, such as Intertropical Convergence Zones (ITCZs) and monsoons, are complex systems, governed by both large-scale constraints on the atmospheric general circulation and regional interactions with continents and orography, and coupled to the ocean. Monsoons have historically been considered as regional large-scale sea breeze circulations, driven by land-sea contrast. More recently, a perspective has emerged of a Global Monsoon, a global-scale solstitial mode that dominates the annual variation of tropical and subtropical precipitation. This results from the seasonal variation of the global tropical atmospheric overturning and migration of the associated convergence zone. Regional subsystems are embedded in this global monsoon, localized by surface boundary conditions. Parallel with this, much theoretical progress has been made on the fundamental dynamics of the seasonal Hadley cells and convergence zones via the use of hierarchical modeling approaches, including aquaplanets. Here we review the theoretical progress made, and explore the extent to which these advances can help synthesize theory with observations to better understand differing characteristics of regional monsoons and their responses to certain forcings. After summarizing the dynamical and energetic balances that distinguish an ITCZ from a monsoon, we show that this theoretical framework provides strong support for the migrating convergence zone picture and allows constraints on the circulation to be identified via the momentum and energy budgets. Limitations of current theories are discussed, including the need for a better understanding of the influence of zonal asymmetries and transients on the large-scale tropical circulation.

Abstract

Earth's tropical and subtropical rainbands, such as Intertropical Convergence Zones (ITCZs) and monsoons, are complex systems, governed by both large-scale constraints on the atmospheric general circulation and regional interactions with continents and orography, and coupled to the ocean. Monsoons have historically been considered as regional large-scale sea breeze circulations, driven by land-sea contrast. More recently, a perspective has emerged of a Global Monsoon, a global-scale solstitial mode that dominates the annual variation of tropical and subtropical precipitation. This results from the seasonal variation of the global tropical atmospheric overturning and migration of the associated convergence zone. Regional subsystems are embedded in this global monsoon, localized by surface boundary conditions. Parallel with this, much theoretical progress has been made on the fundamental dynamics of the seasonal Hadley cells and convergence zones via the use of hierarchical modeling approaches, including aquaplanets. Here we review the theoretical progress made, and explore the extent to which these advances can help synthesize theory with observations to better understand differing characteristics of regional monsoons and their responses to certain forcings. After summarizing the dynamical and energetic balances that distinguish an ITCZ from a monsoon, we show that this theoretical framework provides strong support for the migrating convergence zone picture and allows constraints on the circulation to be identified via the momentum and energy budgets. Limitations of current theories are discussed, including the need for a better understanding of the influence of zonal asymmetries and transients on the large-scale tropical circulation.

Plain Language Summary

The monsoons are the moist summer circulations that provide most of the annual rainfall to many countries in the tropics and subtropics, influencing over one third of the world's population. Monsoons in different regions have historically been viewed as separate continent-scale 'sea breezes', where land heats faster than ocean in the summer, causing warm air to rise over the continent and moist air to be drawn over land from the ocean. Here we show that recent theoretical advances and observational analyses support a novel view of monsoons as localized seasonal migrations of the *tropical convergence zone*: the band of converging air and rainfall in the tropics embedded within the tropical atmospheric overturning circulation. This updated perspective distinguishes the dynamics of low-latitude ($\sim 10\text{--}25^\circ$ poleward) 'Intertropical Convergence Zones' (ITCZs) from that of monsoons ($\sim 0\text{--}10^\circ$ poleward), explains commonalities and differences in behavior between the regional ITCZs and monsoons, and may help to understand year-to-year variability in these systems, and how the global monsoon might change in future. We end by discussing features that are not yet included in this new picture: the influence of mountains and continent shapes on the circulation and the relationship of the convergence zones with shorter lived weather systems.

1 Introduction

Monsoons are a dominant feature of the tropical and subtropical climate in many regions of the world, characterized by rainy summer and drier winter seasons, and accompanied by a seasonal reversal of the prevailing winds: Fig. 1a shows the difference in precipitation (GPCP; Huffman et al., 2001) and 850-hPa wind velocity (JRA-55; Kobayashi et al., 2015) between June-September and December-March, based on a climatology from 1979-2016. The magenta contour marks regions where local summer minus winter precipitation exceeds 2 mm/day and summer accounts for at least 55% of the annual total precipitation and thus identifies the various monsoon regions around the globe (cf. B. Wang & Ding, 2008; P. X. Wang et al., 2014).

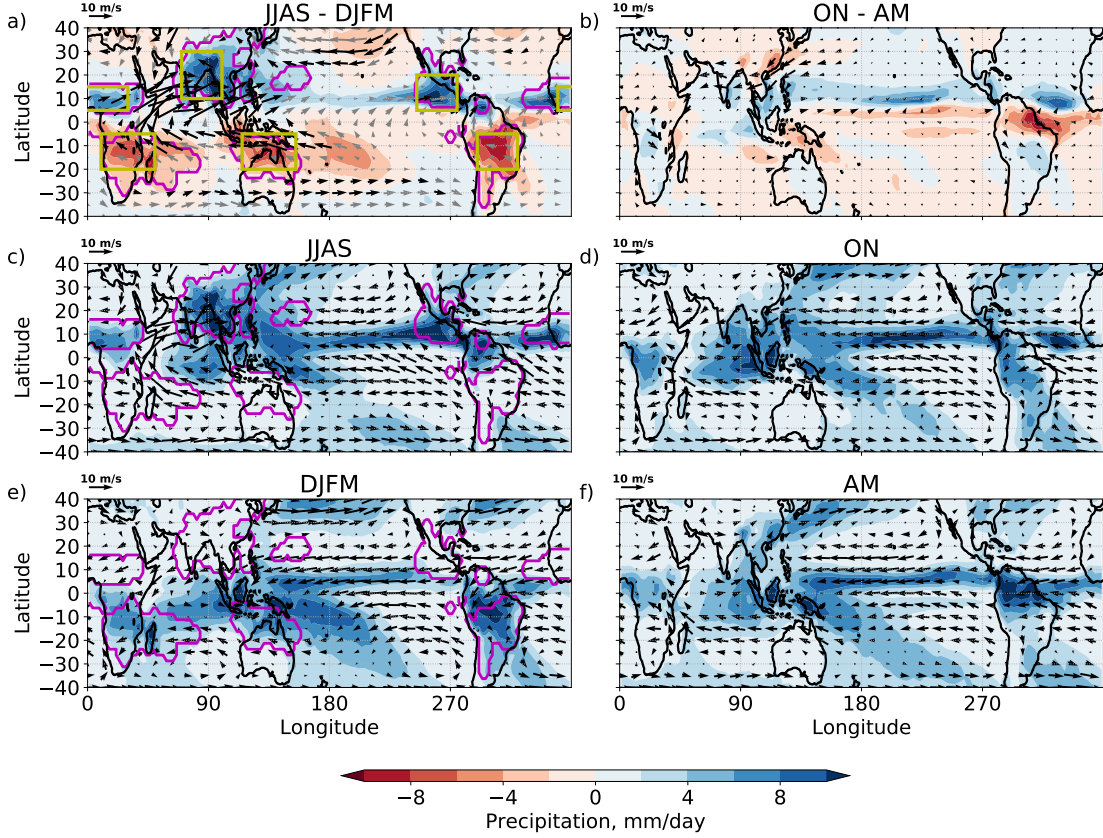


Figure 1. (a) Difference in precipitation (colors, mm/day) and 850-hPa wind speed (arrows, m/s) between Northern Hemisphere summer (defined as June-September) and Southern Hemisphere summer (defined as December-March). (c) and (e) show Northern and Southern Hemisphere summer precipitation and wind respectively. (b), (d) & (f) are as (a), (c) & (e) but for shoulder seasons defined as October & November and April & May. Black arrows in (a) indicate where the wind direction changes seasonally by more than 90° , where this criteria is not met arrows are gray. The magenta contour in (a), (c) & (e) indicates regions where local summer minus winter precipitation exceeds 2 mm/day and summer accounts for at least 55% of the annual total precipitation (cf. B. Wang & Ding, 2008; P. X. Wang et al., 2014). The extent of these regions does not change critically if these criteria are varied. Yellow boxes in (a) approximate these regions for use in Fig. 3.

64 For practical purposes, such as agriculture, it has generally been of interest to explore
 65 the controls on seasonal rainfall at a regional scale. However, empirical orthogonal
 66 function (EOF) analyses of the annual cycle of the global divergent circulation (Tren-
 67 berth, Stepaniak, & Caron, 2000) and of precipitation and lower-level winds (e.g., Fig.
 68 2) reveal a dominant, global-scale solstitial mode, driven by the annual cycle of insola-
 69 tion: the Global Monsoon. On interdecadal to intraseasonal timescales, the local mon-
 70 soons appear to behave largely as distinct systems, albeit with some degree of coordi-
 71 nation via teleconnections to ENSO (B. Wang, Liu, Kim, Webster, & Yim, 2012; Yim,
 72 Wang, Liu, & Wu, 2014). For example, interannual variability in precipitation shows weak

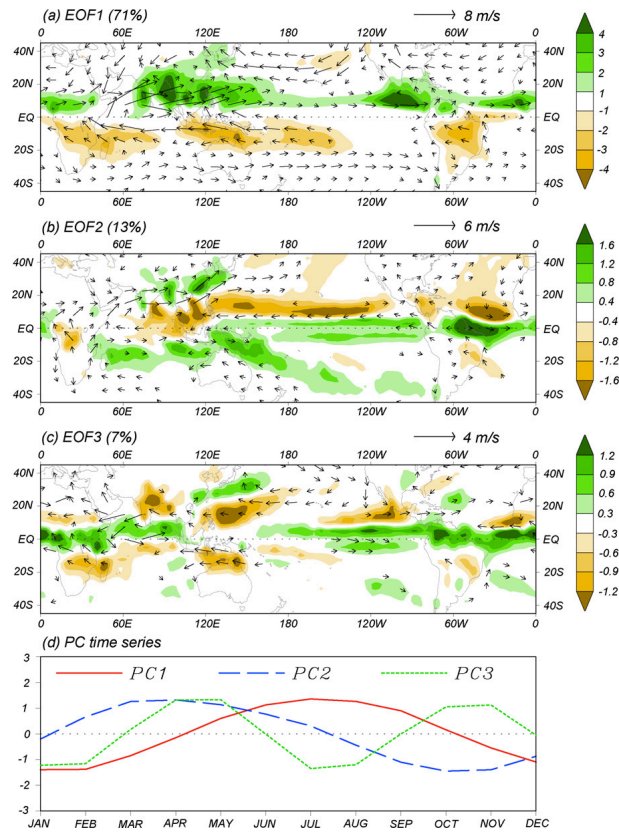


Figure 2. (a–c) The spatial patterns of the first three multi-variable empirical orthogonal functions of the climatological monthly mean precipitation (colors, mm/day) and winds (arrows, m/s) at 850 hPa, and (d) their corresponding normalized principal components. Winds with speed less than 1 m/s are omitted. From B. Wang and Ding (2008). ©Elsevier. Used with permission.

73 correlation between regions (Fig. 3).¹ As paleoclimate proxy datasets have become more
 74 comprehensive and reliable, it has become possible to investigate monsoon variability on
 75 longer timescales. For example, Fig. 4 shows that there were coherent millennial-scale
 76 abrupt changes in precipitation throughout the tropics and subtropics associated with
 77 Heinrich events and Dansgaard-Oeschger (D–O) cycles.² Modeling studies reproduce these
 78 hydrologic changes and demonstrate they are due to sudden changes in sea ice extent
 79 in the North Atlantic (see Pausata, Battisti, Nisancioglu, & Bitz, 2011; Atwood, Dono-
 80 hoe, Battisti, Liu, & Pausata, 2020 and references therein). On longer timescales (~23–
 81 26 kyr), the isotopic composition of the aragonite forming stalagmites throughout the
 82 tropics is strongly related to orbitally induced changes in insolation (see, e.g., Fig. 5).

¹ Note that even within an individual region, the dominant mode of interannual variability may have spatial structure, so that precipitation does not vary coherently across the domain (e.g., Goswami & Ajaya Mohan, 2001).

² Heinrich events are sudden discharges of ice from the Laurentide ice sheet that flood the North Atlantic with freshwater (Heinrich, 1988; Hemming, 2004). D–O cycles are a mode of natural variability that is manifest during (at least) the last ice age. A millennial-scale D–O cycle includes abrupt changes in North Atlantic sea ice extent (see Dansgaard et al., 1993; Dokken, Nisancioglu, Li, Battisti, & Kissel, 2013, and references therein).

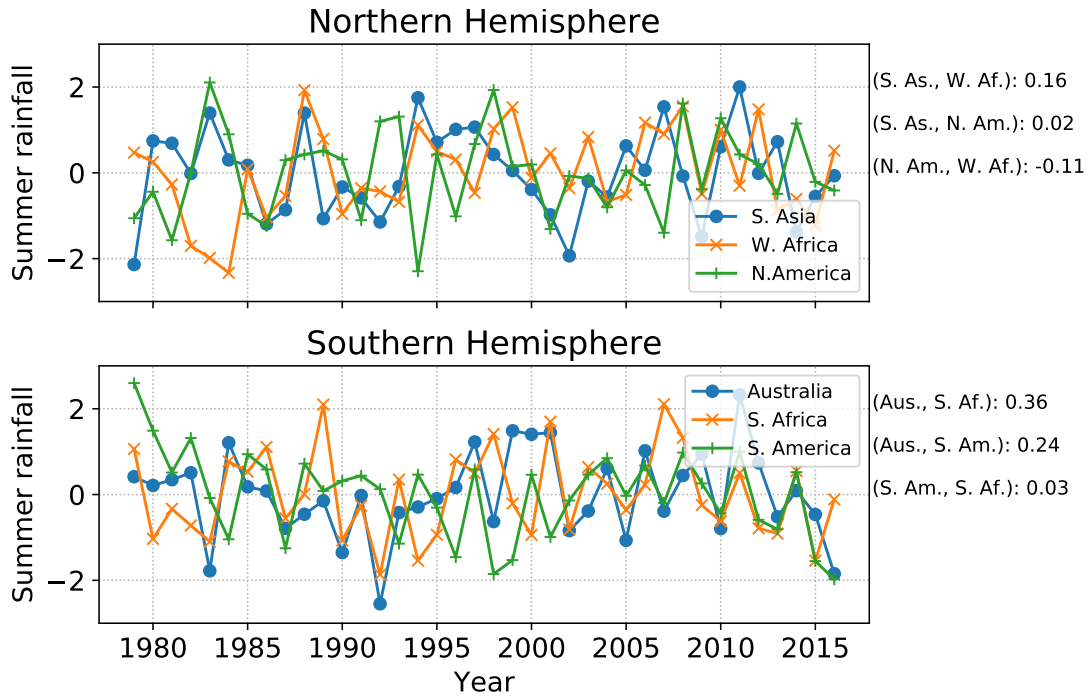


Figure 3. Timeseries of summer-time (June-September mean in the Northern Hemisphere and December-March mean in the Southern Hemisphere) rainfall averaged over the yellow boxes marked in Fig. 1, which are used as approximations to the monsoon regions defined by the magenta contour. For ease of comparison, the timeseries are standardized by subtracting the mean and dividing by the standard deviation. Pearson correlation coefficients are given to the right of the figure; except for the correlation between Australian and Southern African rainfall, correlations are not significantly different from zero ($p=0.10$). Data are taken from the Global Precipitation Climatology Project (GPCP; Huffman et al., 2001) over 1979-2016.

83 Simulations using isotope-enabled climate models reproduce these proxy data and demon-
 84 strate that precession causes coordinated, pan-tropical changes in the strength of the mon-
 85 soons (accentuated in times of high orbital eccentricity) (Battisti, Ding, & Roe, 2014;
 86 Liu, Battisti, & Donohoe, 2017).

87 The evidence for coherent global-scale monsoons raises questions about our physical
 88 understanding of the systems. Historically, the localization of summertime tropical
 89 rainfall around land led to the intuitive interpretation of monsoons as a large-scale sea
 90 breeze, with moist air drawn over the continent in the local summer season, when the
 91 land is warm relative to the ocean, resulting in convective rainfall over land (Halley, 1686).
 92 Traditionally, monsoons were considered distinct phenomena to the Intertropical Con-
 93 vergence Zone (ITCZ), with the latter coincident with the ascending branch of the Hadley
 94 circulation and generally being defined as the location where the trade winds of the North-
 95 ern and Southern Hemispheres converge. This perspective of monsoons as a sea breeze
 96 has been pervasive, despite the fact that land-sea temperature contrast has long been
 97 known to be greatest prior to monsoon onset over India (Simpson, 1921), and that drought
 98 years are accompanied by higher land surface temperatures (Kothawale & Kumar, 2002).
 99 However, consistent with the picture of the dominant global monsoon mode (Trenberth
 100 et al., 2000; B. Wang & Ding, 2008), more recent work suggests a perspective of the re-
 101 gional monsoons as localized and more extreme migrations of the tropical convergence

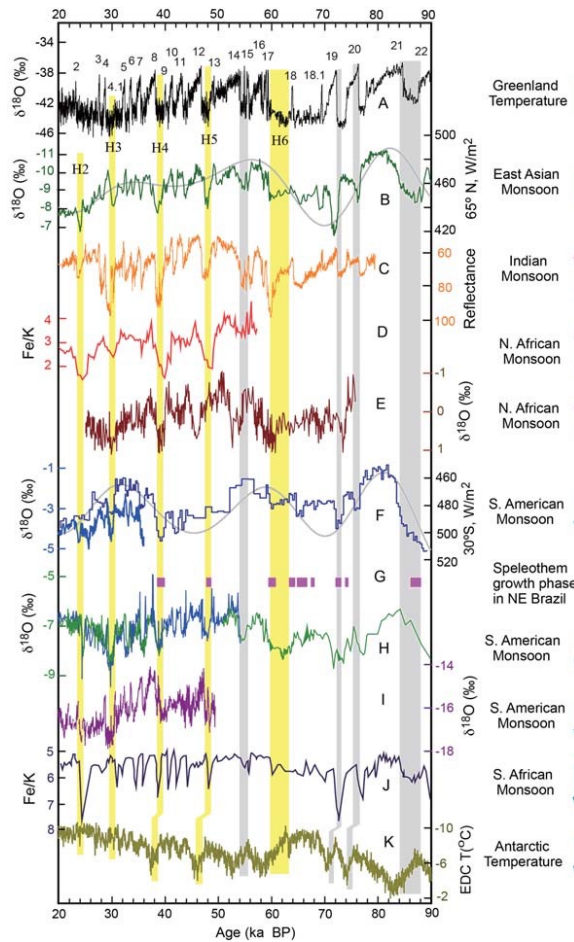


Figure 4. Paleoclimate proxy records from over the past 90,000 years. (a) Greenland ice core $\delta^{18}\text{O}$ record (Svensson et al., 2008, NGRIP). (b) East Asian monsoon record composited by using the Hulu and Sanbao records (H. Cheng et al., 2009). (c) Indian monsoon record inferred from Arabian Sea sediment total reflectance from core SO130-289KL (Deplazes et al., 2013). (d) Bulk Fe/K ratios from core GeoB9508-5 indicate arid (low) and humid (high) conditions in the North African monsoon region (Mulitza et al., 2008). (e) The North African monsoon proxy record based on the age model tuning to the GISP2 chronology (Weldeab, 2012). (f) South American monsoon records from Botuvera Cave (X. Wang et al., 2006, 2007). (g) Northeastern Brazil speleothem growth (wet) periods (X. Wang et al., 2004). (h) South American monsoon record from northern Peru (H. Cheng et al., 2013). (i) South American monsoon record from Pacupahuain Cave (Kanner et al., 2012). (j) Fe/K record (marine sediment core CD154-17-17K) from the southern African monsoon region (Ziegler et al., 2014). (k) Antarctic ice core temperature record (Jouzel et al., 2007, EDC). Numbers indicate Greenland warm phases of D–O cycles. Vertical yellow bars denote Heinrich events (H2–H6), and gray bars indicate correlations between northeastern Brazil wet periods, strong South American events and cold Greenland weak Asian monsoon events. Summer insolation (gray curves) at (b) 65° N (JJA) and (f) 30° S (DJF) (Berger, 1978) is plotted for comparison. Arrows on the right side depict anti-phased changes of monsoons between the two hemispheres. From P. X. Wang et al. (2014). ©Author(s) 2014. CC Attribution 3.0 License.

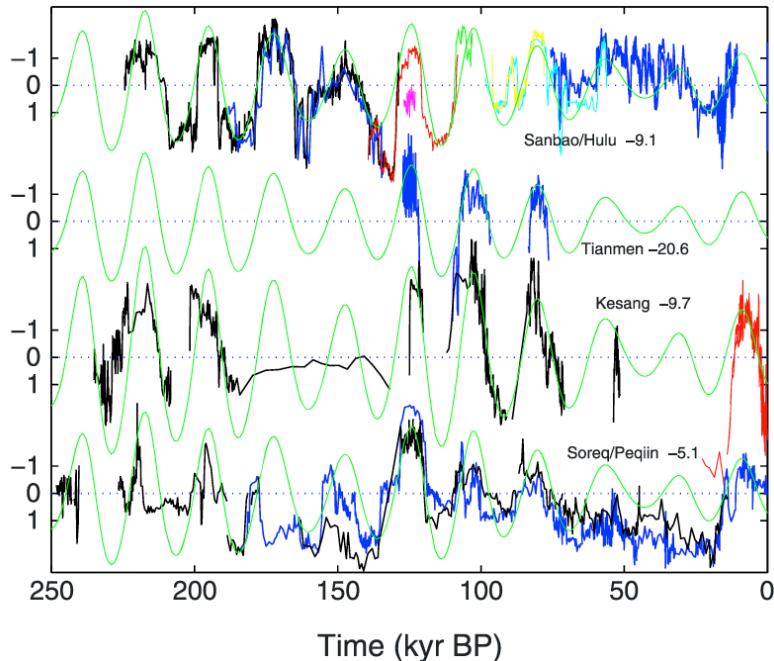


Figure 5. Time series of the oxygen isotopic composition of aragonite $\delta^{18}\text{O}$ (‰) in stalagmites across Asia that are sufficiently long to resolve orbital time scales. For each speleothem, the time average $\delta^{18}\text{O}$ is noted (e.g., Tianmen= -20.6‰) and removed before plotting. Superposed on each record is the summer (JJA) insolation at 30°N (green). For ease of viewing, the insolation has been multiplied by -1 and scaled so the standard deviation of insolation is identical to the standard deviation of the $\delta^{18}\text{O}$ for the respective cave record. From Battisti et al. (2014).

102 zone, which may sit near the Equator forming an ITCZ, or be pulled poleward over the
 103 continent as a monsoon (see Gadgil, 2018, and references therein).

104 Simultaneously, a significant body of work investigating the fundamental dynam-
 105 ics of the monsoon has been undertaken via hierarchical modeling approaches, ranging
 106 from dry axisymmetric models (e.g., Bordoni & Schneider, 2010; Hill, Bordoni, & Mitchell,
 107 2019; Schneider & Bordoni, 2008), to cloudless moist models (e.g., Bordoni & Schnei-
 108 der, 2008; Faulk, Mitchell, & Bordoni, 2017; Geen, Lambert, & Vallis, 2018, 2019; Privé
 109 & Plumb, 2007a), to more comprehensive models including full physics and realistic orog-
 110 raphy (e.g., Boos & Kuang, 2010; Chen & Bordoni, 2014). This hierarchy has allowed
 111 a wide range of factors controlling the structure of tropical precipitation to be explored.
 112 Findings from these studies strongly support the view of monsoons as local expressions
 113 of the global tropical convergence zone, and provide valuable, theoretically grounded in-
 114 sights into the controls on the tropical circulation and precipitation.

115 In this review, we attempt to synthesize the results of studies on the observed char-
 116 acteristics of Earth’s monsoon systems with recent theoretical advances that provide con-
 117 straints on the large-scale dynamics of ITCZs and monsoons, with the aim of taking stock
 118 of the progress achieved and identifying avenues for future work. Note that throughout
 119 the review, ‘monsoon’ refers to the local summer, as opposed to winter, monsoon. Specif-
 120 ically, as we will motivate through discussion of theoretical work, for the remainder of
 121 the paper we reserve the term ‘*monsoon*’ to describe precipitation associated with over-
 122 turning circulations with ascending branches located well poleward of $\sim 10^\circ$ latitude.
 123 We will show that, unlike the ITCZs, monsoons are characterized by angular momen-

124 tum conserving circulations, whose strength is largely determined by energetic constraints.
 125 The term ‘*ITCZ*’ is reserved to describe the zonally oriented precipitation bands that
 126 remain within $\sim 10^\circ$ of the Equator and whose dynamics are much more strongly in-
 127 fluenced by momentum fluxes associated with large-scale transient eddies. The term *con-*
 128 *vergence zone* will be used to refer to the location of both monsoonal and ITCZ pre-
 129 cipitation because, regardless of their governing dynamics, precipitation in both types
 130 of circulation is associated with ascending branches of overturning cells. The zonal and
 131 annual mean tropical convergence zone is referred to as the *ITCZ*.

132 The goals of this article are:

- 133 1. To assess the relevance of theoretical advances (which stem from studies using ide-
 134 alized models) to the real-world monsoons and ITCZs;
- 135 2. To help to motivate relevant simulations from the modeling community to answer
 136 open questions on the dynamics governing tropical convergence zones;
- 137 3. To provide an introduction to both of these aspects for readers new to the field.

138 With these aims in mind, Section 2 discusses theoretical results derived from ide-
 139 alized models, particularly aquaplanets with symmetric boundary conditions and heat-
 140 ing perturbations. Section 3 discusses the features of the observed regional convergence
 141 zones, their combined role in the global monsoon, and the applicability of the dynam-
 142 ical processes identified in idealized models to the various systems. Section 4 explores
 143 the roles of asymmetries in the boundary conditions and transient activity in the mon-
 144 soons and ITCZs. These factors are sometimes overlooked in formulating theories in ide-
 145 alized models. In Section 5 we summarize the successes and limitations of this synthe-
 146 sis of theory and observations, and propose some areas on which to focus future research.

147 **2 Idealized modeling of tropical and subtropical convergence zones**

148 Reanalyses, observations, and state-of-the-art global circulation models (GCMs)
 149 give our best estimates of Earth’s climate. However, when viewed as a whole, the Earth
 150 system is dizzyingly complex, and identifying the processes controlling the various el-
 151 ements of climate is hugely challenging. Idealized models provide a valuable tool for break-
 152 ing down some of this complexity, and for proposing mechanisms whose relevance can
 153 then be investigated in more realistic contexts.³ In this section, we review the use of ide-
 154 alized models in understanding the dynamics of the monsoons and ITCZs.

155 Some key insights into the controls on tropical rainfall and monsoons have come
 156 from a perhaps unexpected source: aquaplanets. Despite lacking zonal asymmetries such
 157 as land-sea contrast, which localize regional monsoons, these models have been shown
 158 to capture the basic elements of a monsoon. For example, in aquaplanets with moist physics
 159 and a low thermal inertia slab ocean, the convergence zone migrates rapidly and far away
 160 from the Equator into the summer hemisphere during the warm season (Bordoni & Schnei-
 161 der, 2008). This migration is associated with a rapid reversal of the upper- and lower-
 162 level wind in the summer hemisphere, and the onset of intense off-equatorial precipita-
 163 tion, similar to the behaviors seen in Earth’s monsoons (e.g., Fig. 6). Thus, in so far as
 164 the rapid development of an off-equatorial convergence zone accompanied by similarly
 165 rapid circulation changes can be interpreted as a monsoon, aquaplanets provide a sim-
 166 ple tool for exploring the lowest-order processes at work. This represents a significant
 167 change in perspective from the classical view of monsoon wind reversal as driven by land-
 168 sea thermal contrast (Halley, 1686), towards a view of monsoons as local and seasonal
 169 manifestations of the meridional overturning circulation.

³ For further discussion of the use of idealized models and the model hierarchy see (Held, 2005; Jeevan-
 jee, Hassanzadeh, Hill, & Sheshadri, 2017; Levins, 1966; Maher et al., 2019)

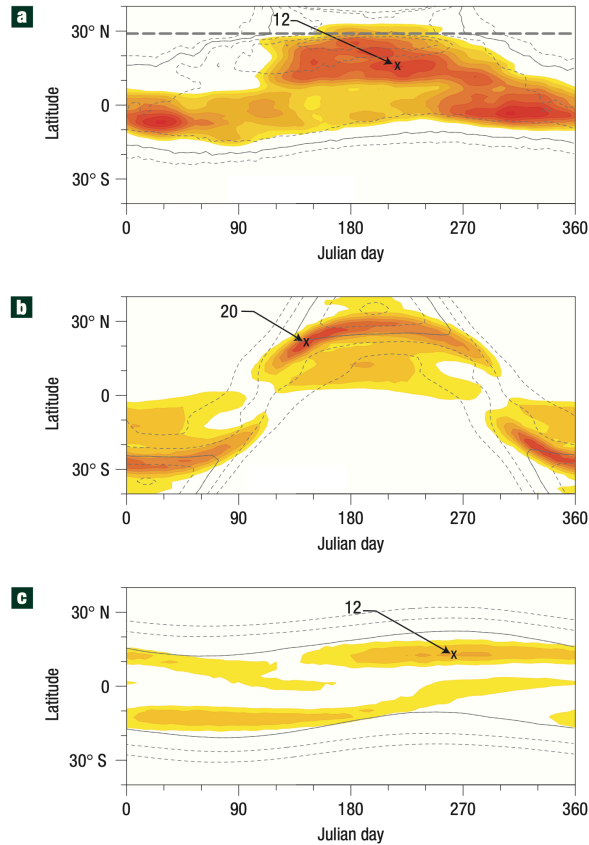


Figure 6. Seasonal cycle of zonal- and pentad-mean precipitation (color contours, data from GPCP 1999-2005) and sea-level air temperature (gray contours, data from the ERA-40 reanalysis (Uppala et al., 2005)) for (a) observations in the Asian monsoon sector ($70\text{--}100^\circ\text{E}$), and for aquaplanet simulations with ocean mixed-layer heat capacity equivalent to (b) 0.5m and (c) 50m of water.¹ The precipitation contour interval is 1 mm/day in (a) and 2 mm/day in (b) and (c), and maxima are indicated by crosses. For sea-level air temperature, the contour interval is 2°C in all panels, and the solid gray line indicates the 24°C isotherm. The thick dashed line in (a) shows the latitude at which the zonal-mean topography in the Asian monsoon sector rises above 3 km . From Bordoni and Schneider (2008). NB. Mixed layer depths here are corrected from Bordoni and Schneider (2008), (S. Bordoni, pers. com., 2020).

170 Different theoretical approaches have been used to interpret the results from these
 171 idealized simulations, primarily using large-scale budgets of energy and angular momen-
 172 tum. The momentum budget gives insight into the drivers and regimes of the overturn-
 173 ing circulation, and how these relate to monsoon onset. The energy budget provides a
 174 framework for understanding the controls on the latitude of the zonally averaged con-
 175 vergence zone, and its meridional migration. In a real-world context, this is useful in in-
 176 terpreting the latitude of tropical rainfall bands, and the meridional extent of Earth's
 177 monsoons. These complementary approaches are discussed in Sections 2.1 and 2.2, re-
 178 spectively.

179

2.1 Dynamical constraints

180

181

182

183

One important constraint on the atmospheric circulation is conservation of angular momentum. Recent results from aquaplanet simulations suggest that this can help to explain controls on the latitude of the convergence zone, the extent of the Hadley circulation, and the rapidity of monsoon onset.

184

185

The axial component of the angular momentum associated with the atmospheric circulation is

$$M = \Omega a^2 \cos^2 \phi + ua \cos \phi, \quad (1)$$

186

187

188

189

190

191

where Ω and a are Earth's rotation rate and radius, u is the zonal wind speed, and ϕ is latitude. Eq. 1 states that the atmosphere's angular momentum comprises a planetary contribution from Earth's rotation, and a contribution from the zonal wind relative to this. In the absence of torques (e.g., from friction, zonal pressure gradients or orography; see Egger, Weickmann, & Hoinka, 2007), M is conserved by an air parcel as it moves meridionally. Above orography, in the zonal mean we can approximate

$$\frac{DM}{Dt} = 0. \quad (2)$$

192

193

194

In the absence of stationary eddies, as is the case in an aquaplanet, substituting Eq. 1 into Eq. 2, linearising about the zonal and time mean state, and considering upper-level flow where viscous damping is weak and can be neglected gives

$$\bar{v} \left(f - \frac{1}{a \cos \phi} \frac{\partial(\bar{u} \cos \phi)}{\partial \phi} \right) - \bar{\omega} \frac{\partial \bar{u}}{\partial p} = \frac{1}{a \cos^2 \phi} \frac{\partial(\overline{u'v'} \cos^2 \phi)}{\partial \phi} + \frac{\partial \overline{u'\omega'}}{\partial p}, \quad (3)$$

195

196

197

198

199

200

201

202

203

204

205

where f is the Coriolis parameter, and v and ω are the meridional and vertical wind components, respectively. Overbars indicate the time and zonal mean, and primes deviations from the time mean. Terms relating to the mean flow have been grouped on the left hand side, while terms relating to the transient eddy fluxes of momentum are grouped on the right. In the upper branch of the Hadley circulation, where meridional streamlines are approximately horizontal (e.g., Fig. 13), the vertical advection term on the left hand side can be neglected. Additionally, meridional eddy momentum flux convergence is generally much larger than the vertical eddy momentum flux convergence outside of the boundary layer (e.g., Schneider & Bordoni, 2008). Utilising the definition of relative vorticity, $\zeta = \hat{\mathbf{k}} \cdot \nabla \times \mathbf{u}$, the leading order balance in Eq. 3 can be expressed in terms of a local Rossby number, $Ro = -\zeta/f$, (cf. Schneider & Bordoni, 2008) as

$$f(1 - Ro)\bar{v} = \frac{1}{a \cos^2 \phi} \frac{\partial(\overline{u'v'} \cos^2 \phi)}{\partial \phi}. \quad (4)$$

206

207

Ro is a non-dimensional metric of how far (small Ro) or close ($Ro = 1$) the circulation is to conservation of angular momentum.

208

2.1.1 The axisymmetric case

209

210

211

212

213

214

215

216

217

218

Considering first the case of an axisymmetric atmosphere, in which there are no eddies, Eq. 4 has two classes of solution. Firstly, the zonal averaged meridional and (by continuity) vertical velocities may be zero everywhere. This corresponds to a radiative-convective equilibrium (RCE) solution. Alternatively, Ro may be equal to 1 and an axisymmetric circulation may exist, so that the zonal and time mean flow conserves angular momentum. Plumb and Hou (1992) and Emanuel (1995) explored the conditions under which either of these cases might occur in dry and moist atmospheres, respectively. Importantly, the RCE solution is not viable if the resulting zonal wind in thermal wind balance with the RCE temperatures violates Hide's theorem (Hide, 1969) by giving rise to a local extremum in angular momentum. Plumb and Hou (1992) demonstrate that

219 for an off-equatorial forcing, this implies the existence of a threshold curvature of the depth-
 220 averaged RCE temperature, above which the RCE solution cannot exist and an overturn-
 221 ing circulation will develop. They also speculate that this threshold behavior in the ax-
 222 isymmetric model might be related to the rapid onset of Earth’s monsoons. The over-
 223 all argument is as follows.

224 Taking the RCE case, in which \bar{v} and $\bar{\omega}$ vanish, gradient wind and hydrostatic bal-
 225 ance can be expressed in pressure coordinates as

$$\frac{\partial}{\partial p} \left[f \bar{u}_e + \frac{\bar{u}_e^2 \tan \phi}{a} \right] = \frac{1}{a} \left(\frac{\partial \bar{\alpha}}{\partial \phi} \right)_p, \quad (5)$$

226 where $\bar{\alpha}$ is specific volume and \bar{u}_e is a RCE zonal wind profile. Note that in the axisym-
 227 metric case, overbars denote only the time mean, as by construction there are no zonal
 228 variations. Assuming the zonal wind speed at the surface is zero, the above can be in-
 229 tegrated down to the surface for a given upper-level wind profile to give an associated
 230 RCE depth-averaged temperature distribution (cf. Lindzen & Hou, 1988; Plumb & Hou,
 231 1992).

232 In modeling Earth’s atmosphere, moist processes must also be accounted for. In
 233 the tropics, frequent, intense moist convection means that in the time mean, the lapse
 234 rate is approximately moist adiabatic, so that the saturation moist entropy of the free
 235 atmosphere is nearly equal to the subcloud moist entropy, s_b (the b denoting subcloud
 236 values) (e.g., Arakawa & Schubert, 1974; Emanuel, Neelin, & Bretherton, 1994). This
 237 is known as *convective quasi-equilibrium* (CQE).⁴ Assuming the tropical atmosphere to
 238 be in CQE, Emanuel (1995) uses Eq. 5 to derive a relation between the angular momen-
 239 tum at the tropopause, M_t , and subcloud equivalent potential temperature, θ_{eb} :

$$c_p(\bar{T}_s - \bar{T}_t) \frac{\partial \overline{\ln \theta_{eb}}}{\partial \phi} = -\frac{1}{a^2} \frac{\tan \phi}{\cos^2 \phi} (\bar{M}_t - \Omega^2 a^4 \cos^4 \phi), \quad (6)$$

240 where T_s and T_t are the RCE temperatures at the surface and tropopause respectively,
 241 c_p is the heat capacity of dry air at constant pressure and θ_{eb} is related to moist entropy
 242 as $s_b = c_p \ln \theta_{eb}$. The condition that no local maximum in angular momentum exist gives
 243 a critical curvature of θ_{eb} :

$$-\left[\frac{\partial}{\partial \phi} \left(\frac{\cos^2 \phi}{\tan \phi} c_p(\bar{T}_s - \bar{T}_t) \frac{\partial \overline{\ln \theta_{eb}}}{\partial \phi} \right) \right]_{crit} = 4\Omega^2 a^2 \cos^3 \phi \sin \phi. \quad (7)$$

244 In an axisymmetric atmosphere, if the left hand side of Eq. 7 is less than the right hand
 245 side, the RCE solution is viable and there is no meridional overturning cell. If this con-
 246 dition is violated, so that the profile of θ_{eb} is supercritical, the RCE solution is not vi-
 247 able and a meridional flow must exist (cf. Emanuel, 1995; Hill et al., 2019; Plumb & Hou,
 248 1992). This condition is illustrated graphically in Fig. 7, which shows the profiles of RCE
 249 zonal wind, angular momentum, and absolute vorticity (proportional to the meridional
 250 gradient of angular momentum) that result from a range of forcings with a local subtrop-
 251 ical maximum (Fig. 7a).⁵ For weak forcing (blue lines), no extrema of \bar{M}_t are produced,
 252 illustrated by the fact that absolute vorticity (Fig. 7d) is positive everywhere. At the
 253 critical forcing profile (gray lines) a saddle point in \bar{M}_t is produced (Fig. 7c), where ab-
 254 solute vorticity is 0. Beyond this point, the profiles of \bar{u} that are in gradient wind bal-
 255 ance with the forcing are such as to produce extrema in \bar{M}_t , and are in violation of Hide’s
 256 theorem (Hide, 1969) so that a Hadley circulation must develop.

⁴ NB. One important assumption in CQE is that it holds for large spatial and temporal scales compared to the convective scales, so that convection can be assumed to be in quasi-equilibrium with its large-scale environment. On exactly what scales this breaks down is an open question.

⁵ This figure, taken from Hill et al. (2019), corresponds to a dry atmosphere, (cf. Plumb & Hou, 1992), but the behavior is equivalent to that for Eq. 7.

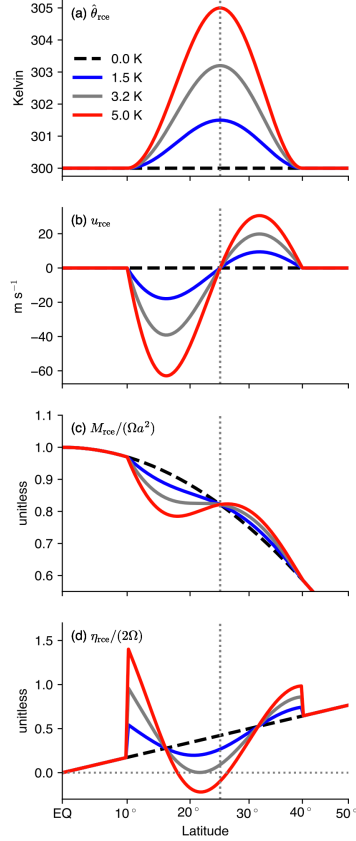


Figure 7. Illustration of the effects of a subcritical (blue lines), critical (gray lines) or supercritical (red lines) RCE potential temperature profile. Forcing profiles, shown in (a), are based on those used by Plumb and Hou (1992). The remaining panels show (b) zonal wind (m s^{-1}), (c) absolute angular momentum, normalized by the planetary angular momentum at the Equator, (d) absolute vorticity, normalized by twice the planetary rotation rate. From Hill et al. (2019). ©American Meteorological Society. Used with permission.

257 The above arguments assess the conditions under which a Hadley circulation will
 258 exist in an axisymmetric atmosphere. Privé and Plumb (2007a) further showed that this
 259 framework can give some insight into the controls on the latitude of the convergence zone.
 260 They noted that, if the overturning circulation conserves angular momentum in the free
 261 troposphere, the circulation boundary for a vertical streamline must be located in a re-
 262 gion of zero vertical wind shear. Where CQE applies, so that free tropospheric temper-
 263 atures are coupled to lower-level θ_{eb} , this implies that the zero streamfunction contour
 264 must occur in a region of zero horizontal gradient of θ_{eb} (i.e. where θ_{eb} maximizes). Most
 265 of the ascent in the circulation ascending branch, and consequently the precipitation, will
 266 occur just equatorward of this maximum. They additionally noted that either the max-
 267 imum in θ_{eb} or the maximum in moist static energy (MSE), h , could also be used to es-
 268 timate the latitude of the convergence zone (see their Section 5)⁶, as the two variables

⁶ θ_e is useful due to its relationship to moist entropy, which for example allows the substitution of a Maxwell relation into Eq. 5 (Emanuel, 1995). However, MSE is a linear quantity that is straightforward to calculate, and so is more widely used.

269 are related by

$$\partial\theta_{eb} \approx \frac{1}{T_b} \partial h_b, \quad (8)$$

$$h = c_p T + L_v q + gz. \quad (9)$$

270 In the above, T is temperature, q is specific humidity, z is height, L_v is the latent heat
 271 of vaporisation of water, c_p is the specific heat capacity and g is gravitational acceler-
 272 ation.

273 **2.1.2 Eddy-permitting solutions**

274 Conservation of angular momentum provides important constraints on the existence
 275 and extent of axisymmetric overturning circulations. However, it is now well known that
 276 extratropical eddies generated in midlatitude baroclinic zones propagate into the sub-
 277 tropics where they break, and have non-negligible impact on the Hadley circulation (e.g.,
 278 Becker, Schmitz, & Geprägs, 1997; C. C. Walker & Schneider, 2006). In particular, as
 279 transport of angular momentum by large-scale eddies becomes non-negligible, the asso-
 280 ciated eddy momentum flux convergence in Eq. 4 can no longer be neglected. In the limit
 281 of small Ro , the advection of zonal momentum by the zonal mean meridional flow is neg-
 282 ligible, and the dominant balance is between the Coriolis effect on the zonal mean merid-
 283 ional flow and the eddy momentum flux divergence. This regime is linear, in that the
 284 mean advection term is negligible, and eddy driven, in that the strength of the overturn-
 285 ing circulation is strongly constrained by the eddy momentum fluxes. As Ro approaches
 286 1, eddy effects become negligible, advection of zonal relative momentum by the mean
 287 meridional circulation is dominant and the circulation approaches conservation of angu-
 288 lar momentum. In reality, cases intermediate between these two limits, with $Ro \sim$
 289 0.5, are also observed, where both nonlinear zonal mean advection and eddy terms are
 290 important (Schneider, O’Gorman, & Levine, 2010).

291 Transitions from regimes with small Ro to regimes with Ro approaching unity have
 292 been connected to the rapid changes in the tropical circulation that occur during mon-
 293 soon onset. Examining the upper-level momentum budget in aquaplanet simulations with
 294 shallow slab oceans (e.g., ~ 1 m) and a seasonal cycle, Bordoni and Schneider (2008)
 295 found that around the equinoxes, the Hadley cells in the two hemispheres are roughly
 296 symmetric and the associated convergence zone is near the Equator, $Ro \lesssim 0.5$ and the
 297 circulation strength is governed by eddies (e.g., Fig. 8a). As the insolation maximum
 298 starts moving into the summer hemisphere, the winter Hadley cell starts becoming cross
 299 equatorial. The zonal mean ascent and precipitation move to a subtropical location in
 300 the summer hemisphere (e.g., Fig. 6), and upper-level tropical easterlies develop. The
 301 latter limit the ability of eddies from the winter hemisphere to propagate into the low
 302 latitudes, and the circulation shifts quickly towards the $Ro \sim 1$ angular momentum con-
 303 serving flow regime, at the same time strengthening and expanding rapidly (e.g., Fig.
 304 8b). As the cross-equatorial circulation approaches conservation of angular momentum,
 305 the dominant balance becomes between the terms on the left hand side of Eq. 3, with
 306 the eddy terms a small residual. Once in this regime, the circulation strength is no longer
 307 constrained by the zonal momentum budget, which becomes a trivial balance, but is in-
 308 stead constrained by the energy budget, and so responds strongly to the thermal forc-
 309 ing.

310 The rapid meridional migrations of the convergence zone in the aquaplanet are a
 311 result of a positive feedback relating to advection of cooler and drier air up the MSE gra-
 312 dient in the lower branch of the winter Hadley cell (Bordoni & Schneider, 2008; Schnei-
 313 der & Bordoni, 2008). As summer begins the summer hemisphere warms via diabatic
 314 fluxes of MSE into the air column. This pulls the lower-level peak in MSE and, in ac-
 315 cordance with the arguments of Privé and Plumb (2007a), pulls the ITCZ off of the Equa-
 316 tor. Simultaneously, the winter Hadley circulation begins to redistribute MSE, advect-

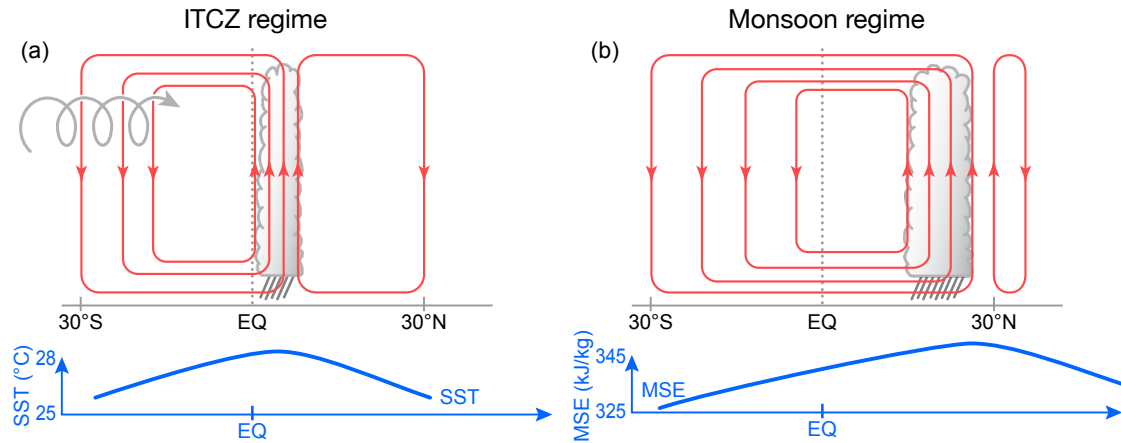


Figure 8. Schematic illustration of the two regimes of the meridional overturning circulation identified in aquaplanets (Bordoni & Schneider, 2008; Schneider & Bordoni, 2008). The gray cloud denotes clouds and precipitation, red contours denote streamfunction. (a) Convergence zone is an ITCZ located near to the Equator, and approximately co-located with the peak SST. Hadley cells are significantly eddy driven, as indicated by the helical arrow. (b) Convergence zone is monsoon-like, located farther from the Equator, with the mid-tropospheric zero contour of the streamfunction aligned with the MSE maximum (Privé & Plumb, 2007b) and precipitation falling just equatorward of this. The winter Hadley cell crosses the Equator and is near angular-momentum conserving, with eddies only weakly influencing the overturning strength. The summer Hadley cell is comparatively weak, if present at all. Known physics of these regimes is summarized in Table 1. Illustration by Beth Tully.

317 ing cooler and drier air up the MSE gradient. This pushes the lower-level MSE maxi-
 318 mum farther off the equator. The overturning circulation strengthens, further increas-
 319 ing the lower-level advection of cool air, and expanding the upper-level easterlies, allow-
 320 ing the circulation to become further shielded from the eddies and amplifying its response
 321 to the thermal forcing. It is important to note that in this view land is necessary for mon-
 322 soon development only insofar as it provides a lower boundary with low enough thermal
 323 inertia for the MSE to adjust rapidly and allows the feedbacks described above to act
 324 on intraseasonal timescales. Behavior consistent with these feedbacks has been observed
 325 in Earth’s monsoons, and will be discussed in more detail in Section 3.

326 **2.1.3 Hadley cell regimes and cell extent**

327 The idealized modeling work discussed above indicates that the Hadley cells in an
 328 aquaplanet change their circulation regime over the course of the year, shifting rapidly
 329 between an eddy-driven ‘ITCZ’ regime and a near angular momentum conserving ‘mon-
 330 soon’ regime. In addition, that the cross-equatorial Hadley cell approaches angular
 331 momentum conservation suggests that axisymmetric theories (e.g., Eq. 7) might not be ap-
 332 plicable to the understanding of the zonal and annual mean Hadley cell, but might pro-
 333 vide important constraints on monsoonal circulations, which do approach an angular
 334 momentum conserving state. The relationship between these two regimes and the latitude
 335 of the convergence zone raises further questions: How far into the summer hemisphere
 336 must the Hadley cell extend for the regime transition, and associated rapid shift in con-
 337 vergence zone latitude, to occur? Does the latitude at which the convergence zone shifts
 338 from being governed by ‘ITCZ’ to ‘monsoon’ dynamics in aquaplanets relate to the ob-

339 served latitudes of the ITCZs and monsoons? If the upward branch of the Hadley cell
 340 follows the peak in MSE (Privé & Plumb, 2007a), what governs the extent of the cross-
 341 equatorial cell, e.g., is a pole-to-pole cell possible?

342 Geen et al. (2019) investigate the first of the above questions. By running aqua-
 343 planet simulations under a wide range of conditions, including different slab ocean depths,
 344 year lengths, and rotation rates, they investigated how the convergence zone latitude and
 345 migration rate were related, and how these factors varied over the year. They found that,
 346 at Earth’s rotation rate, the convergence zone appeared least stable (migrated poleward
 347 fastest) at a latitude of 7° , suggesting that, in an aquaplanet, this may be the poleward
 348 limit of the rising branch of an eddy-driven overturning circulation; i.e., the poleward
 349 limit of an ITCZ. Beyond this latitude there is a rapid transition to a monsoon circula-
 350 tion characterized by an overturning circulation with a rising branch far off the Equator
 351 and weak eddy momentum transports. In their simulations, this ‘transition latitude’
 352 does not vary significantly with surface heat capacity or year length, but it does increase
 353 with decreasing planetary rotation rate. Although the mechanism setting the transition
 354 latitude is not yet fully understood, they suggest that this 7° threshold might give a guide-
 355 line for where the tropical precipitation is dynamically associated with a near-equatorial
 356 ‘ITCZ’ vs. a monsoon system.

357 Consistent with these results, simulations introducing zonally symmetric continents
 358 in the Northern Hemisphere with southern boundaries at various latitudes suggest that
 359 monsoon circulations extending into the subtropics only develop if the continent extends
 360 equatorward of 20° latitude, into tropical latitudes. For continents with more poleward
 361 southern boundaries, the main precipitation zone remains close to the Equator and moves
 362 more gradually into the summer hemisphere. The absence of regions of low thermal inertia
 363 at tropical latitudes in this second case prevents the establishment of a reversed
 364 meridional MSE gradient and, with it, the rapid poleward displacement of the circula-
 365 tion ascending branch and convergence zone; i.e., it prevents a monsoon circulation (Hui
 366 & Bordoni, submitted.). Table 1 summarizes the characteristics and dynamics of the over-
 367 turning (Hadley Cells) associated with the ITCZ and monsoon regimes.

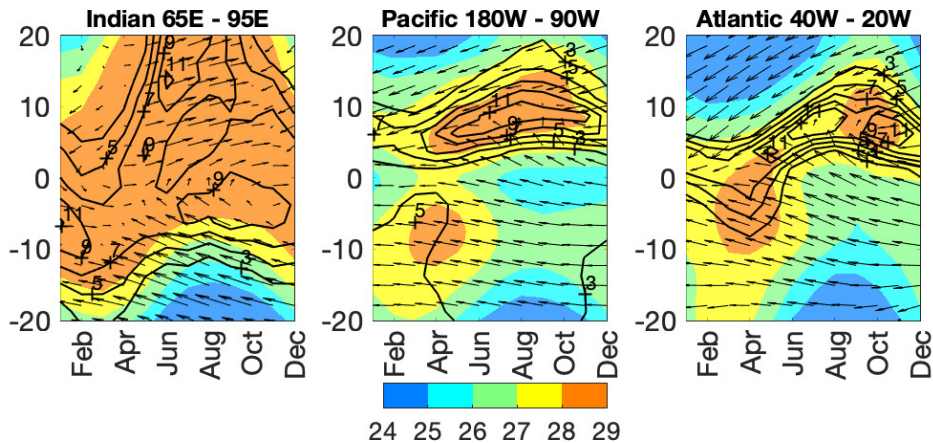


Figure 9. Hovmoller diagram of the climatological SST and 10m wind averaged across the (left) Indian, (center) eastern half of the Pacific and (right) Atlantic basin. SST is shaded (in $^\circ\text{C}$) and precipitation is contoured (contour interval 2 mm/day). The wind vectors are relative to the maximum in each panel. Precipitation data are from CMAP 1979-2017 (Xie & Arkin, 1997a), SST data are from HADISST 1870-2017 (Rayner et al., 2003), and wind data are from ERA-Interim 1979-2017 (Dee et al., 2011). From Battisti et al. (2019). ©American Meteorological Society. Used with permission.

Table 1. Characteristics of Hadley cell regimes associated with the limits of Eq. 4. The transition between the two regimes is determined by the criteria in Eq. 7.

Property	Regime	
	ITCZ	Monsoon
Position of convergence zone	Within $\sim 10^\circ$ of the Equator	Subtropics, up to $\sim 30^\circ\text{N/S}$
Physics setting convergence zone position	Under development	Under development
Strength of overturning cell/precipitation	Eddy momentum fluxes	Energetic controls (still under development)

368 In contrast with the idealized model results of Geen et al. (2019), the observed ITCZs
369 over the Atlantic and Pacific migrate as far poleward as 10° from the Equator over the
370 year (see Figs. 1 and 9). There is considerable evidence that the latitude of these ITCZs
371 is a result of a symmetric instability in the boundary layer flow (Levy & Battisti, 1995;
372 Stevens, 1983; Tomas & Webster, 1997). Symmetric instability is a two-dimensional (latitude-
373 height) instability that results from the joint criteria of conservation of angular momen-
374 tum and potential temperature (potential vorticity).⁷ The instability in the boundary
375 layer flow is set up by cross-equatorial pressure gradients, driven by equatorially asym-
376 metric boundary layer heating. In the case of the Pacific and Atlantic ITCZs, the insta-
377 bility results from the low-latitude, meridionally-asymmetric sea surface temperature (SST)
378 distribution that is set up by the Andes and from meridionally asymmetric land heat-
379 ing over Africa respectively (see Section 4.1.3). The result of the instability is a band
380 of divergence in the boundary layer that lies between the Equator and the latitude of
381 neutral stability, flanked by a narrow zone of convergence that lies just poleward and pro-
382 vides the moisture convergence that fuels the ITCZ convection (Tomas & Webster, 1997).
383 Monsoon flows have also been observed to be symmetrically unstable (e.g., Tomas & Web-
384 ster, 1997), with the instability in this case generated by the seasonally varying merid-
385 ional pressure gradient set up by the insolation.

386 **2.1.4 Extratropical limit to monsoons**

387 The application of the theoretical concepts discussed in Sections 2.1.1 and 2.1.2 to
388 Hadley cell extent has been addressed in recent work by Faulk et al. (2017), Hilgenbrink
389 and Hartmann (2018), Hill et al. (2019) and Singh (2019). Faulk et al. (2017) performed
390 a series of simulations using an eddy-permitting aquaplanet model in which they var-
391 ied rotation rate under seasonally varying insolation. They found that, at Earth’s ro-
392 tation, the MSE maximized at the summer pole, but the convergence zone did not mi-
393 grate poleward of $\sim 25^\circ$ from the Equator even in perpetual solstice simulations, con-
394 trary to expectations from Privé and Plumb (2007a). The influence of eddies on the cross-
395 equatorial circulation was found to be weak, consistent with the suppression of eddies
396 by upper-level easterlies (Bordoni & Schneider, 2008; Schneider & Bordoni, 2008) and
397 justifying the use of axisymmetric based considerations as a starting point for understand-
398 ing the cell extent. Faulk et al. (2017) found that a Hadley circulation existed over the
399 latitudes where the curvature of θ_{eb} was supercritical (see Eq. 7), with the curvature sub-
400 critical in the extratropics.

⁷ For motion on a constant potential temperature (angular momentum) surface, the criteria reduces to the criteria for inertial (convective) instability (Emanuel, 1988; Tomas & Webster, 1997).

401 While these studies have provided novel insight into important features of cross-
 402 equatorial Hadley cells, prognostic theories for their poleward boundary (the zero stream-
 403 function contour) in the summer hemisphere have yet to emerge. Singh (2019) investi-
 404 gated the limitations of CQE-based predictions based on the lower-level MSE maximum.
 405 The vertical instability addressed by CQE is not the only form of convective instabil-
 406 ity in the atmosphere. If vertical wind shear is strong, CQE predicts an unstable state
 407 in which potential energy is released when saturated parcels move along slantwise paths,
 408 along angular momentum surfaces (Emanuel, 1983a, 1983b). Singh (2019) showed that
 409 the extent of the perpetual solstitial overturning cell can be accurately estimated by as-
 410 suming that the large-scale circulation adjusts the atmosphere towards a state that is
 411 neutral to this slantwise convection. When the peak in subcloud moist entropy is rel-
 412 atively close to the Equator, the cell boundary is near vertical and the atmosphere is near
 413 CQE, and this reduces to the condition of Privé and Plumb (2007a).

414 Notably, this developing body of literature indicates that the planetary rotation
 415 rate determines the latitudinal extent of the Hadley cell, potentially limiting the max-
 416 imum latitudinal extent of a monsoon circulation. This might provide a guideline for dis-
 417 tinguishing a monsoon associated with a cross-equatorial Hadley cell and governed by
 418 eddy-less, angular momentum conserving dynamics, where the convergence zone is lo-
 419 cated in the subtropics ($\sim 20-25^\circ$ latitude, e.g., South Asia) from a monsoon that is
 420 strongly influenced by extratropical processes, where summer rainfall is observed at even
 421 higher latitudes (e.g., 35° in East Asia).

422 2.2 Energetic constraints

423 The regional monsoons are an integral part of the tropical convergence zone. As
 424 such, theories that have recently emerged to explore controls on the location of the zon-
 425 ally and annually averaged convergence zone ($\overline{\text{ITCZ}}$) might prove useful to the under-
 426 standing of monsoon dynamics. For example, the $\overline{\text{ITCZ}}$ is located in the Northern Hemi-
 427 sphere, at 1.7°N if estimated by the precipitation centroid; (Donohoe, Marshall, Ferreira,
 428 & Mcgee, 2013), or $\sim 6^\circ\text{N}$ if judged by the precipitation maximum; (e.g., Gruber, Su,
 429 Kanamitsu, & Schemm, 2000). While it is usually the case that the $\overline{\text{ITCZ}}$ is co-located
 430 with SST maxima, both paleoclimate proxies (e.g., Figs. 4 & 5; Arbuszewski, Demenocal,
 431 Cléroux, Bradtmiller, & Mix, 2013; Lea, Pak, Peterson, & Hughen, 2003; McGee,
 432 Donohoe, Marshall, & Ferreira, 2014) and model simulations (Broccoli, Dahl, & Stouf-
 433 fer, 2006; Chiang & Bitz, 2005; Kang, 2020; Kang, Shin, & Xie, 2018; R. Zhang & Del-
 434 worth, 2005) indicate that the location of the $\overline{\text{ITCZ}}$ responds to extratropical forcing,
 435 that is, to forcing remote from its location. Analysis of the atmospheric and oceanic en-
 436 ergy budget has helped to explain these behaviors.

437 Not surprisingly, aquaplanet simulations have been used to examine systematically
 438 controls on the $\overline{\text{ITCZ}}$ latitude by imposing a prescribed hemispherically asymmetric forc-
 439 ing in the extratropics and varying its strength. Kang, Held, Frierson, and Zhao (2008)
 440 found that the atmospheric energy transport associated with the Hadley cell largely com-
 441 pensates for changes in hemispherically asymmetric extratropical surface heating. The
 442 Hadley cell diverges energy away from its ascending branch, i.e. away from the $\overline{\text{ITCZ}}$,
 443 and generally transports energy in the direction of the upper-level meridional flow. Hence
 444 a hemispherically asymmetric atmospheric heating will cause the $\overline{\text{ITCZ}}$ to shift towards
 445 the hemisphere with the greater heating, as illustrated in Fig. 10. Kang et al. (2008) fur-
 446 ther noted that the $\overline{\text{ITCZ}}$ latitude was approximately colocated with the ‘Energy Flux
 447 Equator’ (EFE), the latitude at which the vertically integrated MSE flux is zero, and
 448 that it varied proportionally to the strength of the asymmetric forcing. Anticorrelation
 449 between the $\overline{\text{ITCZ}}$ latitude and the cross-equatorial atmospheric energy transport in the
 450 tropics has since been observed in aquaplanet models with different physical parameter-
 451 izations (Kang et al., 2009), and in models with realistic continental configurations un-
 452 der global warming and paleoclimate scenarios (Donohoe et al., 2013; D. M. W. Frier-

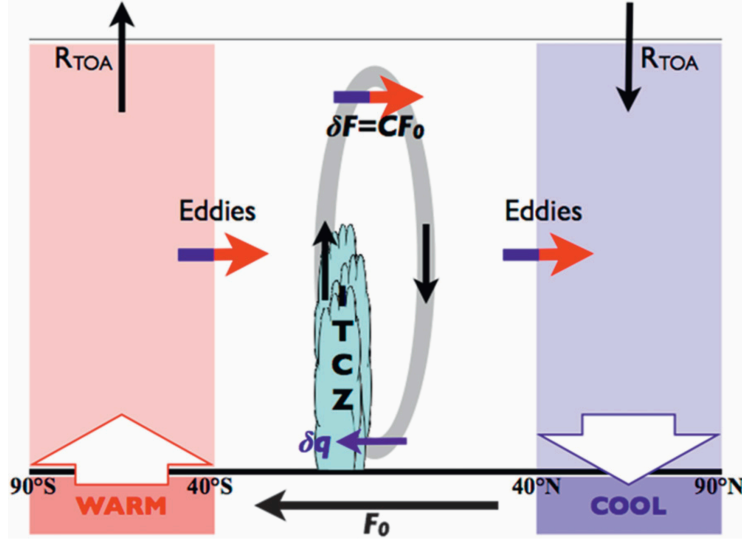


Figure 10. Schematic illustrating the energetics framework to determine the tropical response to extratropical thermal forcing (Kang et al., 2009). Warming is applied to the southern extratropical slab ocean, giving an implied ocean heat transport anomaly F_0 . The atmosphere compensates for the additional warming by altering the top-of-atmosphere net radiative flux (R_{TOA}) and horizontal energy transports by the atmosphere. In the tropics, the gray oval indicates the anomalous Hadley circulation response, the direction of which is represented by black arrows. The blue (red) part of the colored arrow indicates regions where energy transports act to (anomalously) cool (warm) the atmosphere. These energy transports are due to midlatitude eddies and the Hadley circulation. The clockwise anomalous Hadley circulation transports energy northward to cool (warm) the southern (northern) subtropics and largely compensates the warming (cooling) by eddies. From Kang et al. (2009). ©American Meteorological Society. Used with permission.

son & Hwang, 2012). However, the degree of compensation between the imposed heating and the atmospheric energy transport is sensitive to the parameterizations of convection, clouds, and ice (D. M. W. Frierson & Hwang, 2012; Kang et al., 2009, 2008); to the nature of the forcing applied; to whether the response is dominated by the zonal mean circulation or stationary and transient eddies (Roberts, Valdes, & Singarayer, 2017); and to changes in energy transport by the ocean, which has been shown to play a significant role in the energy transport response to an imposed perturbation (Green & Marshall, 2017; Hawcroft et al., 2017; Kang, 2020; Kang et al., 2018; Kay et al., 2016; Levine & Schneider, 2011; Schneider, 2017).

The relationship between the \overline{ITCZ} , EFE, and tropical atmospheric energy transport can be understood more quantitatively using the steady state, zonally averaged, vertically integrated energy budget,

$$\overline{\mathcal{S}} - \overline{\mathcal{L}} - \overline{\mathcal{O}} = \frac{\partial \langle v\bar{h} \rangle}{\partial y}. \quad (10)$$

In the above, \mathcal{S} is the net downward top-of-atmosphere shortwave radiation, \mathcal{L} the outgoing longwave radiation and \mathcal{O} represents any net energy uptake at the surface. Angular brackets denote a vertical integral, and overbars a time and zonal mean. Eq. 10 states that net energy input into the atmospheric column through top-of-atmosphere ra-

469 diative fluxes and surface energy fluxes must be in balance with meridional convergence
 470 or divergence of MSE into the atmospheric column. For small meridional displacements,
 471 δ , this equation can be Taylor expanded around the Equator to 3rd order as (Bischoff
 472 & Schneider, 2014, 2016)

$$\langle \overline{vh} \rangle_\delta = \langle \overline{vh} \rangle_0 + a \partial_y \langle \overline{vh} \rangle_0 \delta + \frac{1}{2} a^2 \partial_{yy} \langle \overline{vh} \rangle_0 \delta^2 + \frac{1}{6} a^3 \partial_{yyy} \langle \overline{vh} \rangle_0 \delta^3, \quad (11)$$

473 where the $_0$ subscript denotes quantities evaluated at the Equator. At the EFE, by def-
 474 inition, the vertically integrated, zonal mean MSE flux, $\langle \overline{vh} \rangle$, is zero. Taking δ as the lat-
 475 itude of the EFE, and substituting in from Eq. 10, gives

$$0 = \langle \overline{vh} \rangle_0 + a(\overline{\mathcal{S}} - \overline{\mathcal{L}} - \overline{\mathcal{O}})_0 \delta + \frac{1}{2} a^2 \partial_y (\overline{\mathcal{S}} - \overline{\mathcal{L}} - \overline{\mathcal{O}})_0 \delta^2 + \frac{1}{6} a^3 \partial_{yy} (\overline{\mathcal{S}} - \overline{\mathcal{L}} - \overline{\mathcal{O}})_0 \delta^3. \quad (12)$$

476 The net energy input ($\overline{\mathcal{S}} - \overline{\mathcal{L}} - \overline{\mathcal{O}}$) is approximately symmetric about the Equator, so
 477 the quadratic term is small relative to the other terms (Bischoff & Schneider, 2016), and
 478 can be neglected. Hence, to a good approximation, Eq. 12 can be written as

$$\delta = -\frac{\langle \overline{vh} \rangle_0}{a(\overline{\mathcal{S}} - \overline{\mathcal{L}} - \overline{\mathcal{O}})_0}. \quad (13)$$

479 Eq. 13 has been shown to give a good estimate of the EFE latitude under a range of warm-
 480 ing scenarios in aquaplanets (Bischoff & Schneider, 2014), and over the annual cycle in
 481 reanalysis (Adam, Bischoff, & Schneider, 2016b). The EFE in turn acts as an indicator
 482 of the $\overline{\text{ITCZ}}$ latitude. More broadly, (Bischoff & Schneider, 2016) found that the first
 483 order approximation is adequate when the net energy input at the Equator is large and
 484 positive, but that the cubic term is needed when it is small or negative. Notably the neg-
 485 ative case corresponds to a double convergence zone.

486 Unfortunately, the convergence zone and EFE latitudes do not covary on all timescales.
 487 In particular these can deviate from one another significantly over the seasonal cycle (e.g.,
 488 Adam et al., 2016b; Wei & Bordoni, 2018). While the EFE denotes the latitude at which
 489 the meridional MSE flux changes sign, the convergence zone is associated with the as-
 490 cending branch of the tropical meridional overturning circulation, which is close to the
 491 latitude where the mass flux changes sign. The energy flux and overturning circulation
 492 are related via the gross moist stability (GMS, defined here following e.g., D. M. W. Frier-
 493 son, 2007; Hill, Ming, & Held, 2015; Wei & Bordoni, 2018, 2020):

$$GMS = \frac{\langle \overline{vh} \rangle}{\Psi_{max}} = \frac{\langle \overline{vh} \rangle}{g^{-1} \int_0^{p_m} \overline{v} dp}. \quad (14)$$

494 In the above, Ψ_{max} is the maximum of the overturning streamfunction, corresponding
 495 to the mass flux by the Hadley cell, and p_m is the pressure level at which this maximum
 496 occurs. Considering Eq. 14 at the Equator, and combining with Eq. 13, we see that the
 497 strength of the Hadley circulation (and hence the position of the convergence zone) will
 498 therefore covary with the EFE provided that the efficiency with which the Hadley cell
 499 transports energy, as captured by GMS, remains approximately constant. However, re-
 500 cent aquaplanet simulations indicate that over the seasonal cycle GMS varies significantly,
 501 and in fact at times becomes negative, allowing the EFE and convergence zone to sit in
 502 opposite hemispheres (Wei & Bordoni, 2018). GMS has also been observed to vary sig-
 503 nificantly under changes to orbital precession and increased CO₂ in aquaplanet simu-
 504 lations (Biasutti & Voigt, 2020; Merlis, Schneider, Bordoni, & Eisenman, 2013). It is also
 505 worth noting that, in addition to variations in GMS, the zonal mean energy flux com-
 506 pensating an energetic forcing may be achieved by transient or stationary eddies, rather
 507 than by changes to the zonal mean overturning circulation (Roberts et al., 2017; Xiang,
 508 Zhao, Ming, Yu, & Kang, 2018). When these factors do not play a significant role, changes
 509 in hemispheric asymmetry in surface energy flux appear to exert a tighter control than
 510 changes in SST on the latitudinal location of tropical precipitation (Kang & Held, 2012).

511 However, recent analysis of the TRACMIP model ensemble (Voigt et al., 2016) indicates
 512 that the significant changes in GMS which occur both over the seasonal cycle and in the
 513 response to increased CO₂ mean that in these cases the convergence zone latitude is more
 514 closely related to changes in SST than to energy flux changes (Biasutti & Voigt, 2020).

515 Despite these limitations, the energetic framework has been a major advance, and
 516 has given insight into variations in tropical rainfall over both the observational and pa-
 517 leo record (see reviews by Kang, 2020; Kang et al., 2018; Schneider, Bischoff, & Haug,
 518 2014, and references therein). One attractive feature of this perspective is that it pro-
 519 vides a simple explanation for why, in the annual and zonal mean, the $\overline{\text{ITCZ}}$ sits in the
 520 Northern Hemisphere (Donohoe et al., 2013; Gruber et al., 2000). The energetic frame-
 521 work neatly shows that the $\overline{\text{ITCZ}}$ latitude can be understood as a result of the net flux
 522 of energy into the Northern Hemisphere by the ocean, in particular due to asymmetry
 523 introduced by the Drake passage (D. M. Frierson et al., 2013; Fućkar, Xie, Farneti, Ma-
 524 rroon, & Frierson, 2013; Marshall, Donohoe, Ferreira, & McGee, 2014). Efforts to extend
 525 this framework to account for zonal asymmetry in the boundary conditions (the ‘Energy
 526 Flux Prime Meridian’ Boos & Korty, 2016) are discussed in Section 3.2.

527 **3 Interpreting observations and modeled response to forcings**

528 In parallel with the theoretical developments described in Section 2, observational
 529 and reanalysis datasets have allowed more detailed analysis of the behavior of Earth’s
 530 monsoons. As discussed in Section 1, one major step has been moving from a perspec-
 531 tive of monsoons as individual, unrelated systems, to a perspective of a global monsoon
 532 manifesting itself into several regional systems (B. Wang & Ding, 2008). In this section,
 533 we look at the insight into the dynamics of Earth’s monsoons gained from observations
 534 and Earth System models, and at how it connects to the theoretical ideas developed us-
 535 ing idealized model simulations discussed in Section 2. First, we give an overview of the
 536 characteristics of Earth’s regional monsoons, ITCZs and the global monsoon. We then
 537 discuss the extent to which theory, particularly that from aquaplanet models, may help
 538 us understand the behavior of these systems.

539 **3.1 The global and regional monsoons**

540 The magenta line in Fig. 1a-c marks out the regional monsoons, indicating areas
 541 where the local difference between summer and winter precipitation exceeds 2 mm/day,
 542 and where summer precipitation accounts for the majority of the annual total. Six re-
 543 gions can be identified: Asia, West Africa, Southern Africa, South America, North Amer-
 544 ica and Australia (cf. S. Zhang & Wang, 2008). The Asian monsoon is the most intense
 545 and largest in scale of these, and is often further divided into three subregions: the South
 546 Asian, East Asian, and Western North Pacific monsoons, as shown in Fig. 11. (B. Wang
 547 & LinHo, 2002).

548 ***3.1.1 Regional monsoon and ITCZ characteristics***

549 *South Asian Monsoon*

550 The South Asian monsoon features a wind reversal from winter easterlies to sum-
 551 mer westerlies at lower levels (e.g., B. Wang & LinHo, 2002). Onset spreads from the
 552 south to the north, with the earliest onset of the system over the Southern Bay of Ben-
 553 gal, between late April and mid-May (Mao & Wu, 2007), reaching Kerala between mid-
 554 May and mid-June (Ananthkrishnan & Soman, 1988; J. M. Walker & Bordoni, 2016;
 555 B. Wang, Ding, & Joseph, 2009). Onset occurs over the South China Sea between early
 556 May and mid-June (B. Wang, LinHo, Zhang, & Lu, 2004).

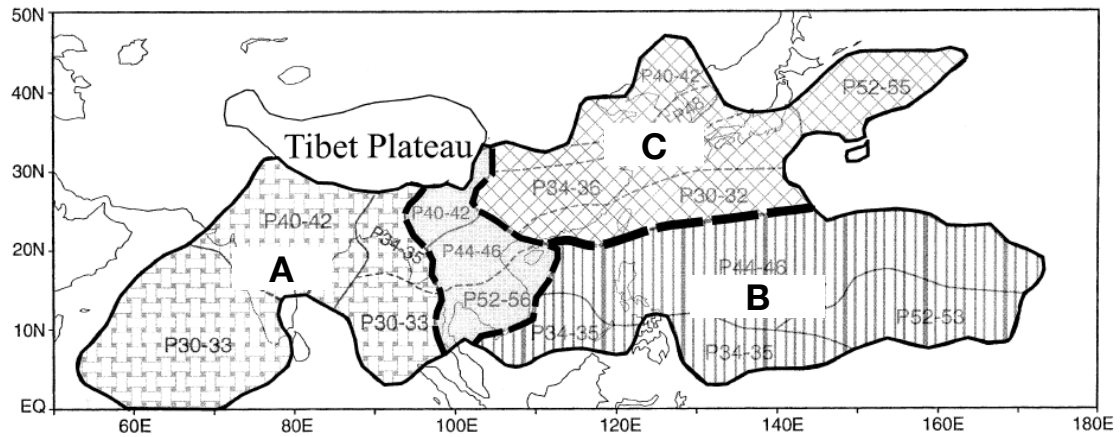


Figure 11. Map showing the division of the Asian monsoon into three subregions. The South Asian monsoon (A) and Western North Pacific monsoon (B) are tropical monsoon regions. A broad corridor in the Indochina Peninsula separates them. The East Asian monsoon (C) is an extratropical ‘monsoon’ (see Section 4.1.1). Numbers indicate the pentad range during which the peak monsoon rainfall occurs. Adapted from B. Wang and LinHo (2002). ©American Meteorological Society. Used with permission.

557 The wet season over India generally lasts from June to September, during which
 558 time about 78% of the total annual rain falls over India (Parthasarathy, Munot, & Kothawale,
 559 1994). The rain band withdraws towards the Equator between late September and early
 560 November (B. Wang & LinHo, 2002).

561 *East Asian ‘Monsoon’*

562 While the South Asian monsoon is confined to be equatorward of $\sim 30^\circ\text{N}$, the East
 563 Asian monsoon extends north of this into the extratropics. Although the monsoon on-
 564 set over the South China Sea has been considered a precursor to the East Asian mon-
 565 soon onset (Martin et al., 2019; B. Wang et al., 2004), some authors (e.g., B. Wang &
 566 LinHo, 2002) consider it as an entirely subtropical system. A key element of the East
 567 Asian monsoon is an east-west oriented band of precipitation, known as Meiyu in China
 568 and Baiu in Japan, that is accompanied by a wind reversal from winter northerlies to
 569 summer southerlies. The Meiyu-Baiu front brings intense rainfall to the Yangtze River
 570 valley and Japan from mid-June to mid-July, after which it breaks down and allows rain-
 571 fall to extend into northern China and Korea. Prior to the onset of the Meiyu-Baiu front,
 572 South China experiences periods of rainfall in the form of the South China spring rain,
 573 intensifying from mid-March to May (Linho, Huang, & Lau, 2008). A thorough review
 574 of the East Asian monsoon’s characteristics, including its onset and development, gov-
 575 erning processes and teleconnections is given in Ding and Chan (2005); see also Section
 576 4.1.1.

577 *Western North Pacific Ocean Monsoon*

578 Monsoon rains arrive later over the western subtropical North Pacific ocean (see
 579 Fig. 11) than the South and East Asian sectors, and last from July to October/November
 580 (B. Wang & LinHo, 2002). The monsoon advances from the south-west to north-east in
 581 a stepwise pattern associated with shifts in the Western North Pacific subtropical high
 582 (R. Wu & Wang, 2001), while withdrawal occurs from the north-west to south-east (S. Zhang
 583 & Wang, 2008). A predominantly zonally oriented change in wind direction is seen be-

584 tween winter and summer, associated with a weakening of the low-latitude easterly flow
 585 as the Western North Pacific subtropical high shifts eastward (e.g., Fig. 1).

586 *Australian Monsoon*

587 The Australian monsoon develops over Java in October–November, and progresses
 588 southeastward, reaching northern Australia in late December (Hendon & Liebmann, 1990;
 589 S. Zhang & Wang, 2008). During austral summer, the low-latitude easterlies over the
 590 western Maritime Continent reverse to a southwesterly flow, as seen in Fig. 1b and c.
 591 Monsoon withdrawal occurs over northern Australia and the southeastern Maritime Con-
 592 tinent through March, with the wet season persisting into April over Java (S. Zhang &
 593 Wang, 2008).

594 *West African Monsoon*

595 The West African monsoon begins near the Equator, with intense rainfall over the
 596 Gulf of Guinea in April. This continues through to the end of June, with a second max-
 597 imum developing near 10°N in late May. The peak precipitation is observed to jump rapidly
 598 to this second maximum in late June, accompanied by a reversal of the wind direction
 599 from north-easterly to south-westerly to the south of this maximum (Sultan & Janicot,
 600 2003). Precipitation weakens from August to September and the peak rainfall migrates
 601 back towards the Equator. Over the Sahel, the monsoon precipitation accounts for 75-
 602 90% of the total annual rainfall (Lebel, 2003). Another notable feature in this region is
 603 the presence of a secondary shallow meridional circulation, with dry air converging and
 604 ascending over the Sahara, where sensible heating is strong, and a return flow at 500-
 605 750 hPa (Hagos & Cook, 2007; Shekhar & Boos, 2017; Trenberth et al., 2000; C. Zhang,
 606 Nolan, Thorncroft, & Nguyen, 2008). The precise seasonality of this shallow circulation
 607 was found to vary between the NCEP1, NCEP2 and ERA-40 reanalyses by C. Zhang
 608 et al. (2008). We find that in the JRA-55 data used here the seasonality is most consis-
 609 tent with that of ERA-40 in that study, with the return flow present year-round, but strength-
 610 ening semi-annually in boreal winter from late November to late March and boreal sum-
 611 mer from mid-May to mid-October (not shown).

612 *Southern African Monsoon*

613 The Southern African monsoon is offset longitudinally to the east of its Northern
 614 Hemisphere counterpart. The global monsoon onset metric of S. Zhang and Wang (2008)
 615 indicates that the rainy season begins in November over Angola and the southern DRC,
 616 and extends southeastward over the continent, progressing over southern Tanzania, Zam-
 617 biala and out over the ocean over northern Madagascar through December, and reaching
 618 Zimbabwe, Mozambique, and as far as the northeast of South Africa by January. The
 619 system extends out over the Southwestern Indian Ocean through January and Febru-
 620 ary. Withdrawal occurs directed towards the north and west from February to April. In
 621 austral winter, the prevailing wind is southeasterly, but in summer this reverses to a weak
 622 northeasterly flow, with stronger northeasterly flow to the north of the region, over the
 623 Horn of Africa, as seen in Fig. 1c. Although, as we will show, the seasonality of both the
 624 circulation and precipitation in this region is consistent with monsoon dynamics, the sum-
 625 mertime precipitation over this region is more often referred to as the ‘Southern African
 626 rainy season’, and it is only with the advent of the Global Monsoon perspective that this
 627 system is gaining more attention as a monsoon (e.g., S. Zhang & Wang, 2008).

628 *North American Monsoon*

629 The North American monsoon is observed as a marked increase in precipitation
 630 over Mexico and Central America, beginning in June–July, and withdrawing through Septem-
 631 ber and October (Adams & Comrie, 1997; Barlow, Nigam, & Berbery, 1998; Ellis, Saf-
 632 fell, & Hawkins, 2004). S. Zhang and Wang (2008) observed that onset (withdrawal) over
 633 this area occurs in a northward (southward) moving band. There is no large-scale re-

634 versal of the winds in this region (see Figs. 1b and 1c). However, the northwesterly flow
 635 down the coast of California observed in boreal winter weakens in boreal summer, the
 636 southeasterly flow over the east coast of Mexico strengthens, and the low-latitude east-
 637 erlies over the eastern Pacific weaken in the Northern Hemisphere (e.g., Fig. 7 of Bar-
 638 low et al., 1998). In addition, at a smaller scale, the lower-level wind direction reverses
 639 over the Gulf of California from northerly to southerly flow (Bordoni, Ciesielski, John-
 640 son, McNoldy, & Stevens, 2004).

641 *South American Monsoon*

642 The monsoon season in South America begins in October, with an abrupt shift of
 643 convection southward over the Amazon river basin (Marengo et al., 2012). The precip-
 644 itation progresses southeastward through November and December (S. Zhang & Wang,
 645 2008). Withdrawal occurs from March to May, with the rain-band returning northward.
 646 During austral winter, the prevailing 850-hPa winds over the continent are predominantly
 647 easterly between 10°S and 10°N, but in summer the flow becomes northeasterly and cross
 648 equatorial, and a northwesterly jet, the South American Low-Level jet, develops along
 649 the east side of the Andes (Marengo et al., 2012). An upper-level anticyclone is observed
 650 over Bolivia, and a lower-level cyclone develops over northern Argentina (Rao, Caval-
 651 canti, & Hada, 1996). Central Brazil receives over 70% of its annual rainfall during the
 652 monsoon season, between September and February (Rao et al., 1996).

653 *The Atlantic and Pacific ITCZs*

654 The latitudinal position of the ITCZs in the Atlantic and Pacific also has a distinct
 655 seasonal cycle, as can be seen from the north-south dipole in the October/November-
 656 April/May precipitation difference, shown in Fig. 1b. Precipitation associated with the
 657 Atlantic and Pacific ITCZs reaches farthest north in October and farthest south (but
 658 still north of the Equator; see Section 4.1.3) in March about three months after the bo-
 659 real and austral solstice, respectively (Fig. 9) due to the large heat capacity of the up-
 660 per ocean that participates in the seasonal cycle.

661 *3.1.2 The Global Monsoon*

662 The regional monsoons exhibit a diverse range of behaviors, but some common fea-
 663 tures can be identified. From Fig. 1a, it can be seen that most monsoon regions feature
 664 anomalous westerly lower-level flow in their summer season, with a cross-equatorial com-
 665 ponent directed into the summer hemisphere. However, comparing Figs. 1b and c shows
 666 that these anomalies are not always sufficient to cause a local reversal of the wind di-
 667 rection. Onset generally occurs as a poleward advancement of rainfall off of the Equa-
 668 tor, often with an eastward directed progression. Onset also sometimes features sudden
 669 jumps or steps in the latitude (poleward) and longitude of precipitation, as observed over
 670 South Asia, West Africa, the Western North Pacific, and South America.

671 These common features are particularly evident in EOF analyses of the annual cy-
 672 cle of the global divergent circulation (Trenberth et al., 2000) and of precipitation and
 673 lower-level winds (B. Wang & Ding, 2008). These reveal a global-scale solstitial mode,
 674 that accounts for 71% of the combined annual variance in precipitation and surface winds,
 675 and closely reflects the summer-winter differences in precipitation (compare Fig. 1a and
 676 Fig. 2a). B. Wang and Ding (2008) also identified a second major mode, an equinoctial
 677 asymmetric mode that reflects spring-fall asymmetry (compare Fig. 1b and Fig. 2b). This
 678 mode is particularly evident in the ITCZs, relating to their delayed seasonality. These
 679 dominant modes motivate a perspective of a global monsoon system that is driven by
 680 the annual cycle of insolation, and so can be expected to respond to orbital forcings in
 681 a coherent manner. The global monsoon might be interpreted as the seasonal migration
 682 of the convergence zone into the summer hemisphere throughout the year, with regional
 683 monsoons corresponding to locations where this migration is enhanced, and with cou-

684 pling between the zonal and meridional overturning circulations contributing to this lo-
 685 calisation of rainfall (Trenberth et al., 2000; B. Wang & Ding, 2008; Webster et al., 1998).

686 This perspective is further supported by paleoclimate reconstructions, present-day
 687 observations, and model simulations, which have begun to elucidate how the regional mon-
 688 soons and ITCZs vary under a range of external and internal forcings. Forcings that pre-
 689 ferentially warm or cool one hemisphere relative to the other - such as Heinrich events,
 690 changes in Earth’s axial precession and high latitude volcanic eruptions - are found to
 691 intensify the monsoons of the warmer hemisphere, and to weaken the monsoons of the
 692 cooler hemisphere (e.g., An et al., 2015; Atwood et al., 2020; Battisti et al., 2014; H. Cheng,
 693 Sinha, Wang, Cruz, & Edwards, 2012; Eroglu et al., 2016; Liu & Battisti, 2015; Pausata
 694 et al., 2011; P. X. Wang et al., 2014, and see Figs. 4 and 5).

695 3.2 Aquaplanet-like monsoons

696 Aquaplanet-based theoretical work, as discussed in Section 2, has used symmetric
 697 boundary conditions to study the fundamental processes governing the zonal mean
 698 convergence zone, Hadley cells, and global monsoon. In contrast, the bulk of studies us-
 699 ing observations, reanalysis, and Earth System models have tended to focus on the mech-
 700 anisms controlling regional monsoons. While local factors are important in determin-
 701 ing the seasonal evolution and the variability of the individual monsoon systems, we ar-
 702 gue here that aquaplanet results can inform us of unanticipated commonalities in the
 703 dynamics of the monsoons, and help us interpret the behaviors observed. Of the two per-
 704 spectives discussed in Section 2 the energetic approach has received more attention (Bi-
 705 asutti et al., 2018; Kang, 2020; Kang et al., 2018; Schneider et al., 2014), perhaps due
 706 to the relative ease with which the relevant diagnostics can be evaluated and the intu-
 707 itive picture it presents (Fig. 10). In this section we explore where these approaches can
 708 provide insight into the dynamics of Earth’s monsoons. Section 4 discusses regions where
 709 zonal asymmetry limits the relevance of the aquaplanet theories.

710 3.2.1 *Insight from the momentum budget and CQE considerations*

711 For an aquaplanet, the momentum framework, combined with the assumption of
 712 CQE, indicates that:

- 713 1. Convergence associated with a cross-equatorial ‘monsoon’ meridional overturn-
 714 ing circulation lies just equatorward of the peak in subcloud MSE or θ_{eb} (Emanuel,
 715 1995; Privé & Plumb, 2007a, 2007b).
- 716 2. Meridional overturning cells associated with monsoons approach conservation of
 717 angular momentum more than cells associated with ITCZs, and consequently are
 718 more strongly coupled to meridional MSE gradients (Schneider & Bordoni, 2008).
- 719 3. Rapid transitions can occur between an ITCZ regime with two eddy-driven Hadley
 720 cells and an angular momentum conserving monsoon regime with one dominant
 721 cell that extends into the summer hemisphere (cf. Figs. 8a and 8b). These tran-
 722 sitions are mediated by feedbacks relating to advection of MSE in the lower branch
 723 of the Hadley circulation, and suppression of eddies by upper-level easterlies (Bor-
 724 doni & Schneider, 2008, 2010; Schneider & Bordoni, 2008).
- 725 4. At Earth’s rotation rate, the transition from the eddy-driven to angular momen-
 726 tum conserving Hadley cell regime appears to occur at $\sim 7^\circ$ latitude on an aqua-
 727 planet with zonally symmetric boundary conditions (Geen et al., 2019).
- 728 5. At Earth’s rotation rate, convergence zones within the ascending branches of mon-
 729 soons appear to be unable to migrate farther than $\sim 25^\circ$ from the Equator (Faulk
 730 et al., 2017; Hill et al., 2019; Singh, 2019).

731 The above ideas were developed in a very idealized framework, but some consistent be-
 732 havior has been observed on Earth. Nie, Boos, and Kuang (2010) investigated whether
 733 the CQE assumption was relevant locally in the regional monsoons. By analysing ERA-
 734 40 and Tropical Rainfall Measuring Mission (TRMM) data, they demonstrated that, in
 735 the South Asian, Australian, and African monsoons, maxima of θ_{eb} and free-troposphere
 736 saturation equivalent potential temperature, θ_e^* , are approximately colocated, and peak
 737 precipitation indeed lies just equatorward of the peak in subcloud MSE, consistent with
 738 CQE (Fig. 12). The picture in Northern Africa is slightly complicated by remote upper-
 739 tropospheric forcing due to the Rossby wave induced by the South Asian summer mon-
 740 soon, but the ridge of θ_e^* nonetheless reflects the structure of θ_{eb} over the Sahel (Fig. 12b).
 741 In South Asia gradients of θ_{eb} are tightly set by topography and the maximum in upper-
 742 level temperature is not centered over the Tibetan Plateau (Fig. 12a). These findings
 743 led to re-interpretation of the role of topography in driving a strong monsoon in the re-
 744 gion, with the elevated topography now recognized as a mechanical barrier to cold, dry
 745 air from the north that generates a strong θ_{eb} maximum, rather than influencing the mon-
 746 soon primarily via elevated heating (Boos & Kuang, 2010, 2013).

747 CQE does not hold well in the Americas or East Asia. Over North America, maxi-
 748 ma of θ_e^* and θ_{eb} occur at different latitudes; the reason for this is not clear but may re-
 749 late to advective drying of the lower troposphere. In South America the θ_{eb} distribution
 750 has a broad maximum extending from the Equator to 20° S, while θ_e^* has a more local-
 751 ized peak at 20° S. In East Asia, a tropical peak of precipitation is found just equator-
 752 ward of the peak in θ_{eb} , but the maximum of θ_e^* occurs farther north, just south of the
 753 precipitation associated with the Meiyu-Baiu front. The Atlantic ITCZ and the Pacific
 754 ITCZ (sufficiently west of North America) both approximately follow CQE in boreal sum-
 755 mer (Figs. 12b & c), but in boreal winter the maxima of precipitation and θ_{eb} remain
 756 in the Northern Hemisphere, while the maxima of θ_e^* shift equatorward (Figs. 12e & f).
 757 Further discussion of these regions is given in Section 4.1.3. It is also worth noting that
 758 while CQE does not hold in all locations, tropical precipitation is generally located close
 759 to or just equatorward of the maximum θ_{eb} throughout the year (see Fig. 12). θ_{eb} ap-
 760 pears a useful indicator of where precipitation will fall, even where this does not take the
 761 form of intense, deep convection in a monsoonal overturning circulation. Over ocean this
 762 is unsurprising, as θ_{eb} is strongly coupled to the SST. However, that this holds over land
 763 reinforces the emerging view of monsoon precipitation being governed by MSE, rather
 764 than surface temperature.

765 Also consistent with the idealized modeling work, seasonal changes in the charac-
 766 ter of the overturning circulation have been observed in the regional monsoons. The Hadley
 767 circulation over the South Asian monsoon region in particular has been highlighted as
 768 showing rapid transitions between an eddy-driven and an angular momentum conserv-
 769 ing Hadley circulation that are similar to those seen in aquaplanet simulations. In this
 770 region, precipitation migrates rapidly off the Equator to $\sim 25^\circ$ and the summertime cir-
 771 culation is nearly angular momentum conserving (Bordoni & Schneider, 2008; Geen et
 772 al., 2018; J. M. Walker & Bordoni, 2016). To give an indication of other regions where
 773 angular momentum conservation may apply, Fig. 13 shows the local overturning circula-
 774 tion, defined using the divergent component of the meridional wind (e.g., Schwendike
 775 et al., 2014; G. Zhang & Wang, 2013) for each of the monsoon regions marked in Fig.
 776 1. Angular momentum contours are plotted in gray. The upper-level summertime over-
 777 turning circulation becomes roughly aligned with angular momentum contours in the deep
 778 tropics in the South Asian, West and Southern African monsoon regions. In contrast,
 779 the overturning circulations over Australia and the Americas are not angular momen-
 780 tum conserving, even very close to the Equator. The case of Australia highlights that
 781 regions where CQE applies may not reflect those where the circulation conserves angu-
 782 lar momentum.

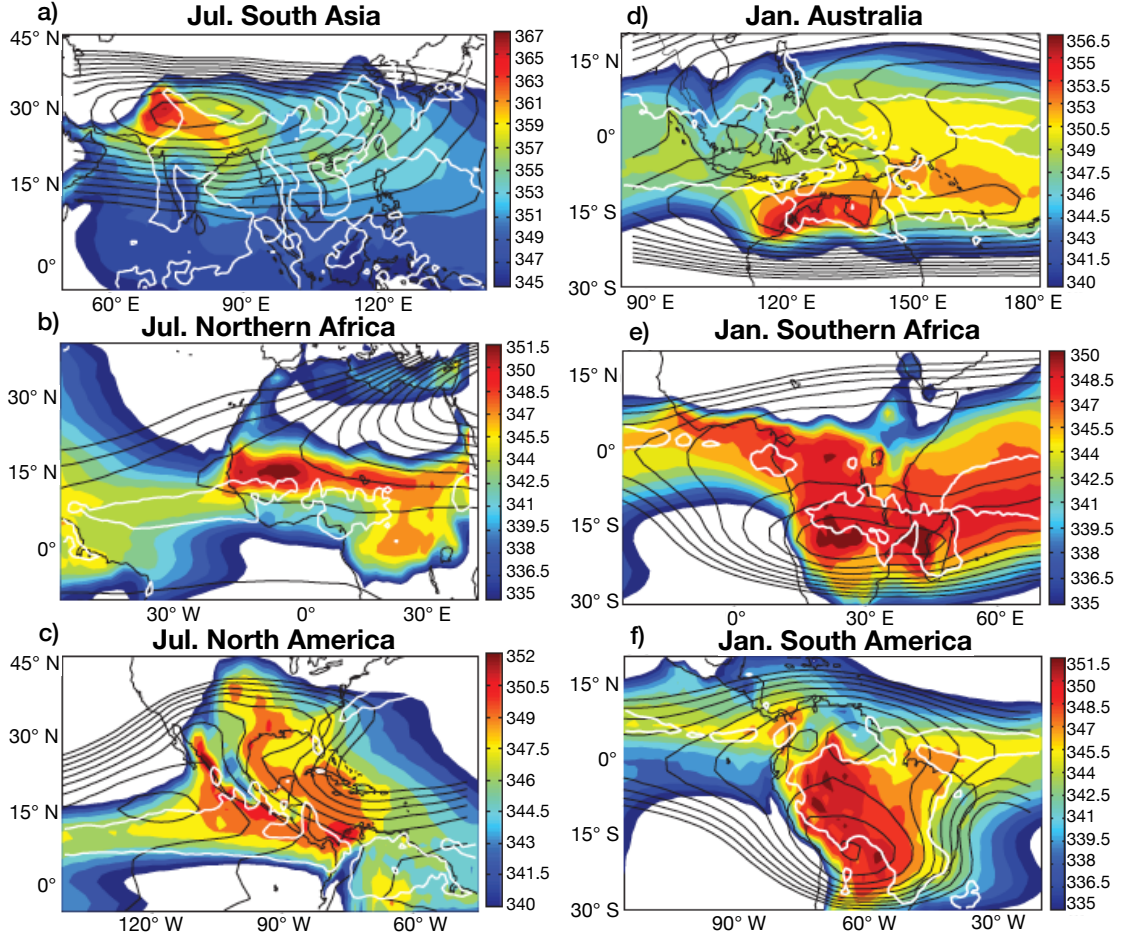


Figure 12. Evaluation of CQE for the (a) South Asia, (b) northern Africa, (c) North America, (d) Australia, (e) southern Africa and (f) South America monsoons. Colors show subcloud equivalent potential temperature, θ_{eb} . The black contour is the free-troposphere saturation equivalent potential temperature, θ_e^* , averaged from 200 to 400 hPa. The white contour indicates the region that has precipitation greater than 6 mm day^{-1} . The θ_e^* contours start from (a) 345 K, (b) 340 K, (c) 340 K, (d-f) 341 K and the respective interval is (a) 1 K, (b) 1 K, and (c-f) 0.5 K. Adapted from Nie et al. (2010). ©American Meteorological Society. Used with permission.

783 Findings from aquaplanets show consistency with climatological behavior of some
 784 regional monsoons, although it is clear that there is still more to be learned. Awareness
 785 of the relevance of the lower-level MSE and upper-level wind structures to the meridional
 786 overturning circulation may additionally help in understanding present day variability
 787 of the monsoons and model projections of future climate. For example, Hurley
 788 and Boos (2013) used reanalysis and observational datasets to explore whether variability
 789 in monsoon precipitation could be connected to variability in θ_{eb} , as expected theoretically
 790 in a monsoon circulation. Even removing the signal of variability linked to ENSO,
 791 they found that positive precipitation anomalies in the American, African, South Asian
 792 and Australian monsoons were associated with enhanced θ_{eb} , consistent with previous
 793 findings over West Africa (Eltahir & Gong, 1996). In addition, variability in θ_{eb} was found
 794 to be due primarily to variability in moisture rather than in temperature, with strong
 795 monsoon years associated with enhanced specific humidity near the climatological θ_{eb}
 796 maximum, with temperature anomalies of the opposite sign (see also J. M. Walker, Bor-

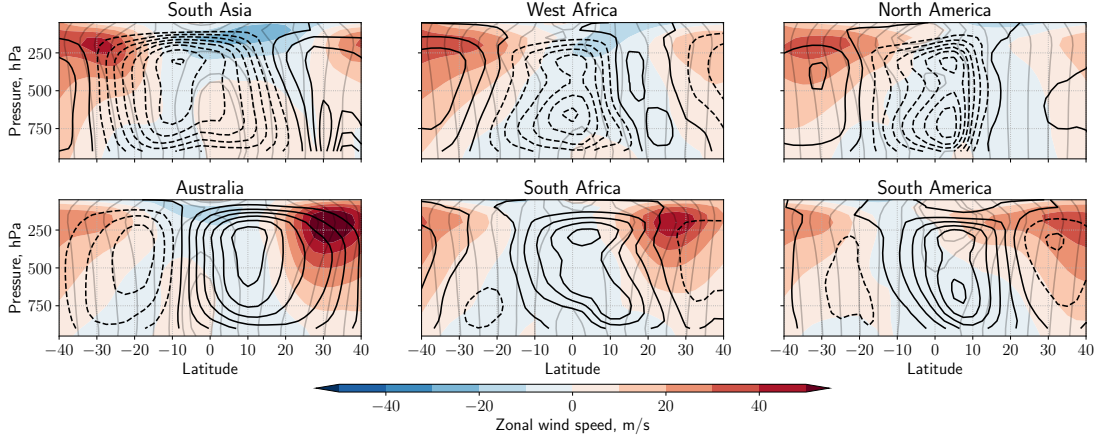


Figure 13. Black contours show local summer (June-September or December-March) meridional overturning circulations for: South Asia (70-100°E), West Africa (10°W-30°E), North America (85-115°W), Australia (115-155°E), South Africa (10-50°E), South America (40-70°W). This is computed by vertically integrating the divergent component of the meridional wind, averaged in longitude, from the top of the atmosphere to the surface (cf. Schwendike et al., 2014; G. Zhang & Wang, 2013). Shading shows zonal wind. Light gray contours indicate absolute angular momentum per unit mass, with contours at $\Omega a^2 \cos^2 \phi_i$ ($\phi_i = 0^\circ, \pm 5^\circ \pm 10^\circ, \dots$).

797 doni, & Schneider, 2015). This clearly contradicts the classical sea-breeze view of the mon-
 798 soons, but is consistent with the CQE perspective. Shaw and Voigt (2015) showed that
 799 the CQE perspective can help to explain the weak response of the Asian monsoons to
 800 global warming seen in climate model projections. Using data from the Atmospheric Model
 801 Intercomparison Project (AMIP) experiments, they compared the circulation response
 802 to a quadrupling of CO₂ with fixed SSTs (AMIP4xCO₂) with the response to a uniform
 803 4K increase in SST (expected due to a 4x increase in CO₂), but with no CO₂ increase
 804 (AMIP4K). They found that the CO₂ forcing led to θ_{eb} changes that supported a more
 805 intense monsoon, but the SST forcing led to opposite θ_{eb} changes which, they argued,
 806 led to a weak net response to an increase in CO₂.

807 The tight, albeit diagnostic, relationship between lower-level MSE and precipita-
 808 tion (Fig. 12) makes assessment of the influence of forcings or teleconnections on the MSE
 809 budget (e.g., via advection, enhanced evaporation etc.) an intuitive focus for research
 810 into monsoon variability and future change. The connection to the upper-level momen-
 811 tum budget and Hadley cell regimes has not yet been so comprehensively investigated.
 812 However, it has been observed that anomalous upper-level easterlies and westerlies are
 813 associated with anomalous upper-level divergence and convergence in monsoon regions
 814 in a sense that is consistent with the aquaplanet regimes. For example, on intraseasonal
 815 and interannual timescales over South Asia and West Africa, anomalously wet conditions
 816 are associated with easterly upper-level zonal wind anomalies, westerly lower-level zonal
 817 wind anomalies, and expansion and strengthening of the meridional overturning, with
 818 the opposite applying in dry phases (Goswami & Ajaya Mohan, 2001; Sultan & Janicot,
 819 2003; J. M. Walker et al., 2015). However, these circulations are zonally confined, and
 820 terms in the momentum budget that are trivially zero in an aquaplanet might play a more
 821 dominant role. More work is needed to understand the leading order momentum bud-
 822 get in the different monsoon regions and if and to what extent conservation of angular
 823 momentum is approached even at the regional scale.

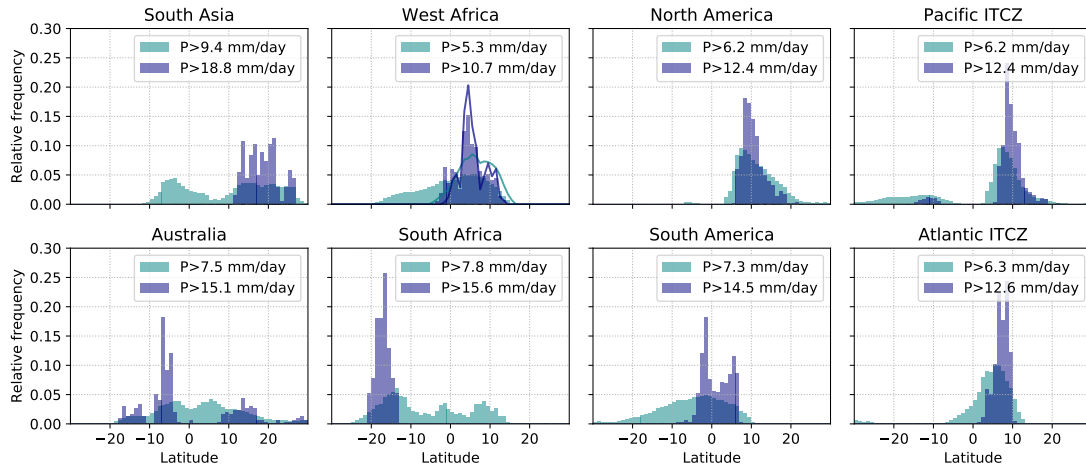


Figure 14. Relative frequency distributions of latitudes where the strongest precipitation falls in the regional monsoons and ITCZs. Monsoon regions are defined as in Fig. 1, and ITCZs as in Fig. 4.1.3. For West Africa, lines show the distribution for -10 to 10°E . Data are from a linearly detrended pentad-mean climatology of GPCP precipitation data spanning 1997–2014.

824 The recent findings summarized in points (4) and (5) above suggest that planetary
 825 rotation constrains the latitude at which the overturning circulation tends to transition
 826 from an eddy-driven to an angular momentum conserving regime, and the maximum lat-
 827 itude that the convergence zone can reach. The implications for Earth’s tropical circu-
 828 lations remain to be explored. However, one could imagine that these latitudinal bounds
 829 might provide information on what circulation regime we expect to be associated with
 830 ascending air and precipitation at a given latitude. Fig. 14 shows the relative frequency
 831 distribution of precipitation that exceeds some threshold (see legends) in each monsoon
 832 region and ITCZ.⁸ In the South Asian, Australian and Southern African monsoon re-
 833 gions, the distribution suggests multiple preferred locations for strong precipitation to
 834 fall. Over South Asia and South Africa, the strongest precipitation (dark blue) is located
 835 in monsoon convergence zones, poleward of 10° . Over the Australian sector, intense pre-
 836 cipitation appears to occur most often nearer the Equator, though smaller peaks are found
 837 poleward of 10° in both hemispheres. In the Northern Hemisphere a small peak is also
 838 seen poleward of 25° ; these peaks reflect rainfall in the Western North Pacific and East
 839 Asian monsoons. Looking at the West Africa region as defined in Fig. 1 (-10 – 30°E), a
 840 broad peak is seen. Limiting the region to -10 – 10°E (as studied by e.g., Sultan & Jan-
 841 icot, 2003) two peaks emerge: a larger peak at $\sim 5^{\circ}$ and a second peak at $\sim 10^{\circ}$. In
 842 the other monsoon regions and ITCZs a single peak is seen, suggesting no change in pre-
 843 cipitation regime over the year.⁹

844 Fig. 15 shows the mass flux associated with meridional and zonal overturning cir-
 845 culations for May to September and November to March (cf. Schwendike et al., 2014).

⁸ Specifically the procedure followed is as follows: (1) Weight precipitation to account for decrease in grid box size with latitude. (2) Find the maximum value of (weighted) precipitation within the region. (3) Calculate thresholds as $1/3$ and $2/3$ of this maximum, this allows for different rainfall intensities between regions. (4) For each threshold, count gridboxes in the region (over longitude and time) where the threshold is exceeded and sum the counts zonally to give a frequency distribution. (5) Normalize the total counts at each location by the domain total counts to obtain the relative frequency.

⁹ The distributions over South America and the Pacific ITCZ show some hint of secondary peaks, likely from the Atlantic ITCZ and South Pacific Convergence Zone respectively (cf. Fig. 1).

846 Gray shading indicates the region between 10-25° from the Equator. Consistent with the
 847 findings of Faulk et al. (2017) for the aquaplanet circulation, the upward mass fluxes as-
 848 sociated with the Hadley cell are confined to within 25° of the Equator. One might fur-
 849 ther speculate that circulations for which the upward mass flux and intense rain are con-
 850 centrated between 10-25° from the Equator (Asia, Southern Africa) might bear similar-
 851 ities to the aquaplanet angular momentum conserving regime, while those where ascent
 852 and precipitation largely remain equatorward of 10° (Australia and South America) might
 853 behave more like the aquaplanet eddy-driven regime. Figs. 13 and 15 suggest this idea
 854 shows promise, with, for example, the summer overturning circulation over Australia re-
 855 maining in an eddy-driven regime, while the circulation over areas such as South Asia
 856 and Southern Africa becomes more aligned with angular momentum contours. These cat-
 857 egorisations of the various flow regimes associated with tropical rainfall could be of use
 858 in interpreting the responses of different regions to external forcings. We note that while
 859 Fig. 14 supports the idea of multiple preferred precipitation regimes at a given longi-
 860 tude, both Figs. 14 and 15 indicate that the critical latitude for delineating the ITCZ
 861 and monsoon regimes is ~12-15° rather than the ~7° threshold found in aquaplanets.
 862 It remains to be explored if and how asymmetric boundary conditions and/or other pro-
 863 cesses and feedbacks that are absent in the aquaplanets might give rise to quantitative
 864 differences in regional critical latitudes.

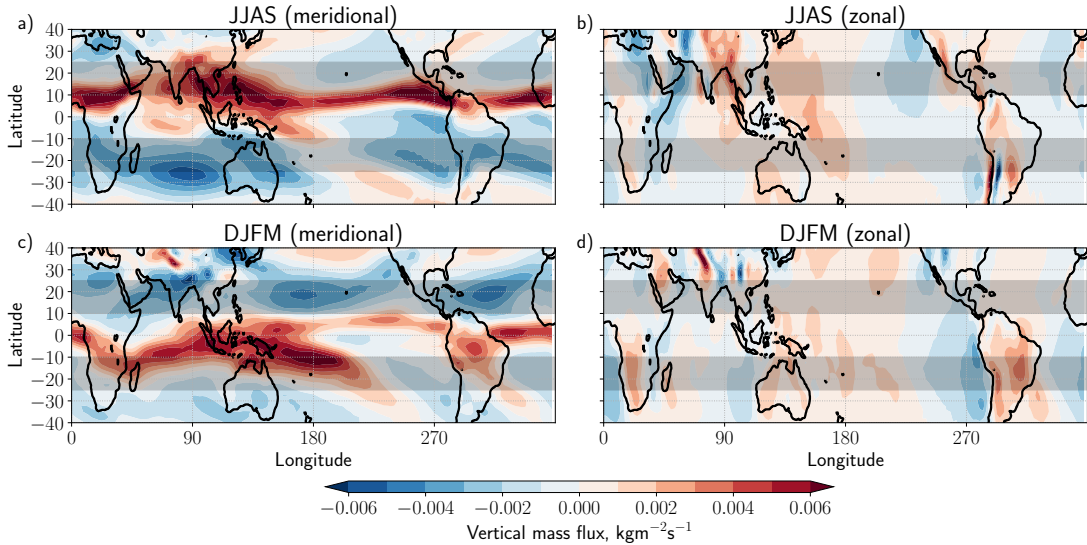


Figure 15. Vertical mass flux at 500 hPa, calculated from JRA-55, associated with (a) the di-
 vergent meridional circulation and (b) the divergent zonal circulation (cf. Schwendike et al., 2014)
 in boreal summer, defined as in Fig. 13. (c) and (d) are as (a) and (b) but for austral summer.
 Gray shading highlights the regions between 10 and 25°N/S, see discussion in text.

865 While the aquaplanet results provide a common framework for interpreting regional
 866 monsoons and their variability, some caveats must be remembered. The regional mon-
 867 soons are local systems with overturning associated with both meridional and zonal flows
 868 (e.g., Fig. 15). Simple symmetric theories do not necessarily extend straightforwardly
 869 to these cases, with stationary waves modifying the momentum and energy budgets (Shaw,
 870 2014). Also, in addition to the deep, moist convective overturning circulation, the West
 871 and Southern African and Australian monsoons feature a shallow, dry circulation whose
 872 ascent is collocated with the peak in potential temperature (e.g., Hagos & Cook, 2007;
 873 Nie et al., 2010; Trenberth et al., 2000; C. Zhang et al., 2008); advective drying by this
 874 shallow circulation appears to suppress monsoon precipitation (Shekhar & Boos, 2017;

Zhai & Boos, 2017). Shekhar and Boos (2016) used idealized model simulations to explore whether the CQE and energetic perspectives could still characterize the ITCZ latitude in the presence of a shallow circulation. In such cases the ITCZ was no longer well characterized by the maximum subcloud MSE, but the maximum of a weighted average of lower tropospheric MSE, from 20 hPa above the surface to 500 hPa, was more consistently located close to the ITCZ. They suggest this weighted average accounts for the entrainment of low-MSE air into deep convective updrafts.

3.2.2 Applications of the EFE framework

As reviewed in Section 2.2., the vertically integrated atmospheric energy budget provides a complementary approach to understanding constraints on tropical rainfall. An elegant finding from applying this in aquaplanets is that the convergence zone approximately follows the EFE, so that changes in zonal mean convergence zone latitude can be linked to changes in net forcing not only in the tropics, but also at higher latitudes (see Section 2.2 and e.g., Bischoff & Schneider, 2014; Kang et al., 2008). Additionally, the MSE budget allows for a more mechanistic understanding of the local response to such changes. Recent reviews have discussed the energetic perspective of the convergence zone (Kang, 2020; Kang et al., 2018; Schneider et al., 2014) and its application to Earth’s monsoons (Biasutti et al., 2018), and so only a brief discussion is given here.

The latitude of the zonally averaged convergence zone is strongly anticorrelated with the zonally averaged meridional atmospheric energy transport at the Equator, and correlated with the EFE latitude. This relation holds in both observations and under a range of modeled forcing scenarios (although it breaks down where the convergence zone shifts far from the Equator over the seasonal cycle; Adam et al., 2016b; Bischoff & Schneider, 2014; Donohoe et al., 2013). This relationship helps to explain why the $\overline{\text{ITCZ}}$ is north of the Equator (Marshall et al., 2014).

Extending this framework to local cases has proved more challenging. Boos and Korty (2016) used the longitudes where the zonally divergent column integrated MSE flux vanishes, and has positive zonal gradient, to define ‘Energy Flux Prime Meridians’ (EFPMs). Two EFPMs can be identified in each season: over the Bay of Bengal and Gulf of Mexico/Caribbean Sea in boreal summer, and over the Western Pacific and South America in austral summer. They showed that this extended theory gives some basic insight into how localized shifts in precipitation with ENSO relate to anomalous energy transports. Adam, Bischoff, and Schneider (2016a) defined the zonally varying EFE as the latitude at which the meridionally divergent column integrated MSE flux vanishes and has positive meridional gradient. This was found to approximate the seasonal cycle of convergence zone migrations over Africa, Asia and the Atlantic. However, the influence of the Walker cell limited the local EFE’s usefulness over the Pacific, and the EFE deviates from the convergence zone in the solstitial seasons that are particularly relevant to the monsoons.

As with the momentum budget framework, while the EFE framework is valuable in explaining some features of the overturning circulation, limitations must be remembered. Relating changes in the latitude of the convergence zone to that of the zonally averaged EFE assumes that the response to forcing is via changes to the meridional overturning circulation, and neglects changes to the GMS. Such changes have been shown to be non-negligible both over the seasonal cycle and in the response to orbital and greenhouse gas forcings (Merlis et al., 2013; Seo, Kang, & Merlis, 2017; Smyth, Hill, & Ming, 2018; Wei & Bordoni, 2018). In addition, Biasutti et al. (2018) noted that while the EFE predicts changes to the convergence zone latitude once the net energy imbalance is known, changes in ocean energy transport, and feedbacks internal to the atmosphere, can result in a net imbalance different to that expected from an imposed external forcing, including orbital forcing (Liu et al., 2017). More generally, even when the energy budget frame-

926 work correctly places the location of the zonal mean convergence zone, the latter can rep-
 927 resent an average over zonally asymmetric contributions that are much greater than the
 928 zonal average (Atwood et al., 2020).

929 **3.2.3 Reconciling the momentum budget/CQE and EFE perspectives**

930 The two perspectives discussed so far in this review have emerged via separate con-
 931 sideration of the momentum and energy budgets, and a unified theory for monsoon cir-
 932 culations remains an outstanding challenge (e.g., Biasutti et al., 2018; Hill, 2019). Com-
 933 mon to both pictures is consideration of processes that can alter the distribution of MSE
 934 either in the boundary layer or in a vertically integrated sense, and this might provide
 935 a bridge to fill the gaps between these two frameworks.

936 The local, vertically integrated MSE budget has long been used to diagnose the dis-
 937 tribution of tropical precipitation. Chou and Neelin (2001) and Chou and Neelin (2003)
 938 analysed the column integrated MSE budget in the South American and North Amer-
 939 ican, Asian and African monsoon regions respectively. They identified three key processes
 940 governing the MSE distribution and thus determining the extent of tropical rainfall over
 941 land: advection of high or low MSE air into the region, soil-moisture feedbacks, and the
 942 interaction between the convergence zone and the Rossby wave induced subsidence, which
 943 occurs to the west of monsoon heating (the interactive Rodwell-Hoskins mechanism; see
 944 Rodwell and Hoskins (2001)). The column integrated MSE budget has also allowed in-
 945 vestigation of the mechanisms determining the differing responses of models to intuitively
 946 similar forcing scenarios (e.g. D’Agostino, Bader, Bordoni, Ferreira, & Jungclaus, 2019),
 947 and the different responses of model variants to the same forcing (e.g Hill, Ming, Held,
 948 & Zhao, 2017; Hill, Ming, & Zhao, 2018).

949 Provided CQE holds, so that the tropical atmosphere is near a moist neutral state,
 950 the horizontal distribution of column integrated moist static energy will be strongly tied
 951 to the distribution of subcloud moist static energy. This may allow connections to be
 952 made between the constraints arising from the momentum and energetic frameworks, at
 953 least in the zonal mean. Precipitation appears to track subcloud MSE throughout the
 954 year whether CQE holds or not, and there is likely more to explore about how the bound-
 955 ary layer dynamics and large-scale overturning circulation interact (e.g., Adames & Wal-
 956 lace, 2017; Biasutti & Voigt, 2020; Chiang, Zebiak, & Cane, 2001; Duffy, O’Gorman, &
 957 Back, 2020).

958 **4 Beyond the aquaplanet perspective**

959 The theories that have emerged from the aquaplanet perspective have begun to prove
 960 useful in interpreting the climatology and variability of the tropical monsoon systems
 961 on both regional and global scales, particularly where their dynamics show similarities
 962 to that of the convergence zone in an aquaplanet. Synthesising idealized modeling work
 963 with observational and realistic modeling studies suggests a picture that is consistent with
 964 a view of the monsoons and ITCZs as local migrations of the tropical convergence zone:

- 965 1. In the zonal mean, the latitude of the convergence zone is set by energetic con-
 966 straints (Fig. 10).
- 967 2. Locally and seasonally, the convergence zone location appears governed by the MSE
 968 distribution, which can be understood via the regional MSE budget (Fig. 12).
- 969 3. When the convergence zone is near the Equator (i.e., is an ITCZ), the overturn-
 970 ing circulation is strongly influenced by extratropical eddies (Fig. 8a). Once it is
 971 far from the Equator, the cross-equatorial (winter) Hadley cell may approach an
 972 angular momentum conserving monsoon regime (Figs. 8b & 13).

- 973 4. Some regional variability in monsoon precipitation on interannual timescales (and
 974 perhaps subseasonal timescales) appears related to local variations in MSE which,
 975 where CQE applies, is connected to variations in the Hadley circulation.
 976 5. Global variability in the latitude of the zonal mean convergence zone on interdecadal
 977 and longer timescales is driven by variations in the hemispheric energy budgets,
 978 with consequences for regional monsoon rainfall.

979 However, there are important influences on the regional monsoons and ITCZs that
 980 are not well accounted for by the above, in particular, the role of the continental con-
 981 figuration and geometry; these are discussed in Section 4.1. The interplay of the two con-
 982 vergence zone regimes with the transients that comprise the climatological precipitation
 983 are discussed in Section 4.2.

984 4.1 Asymmetries in the boundary conditions

985 Zonal asymmetries, such as land-sea contrast, orography, and the ocean circula-
 986 tion, introduce complications unaccounted for by the simple aquaplanet framework. Re-
 987 gional convergence that cannot be captured by the symmetric picture includes the Meiyu-
 988 Baiu frontal zone, the South Pacific Convergence Zone (SPCZ), the South Atlantic Con-
 989 vergence Zone (SACZ), and the South Indian Convergence Zone, which extends off the
 990 southeast coast of Southern Africa (Cook, 2000; Kodama, 1992). In particular, the East
 991 Asian and South American ‘monsoons’ require us to step beyond the perspective of an-
 992 gular momentum conserving monsoons and eddy-driven ITCZs. In addition, the season-
 993 ality of the Atlantic and Pacific ITCZs is strongly influenced by localized atmosphere-
 994 ocean feedbacks.

995 4.1.1 East Asia - a frontal monsoon

996 While the South Asian monsoon fits well with the theoretical paradigm emerging
 997 from idealized work, the circulation over East Asia behaves very differently. Here, wind
 998 reversal is predominantly meridional, and monsoon precipitation extends north into the
 999 subtropics (zone B in Fig. 11). Summer precipitation is concentrated in a zonal band
 1000 at $\sim 35^\circ$ known as the Meiyu-Baiu front, which forms north of the high MSE air mass
 1001 centered over South Asia and the Bay of Bengal (Ding & Chan, 2005, and references therein).
 1002 This front migrates northward in steps over the summer season, as detailed in Section
 1003 3.1.

1004 Unlike in tropical monsoon regions, in the Meiyu-Baiu region the net energy in-
 1005 put into the atmospheric column is negative. Vertical upward motion and convection in
 1006 the front (with associated energy export) require MSE convergence, which is provided
 1007 by horizontal advection, with interactions between the Tibetan Plateau and the west-
 1008 erly jet playing a key role (Chen & Bordoni, 2014; Chiang, Kong, Wu, & Battisti, 2020;
 1009 Molnar, Boos, & Battisti, 2010; Sampe & Xie, 2010). Comparing the monsoon season
 1010 precipitation in this region in numerical experiments with and without the Tibetan Plateau
 1011 indicates that, when the plateau is removed, precipitation is weakened and is no longer
 1012 focused into the front (Chen & Bordoni, 2014; Chiang et al., 2020). Analysis of the MSE
 1013 budget of these simulations suggests that the Plateau chiefly reinforces convergence into
 1014 the Meiyu-Baiu region by strengthening the southerly stationary wave downstream. The
 1015 westerly jet off the eastern flank of the Plateau additionally appears to act as an anchor
 1016 for transient precipitating weather systems, focusing precipitation along the front (Mol-
 1017 nar et al., 2010; Sampe & Xie, 2010).

1018 Over the summer season, the East Asian Summer monsoon features two abrupt north-
 1019 ward jumps of the precipitation, with three stationary periods (Ding & Chan, 2005). This
 1020 intraseasonal evolution of the monsoon has also been suggested to relate to interactions
 1021 between the Plateau and westerly jet, with the migration of westerlies from the south

1022 of the Plateau to the north causing the first abrupt jump and the development of the
 1023 Meiyu-Baiu front, and the northward migration of westerlies away from the Plateau caus-
 1024 ing the second (Kong & Chiang, 2020; Molnar et al., 2010). A series of recent papers has
 1025 examined implications of this interaction for interpretation of changes to the East Asian
 1026 summer monsoon over the paleoclimate record (Chiang et al., 2015) and the Holocene
 1027 (Kong, Swenson, & Chiang, 2017), and for interannual variability of the East Asian sum-
 1028 mer monsoon (Chiang, Swenson, & Kong, 2017), with the hypothesis appearing able to
 1029 explain all cases.

1030 *4.1.2 South America - a zonal monsoon*

1031 Similarities have been noted between the South American and East Asian mon-
 1032 soons; however, studies indicate that diabatic heating over land is most important in gen-
 1033 erating the upper-level monsoon anticyclone over South America (Lenters & Cook, 1997).
 1034 One important difference is that the Andes form a narrow, meridionally oriented bar-
 1035 rier from the tropics to subtropics. This acts to divert the easterly flow from the Atlantic
 1036 to the south, concentrating it into the South American Low-Level Jet (Byerle & Pae-
 1037 gle, 2002; Campetella & Vera, 2002) and inducing adiabatic ascent (Rodwell & Hoskins,
 1038 2001). In austral summer, the result is a zonally convergent mass flux of similar mag-
 1039 nitude to the meridionally convergent component (Fig. 15), which extends the summer
 1040 precipitation southward.

1041 *4.1.3 The Atlantic and Pacific ITCZs and the North American mon-* 1042 *soon*

1043 Except for in the far western tropical Atlantic where the ITCZ dips slightly south
 1044 of the Equator in March and April, the ITCZ is north of the Equator year-round in the
 1045 Atlantic and Pacific (Fig. 9). One important factor for the off-equatorial location of the
 1046 Atlantic ITCZ appears to be the land monsoon heating and the geometrical asymme-
 1047 try in tropical Africa (Rodwell & Hoskins, 2001). Specifically, the austral summer mon-
 1048 soon in southern Africa forces subsidence to the west and causes a subtropical high to
 1049 build over the southern subtropical Atlantic, increasing the southeasterly trade winds
 1050 which act to cool the ocean by enhanced turbulent energy fluxes. Together, the subsi-
 1051 dence and cool water suppress convection south of the Equator in the austral summer
 1052 and fall. In addition, in boreal summer the west African monsoon forces a strong local
 1053 Hadley circulation that also causes subsidence in the sub-tropical south Atlantic that
 1054 supports the formation of stratus clouds which further cool the ocean during austral win-
 1055 ter. Hence, the ITCZ does not transit into the Southern Hemisphere in austral summer.

1056 The ITCZ in the eastern half of the Pacific is also north of the Equator year-round,
 1057 and there is subsidence and cooling in the south-east subtropics. Modeling studies in-
 1058 dicate that this descent can be attributed to several factors. SSTs over the western coast
 1059 of South America are cooler due to coastal upwelling (e.g., Takahashi, 2005), but this
 1060 cooling is largely confined to within 100km of the coast. In response to summer heat-
 1061 ing over the Amazon (Rodwell & Hoskins, 2001), air descends adiabatically over the south-
 1062 east Pacific and flows equatorward. Simulations with and without the Andes suggest orog-
 1063 raphy plays a dominant role. Throughout the year, the extratropical mid-level wester-
 1064 lies incident on the Andes are diverted equatorward, contributing to descent and evap-
 1065 orative cooling of the ocean by the dry subsiding air (e.g., Fig. 9; Rodwell & Hoskins,
 1066 2001; Takahashi & Battisti, 2007). The large-scale descent forced by the Andes causes
 1067 an inversion to form that allows for the development of large-scale stratus clouds that
 1068 cool the ocean for thousands of kilometers offshore (to the Date Line) and suppress con-
 1069 vection over the eastern Pacific, particularly in austral summer. Combined with the atmosphere-
 1070 ocean feedbacks described in the next paragraph, this descent causes the Pacific ITCZ
 1071 to be located exceptionally far north of the Equator throughout the year (Maroon, Frier-

son, & Battisti, 2015; Takahashi & Battisti, 2007).¹⁰ The forcing by the Andes also causes a convergence zone to form that is located and oriented in a fashion similar to the observed SPCZ (Takahashi & Battisti, 2007). It may also partially account for the large seasonal contrast in precipitation in the North American monsoon, which involves an eastward extension of the Pacific ITCZ (Figs. 1 and 15). We note that three other hypotheses have been proposed for why the Pacific ITCZ is north of the Equator all year round (Chang & Philander, 1994; B. Wang & Wang, 1999; Xie & Philander, 1994). However, model experiments that serve as tests of these hypotheses (e.g., Battisti et al., 2014; Philander et al., 1996; Shi, Lohmann, Sidorenko, & Yang, 2020) do not support them. In contrast, the studies that we are aware of that include the Andes in atmospheric GCMs coupled to either a slab or dynamic ocean all produce a single ITCZ in the Northern Hemisphere that is in a very similar position and orientation to the observed ITCZ in the Pacific, and does not transit into the Southern Hemisphere at any time during the calendar year, consistent with observations.

Atmosphere-ocean feedbacks are important for the seasonal cycle in the latitude of the Atlantic and Pacific ITCZs. For example, with the onset of summer in the Northern Hemisphere, water in the Northern Hemisphere subtropics is warmed by increasing insolation (moving the ITCZ northward) which in turn warms the air in the boundary layer above and causes the sea level pressure (SLP) to drop (a hydrostatic response; see Lindzen & Nigam, 1987). The drop in SLP to the north of the Equator increases the cross-equatorial SLP gradient and thus increases the speed of the southeasterly trade winds south of (and along) the Equator, causing more air to converge into the ITCZ. South of the Equator, the strengthened trade winds increase evaporation and thus cools the ocean and the air in the boundary layer above. As a consequence, the meridional pressure gradient is further strengthened, the southerlies flowing across the Equator into the ITCZ are enhanced and the ITCZ is intensified and moves farther north. This positive feedback is known as the wind-evaporation feedback (Chang & Philander, 1994; Xie & Philander, 1994). Although ocean dynamics is not essential to explain the annual cycle in the latitude of the ITCZ (it is reproduced in slab ocean models coupled to atmospheric GCMs), it also plays a role (Mitchell & Wallace, 1992; B. Wang & Wang, 1999).

4.2 The role of transients

Even in an aquaplanet, tropical rainfall does not occur in a zonally uniform, continuously raining band. For simplicity, theoretical studies like those discussed in Section 2 tend to consider time and zonal averages and neglect transient activity except for its contribution to the momentum and energy budgets via eddy fluxes from the extratropics. While the climatological monsoons and ITCZs result from large-scale dynamics acting over a season and longer, the phenomena responsible for the accompanying precipitation are transient and generally of smaller spatial and temporal scales.

Many types of transient activity occur in the tropics. Wheeler and Kiladis (1999) produced wavenumber-frequency spectra of tropical outgoing longwave radiation (OLR), which is used as a proxy for deep convection, and showed that the spectral peaks that emerge are similar to wave modes of the shallow water equations on the beta plane (Matsuno, 1966), providing clear evidence for a strong influence of convectively coupled waves on tropical precipitation. Fig. 16 shows a Wheeler-Kiladis wavenumber-frequency spectrum for Northern Hemisphere summer (Kiladis et al., 2006). In this season, the spectrum of the symmetric component of tropical OLR exhibits three dominant peaks: eastward propagating Kelvin waves, westward propagating waves classed as tropical depres-

¹⁰ In the annual mean, the ITCZ in the Eastern Pacific is found at $\sim 10^\circ\text{N}$, whereas the maximum precipitation in the zonal average $\overline{\text{ITCZ}}$ is at $\sim 6^\circ\text{N}$.

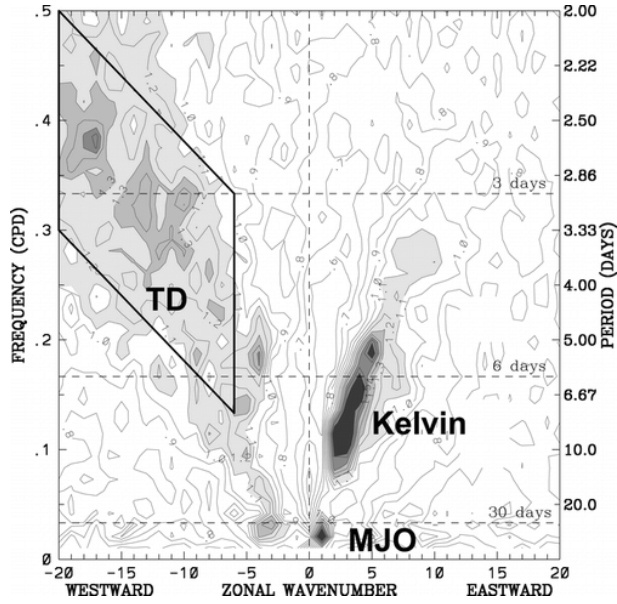


Figure 16. Wavenumber-frequency power spectrum of the symmetric component of OLR for June-August 1979-2003, averaged from 15°N to 15°S, plotted as the ratio of the raw OLR spectrum against a smooth red noise background (see Wheeler & Kiladis, 1999, for details). Contour interval is 0.1. Shading begins at 1.1, where the signal is statistically significant at approximately the 95% level. Peaks associated with the MJO, tropical depressions, and Kelvin waves are identified. From Kiladis et al. (2006). ©American Meteorological Society. Used with permission.

1119 sions, and a low frequency eastward propagating signal associated with the Madden-Julian
 1120 Oscillation (MJO).¹¹

1121 Here we focus first on the synoptic phenomena that both contribute significantly
 1122 to the seasonally averaged precipitation *and* owe their existence to the large-scale cir-
 1123 culation regime discussed in previous sections. This is followed by a discussion of slower,
 1124 larger-scale intraseasonal oscillations, such as the MJO, that interact with the monsoons
 1125 and ITCZs, but do not appear as directly governed by the large-scale background flow
 1126 as the smaller, shorter-lived transients.

1127 **4.2.1 Monsoon transients**

1128 Regional monsoon precipitation has long been observed to be organized by west-
 1129 ward propagating synoptic-scale low-pressure systems, including monsoon depressions,
 1130 observed in the Indian and Australian monsoon regions (e.g., Godbole, 1977; Mooley,
 1131 1973; D. Sikka, 1978), and African Easterly Waves, observed over West Africa (e.g., Burpee,
 1132 1974; Reed, Norquist, & Recker, 1977). Hurley and Boos (2015) produced a global cli-
 1133 matology of monsoon lows. They found that the behavior over India, the western Pa-
 1134 cific and northern Australia showed strong similarities, with a deep warm-over-cold core
 1135 (e.g., Fig. 17a). A second class of systems was seen over West Africa and western Aus-

¹¹ A more detailed discussion of equatorial waves can be found in Roundy and Frank (2004), who develop a climatology, and in a review of the subject by Kiladis, Wheeler, Haertel, Straub, and Roundy (2009).

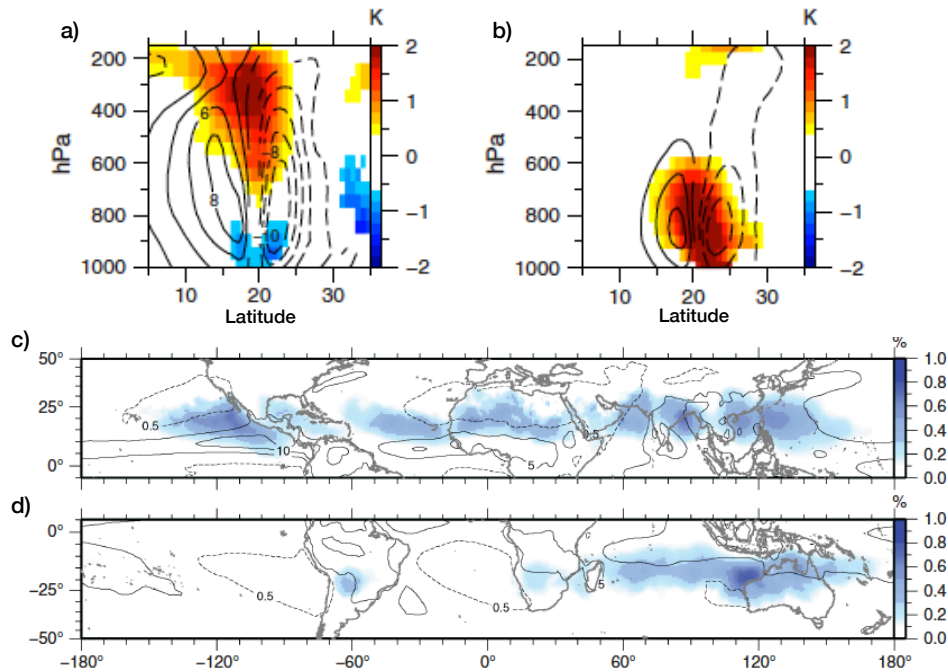


Figure 17. Northern Hemisphere summer (May-September) regional composites of monsoon depressions from ERA-Interim (1979-2012). Composite vertical sections through the storm center of potential temperature (K, shading) and zonal wind (ms^{-1} , contours) anomalies are shown for (a) India and (b) West Africa. Dashed contours are negative. Values are shaded or contoured where a t-test indicates significance at the 5% level. (c) and (d) show the fraction (shading) of total summer precipitation that can be attributed to monsoon lows and monsoon depressions in May-September and November-March respectively. Shading indicates the ratio of the summed precipitation within 500 km of all tracked lows and depressions to the total summer precipitation. Contours reflect the summer climatological precipitation rate. Dashed contours surround dry regions, where precipitation is on average less than 0.5 mm/day. Solid contours indicate wet regions, where precipitation is greater than 5mm/day (5 mm/day contour interval). Adapted from Figs. 9 and 12 of Hurley and Boos (2015). ©2014 Royal Meteorological Society. Used with permission.

1136 tralia, with a shallower warm core (e.g., Fig. 17b). They estimated that organized low-
 1137 pressure systems are responsible for at least 40% of precipitation in monsoon regions (Fig.
 1138 17c,d).

1139 While many questions about their dynamics remain open, recent work indicates
 1140 that monsoon depressions form over South Asia from moist barotropic instability due
 1141 to the meridional shear of the monsoon trough, and are intensified by latent heating (Diaz
 1142 & Boos, 2019a, 2019b). The background monsoonal flow hence is the source of instabil-
 1143 ity for these propagating disturbances and can modulate their variability. For example,
 1144 ENSO causes large-scale changes in the summertime environment that have a modest
 1145 statistical effect on the strength of synoptic scale tropical depressions that propagate from
 1146 the Bay of Bengal to the northwest over India (Hunt, Turner, Inness, Parker, & Levine,
 1147 2016), with La Niña (El Niño) conditions favoring tropical depressions with enhanced
 1148 (weakened) precipitation.

1149 Over Africa and the Atlantic, strong surface heating of the Sahara in summer forces
 1150 a monsoon circulation that is barotropically and baroclinically unstable (Burpee, 1972;
 1151 M.-L. C. Wu, Reale, Schubert, Suarez, & Thorncroft, 2012, and references therein), giving
 1152 rise to African Easterly Waves. While the precise dynamics governing the amplifi-
 1153 cation, propagation and variability of these waves remain unclear, the dynamics of these
 1154 transients is clearly a result of the background large-scale monsoonal flow. Seasons with
 1155 strong African Easterly Wave activity have been found to be associated with a strong
 1156 upper-level easterly jet (Nicholson, Barcion, Challa, & Baum, 2007) and an enhance-
 1157 ment of other equatorial waves, specifically Rossby and westward-moving mixed Rossby-
 1158 gravity wave modes (Y.-M. Cheng, Thorncroft, & Kiladis, 2019; Yang, Methven, Wool-
 1159 nough, Hodges, & Hoskins, 2018).

1160 *4.2.2 Atlantic and Pacific ITCZ transients*

1161 In the tropical Atlantic and Pacific ITCZs, precipitation is strongly modulated by
 1162 easterly waves and other organized synoptic disturbances. African Easterly Waves borne
 1163 from the monsoonal circulation over the Sahel propagate westward into the Atlantic Ocean
 1164 and are the primary precursors of tropical cyclones in the Atlantic. The associated rain-
 1165 fall contributes to the summer precipitation in the Atlantic ITCZ. Easterly waves are
 1166 also found in the tropical east and central Pacific, although the dynamics of these sys-
 1167 tems is different from their Atlantic counterparts. Many easterly waves in the Pacific are
 1168 Mixed Rossby-Gravity waves: antisymmetric equatorially trapped waves with low pres-
 1169 sure centered on 5-10° latitude (Kiladis et al., 2009; Matsuno, 1966). Friction acts to cause
 1170 convergence in the low pressure centers and in the Northern Hemisphere this leads to
 1171 moisture convergence and precipitation (Holton, Wallace, & Young, 1971; Liebmann &
 1172 Hendon, 1990) (the low pressure center in the Southern Hemisphere does not feature pre-
 1173 cipitation because the water is cold and there is strong subsidence). Other convectively
 1174 coupled equatorial waves that contribute to the ITCZ in the central Pacific include Kelvin
 1175 waves (in which convection is not symmetric about the Equator) and inertio-gravity waves
 1176 (Kiladis et al., 2009).

1177 An upper bound on the contribution by transients to ITCZ precipitation can be
 1178 estimated by assuming that all precipitation events lasting more than 24 hours are rel-
 1179 ated to organized synoptic disturbances, in which case the fraction of the total precip-
 1180 itation in the Atlantic and Pacific ITCZs that is due to large-scale organized waves is
 1181 about 40% (White, Battisti, & Skok, 2017). In addition to synoptic scale systems, about
 1182 half of the total precipitation in these ITCZs is in the form of stratiform precipitation
 1183 (Schumacher & Houze Jr, 2003), which is overwhelmingly in the form of long-lived mesoscale
 1184 convective systems (Houze Jr, 2018).

1185 *4.2.3 Other modes of tropical intraseasonal variability*

1186 The above transients appear to be caused by instabilities associated with shear in
 1187 the large-scale circulation, and can be interpreted as a product of the overturning regime
 1188 and local boundary conditions. In addition to these convectively coupled waves gener-
 1189 ated by the large-scale environment, slower, larger-scale disturbances are also observed
 1190 in the tropics. Fig. 16 shows intense activity associated with low wavenumbers and a
 1191 period of 30–60 days. This has been shown to correspond to the MJO; a convectively
 1192 coupled, large-scale equatorially trapped wave that propagates slowly eastward from the
 1193 east coast of Africa to the western-central Pacific, whereafter it continues eastward as
 1194 a Kelvin wave (Madden & Julian, 1971, 1972; C. Zhang, 2005, and references therein).
 1195 The oscillation has strong influences on tropical rainfall, particularly in the Indo-Pacific
 1196 region (see examples below), but the precise mechanism responsible remains a topic of
 1197 extensive ongoing research.

1198 *The Madden Julian Oscillation and the tropical Indian Ocean ‘ITCZ’*

1199 Precipitation in the Indian Ocean sector in austral summer is found between 10°N
 1200 and 15°S, but is concentrated slightly south of the Equator. It can be seen from Fig. 9
 1201 that, unlike the Atlantic and Pacific ITCZs, precipitation in the Indian Ocean is not or-
 1202 ganized into a narrow zonal band due to different physics than is described in Section
 1203 2.1.3 (the zonal asymmetry in SST is insufficient to drive a symmetrically unstable flow).
 1204 Indeed, estimates show that between 30 and 40% of the annual precipitation in the In-
 1205 dian Ocean and Maritime continent (10°N and 10°S, 70°E and 150°E) is associated with
 1206 the MJO (Kerns & Chen, 2020).

1207 *Intraseasonal variability in the Indo-Pacific*

1208 In the Indo-Pacific region, the MJO features trailing Rossby waves with enhanced
 1209 shear zones that angle polewards and westwards from the precipitation center near the
 1210 Equator and support precipitation. Hence, along a fixed longitude, bands of precipita-
 1211 tion appear to propagate poleward from the Equator to about 20°N over India as the
 1212 MJO propagates eastward over the maritime continent (Hartmann & Michelsen, 1989).

1213 In boreal summer, in addition to the MJO, the climate in this region appears to
 1214 be modulated by propagating ‘Boreal Summer Intraseasonal Oscillations’ (BSISO), ob-
 1215 served to have dominant timescales of 10-20 and 30-60 days, and to propagate northward
 1216 over the continent (Annamalai & Slingo, 2001; Goswami & Ajaya Mohan, 2001; Hart-
 1217 mann & Michelsen, 1989; Lee et al., 2013). These oscillations modulate the active and
 1218 break phases of the Indian monsoon, with the tropical convergence zone and associated
 1219 Hadley circulation oscillating between an off-equatorial ‘monsoon’ location, and a near
 1220 equatorial ‘ITCZ’ location (e.g., Annamalai & Slingo, 2001; Goswami & Ajaya Mohan,
 1221 2001; D. R. Sikka & Gadgil, 1980). Like the MJO, the propagation mechanism and pre-
 1222 cise drivers of the BSISOs remain unclear, and are the subject of ongoing research. Some
 1223 authors argue that the BSISOs are distinct from the MJO (e.g Lee et al., 2013; B. Wang
 1224 & Xie, 1997), while others identify them as associated with the MJO (e.g., Hartmann
 1225 & Michelsen, 1989; Jiang, Adames, Zhao, Waliser, & Maloney, 2018).

1226 **5 Conclusions and outlook**

1227 In this article, we have reviewed the theory of monsoons that has resulted in large
 1228 part from idealized models and discussed the behavior of Earth’s monsoons in light of
 1229 the theory. While the regional monsoons have a diverse range of individual features, they
 1230 also have much in common, including enhancement of cross-equatorial and westerly flow
 1231 in the summer season, rapid onset, and development in an off-equatorial direction. In
 1232 addition, regional monsoons often covary as components of a global monsoon, under both
 1233 changes to orbital forcing and internal variations. The theoretical considerations out-
 1234 lined in Section 2 are starting to provide explanations for these behaviors, as presented
 1235 in Section 3, but many open questions remain in how to connect theoretical ideas to ob-
 1236 servations (Section 4). We conclude the review by first discussing these successes and
 1237 challenges, before proposing more specific directions for future research.

1238 **5.1 Successes**

1239 Insight from theory has caused a shift in the understanding of monsoon dynam-
 1240 ics – from that of primarily land-sea contrast driven, sea-breeze-like circulations, to lo-
 1241 calized variations of the tropical overturning circulation and associated convergence zones,
 1242 strongly governed by the momentum and energy budgets.

1243 The momentum budget, Eq. 4, indicates three classes of solution for the Hadley
 1244 circulation: a ‘radiative-convective equilibrium’ regime, $\bar{v} = \bar{w} = 0$; an ‘angular mo-
 1245 mentum conserving’ regime, in which the Rossby number Ro approaches 1 and eddies

Table 2. Suggested classifications of tropical and subtropical convergence zones. Regions are defined as in Fig. 1 & 14. Wind reversal is assessed based on Fig. 1, and the presence of multiple preferred latitudes for rainfall is based on Fig. 14. P_{0-10° , P_{10-25° and P_{25-35° are the area-weighted fractions of precipitation (mm/day) falling in each monsoon/ITCZ region between the indicated latitudes (bounded in longitude by the boxes in Fig. 1), relative to the total evaluated from $0-35^\circ$. Conclusions are not sensitive to small variations in the latitude bounds used; the use of 10° rather than 7° (cf. Geen et al., 2019) here is motivated by discussion in Section 3.2.1. $\phi(\theta_{eb})$ and $\phi(P_{max})$ are the latitudes of maximum season-mean subcloud equivalent potential temperature and precipitation respectively. Precipitation fractions and maxima are calculated using GPCP data and θ_{eb} is calculated using JRA-55 reanalysis, with 1979–2016 used in both cases. Season means over June–Sept are used for Northern Hemisphere monsoons, Dec–March for Southern Hemisphere monsoons, and all months for the Atlantic and Pacific ITCZs.

System	Type	Wind reversal?	Multiple preferred latitudes?	P_{0-10° (%)	P_{10-25° (%)	P_{25-35° (%)	$\phi(\theta_{eb})$ ($^\circ$)	$\phi(P_{max})$ ($^\circ$)
S. Asia	Monsoon	yes	yes	24	57	19	25	21.25
Australia	Hybrid	yes	yes	48	44	8	-7.5	-6.25
W. Africa	Hybrid	yes	yes	58	40	2	12.5	8.75
S. Africa	Monsoon	yes	yes	33	54	13	-12.5	-13.75
N. America	ITCZ extension	no	no	32	55	13	10.	8.75
S. America	Neither	no	yes	41	43	16	-12.5	-6.25
Atlantic	ITCZ	no	no	69	19	12	2.5	6.25
E. Pacific	ITCZ	no	no	50	35	15	7.5	8.75

1246 have a negligible effect; and an ‘eddy-driven’ regime, where Ro is much less than 1 and
 1247 eddies strongly influence the overturning circulation. Our understanding of monsoon dy-
 1248 namics has been greatly advanced by considering the transitions between these regimes,
 1249 and the controls on the latitude of the ascending branch of the circulation.

1250 Constraints on the zonal mean convergence zone latitude have been identified by
 1251 considering the energetics of the circulation, in addition to the momentum budget. If
 1252 the atmosphere is in CQE then, for an angular momentum conserving overturning cir-
 1253 culation, the convergence zone is expected to lie just equatorward of the peak in sub-
 1254 cloud moist static energy (see Privé & Plumb, 2007a, 2007b, and Section 2.1). The sub-
 1255 cloud distribution of MSE therefore strongly constrains the circulation.¹² A related en-
 1256 ergetic constraint is obtained from considering the vertically integrated MSE budget (Eq.
 1257 10). The latitude of the EFE has been found to be approximately colocated with the con-
 1258 vergence zone latitude, allowing the zonal mean convergence zone location to be related
 1259 to the meridional cross-equatorial energy flux and net energy input at the Equator (e.g.,
 1260 Bischoff & Schneider, 2016; Kang, 2020; Kang et al., 2018).

1261 The latitude of the convergence zone is also strongly related to the dynamics that
 1262 govern the Hadley circulation. In aquaplanet simulations when the convergence zone is
 1263 on or near the Equator the circulation is more eddy driven (i.e., an ITCZ), while when
 1264 the convergence zone is far from the Equator the circulation is near angular momentum
 1265 conserving and the strength of the circulation is determined mainly by energetics (Bor-
 1266 doni & Schneider, 2008, 2010; Schneider & Bordoni, 2008). These ‘ITCZ’ and ‘monsoon’
 1267 regimes are illustrated schematically in Fig. 8a and b respectively. When the slab ocean
 1268 in these aquaplanets is thin, and hence the surface thermal inertia low, similar to land,
 1269 a fast transition between these two regimes is observed over the course of the seasonal
 1270 cycle, with the zonal mean convergence zone rapidly moving away from the Equator into
 1271 the summer hemisphere at the start of the summer season. This fast transition is me-
 1272 diated by two feedbacks. Firstly, as the convergence zone shifts off the Equator and the
 1273 Hadley circulation becomes cross equatorial, the lower branch of the Hadley cell advects
 1274 cooler, drier air up the meridional MSE gradient. Combined with the continued diabatic
 1275 warming of the summer hemisphere by the insolation, this has the effect of pushing the
 1276 MSE peak poleward and so shifting the convergence zone farther off the Equator. Sec-
 1277 ondly, as a result of angular momentum conservation, the equatorward upper-level merid-
 1278 ional flow gives rise to upper-level easterlies. These easterlies suppress propagation of
 1279 extratropical eddies into the low latitudes (Charney & Drazin, 1961) and help to kick
 1280 the Hadley cell into the angular momentum conserving regime, so that the meridional
 1281 overturning is strongly responsive to the thermal forcing and strengthens and broadens
 1282 further.

1283 Recent results suggest that in an aquaplanet, the transition between an eddy-driven
 1284 and angular momentum conserving Hadley circulation occurs when the convergence zone
 1285 migrates beyond $\sim 7^\circ$, regardless of slab ocean characteristics (Geen et al., 2019). In
 1286 this review, we have argued that the former regime is relevant to the dynamics of the
 1287 observed ITCZs, while the latter is appropriate for understanding the monsoon circu-
 1288 lations. Another recent strand of research has explored the maximum limits on the mi-
 1289 grations of the convergence zone away from the Equator: in aquaplanets, the convergence
 1290 zone does not migrate more than 25° away from the equator, even when the MSE max-
 1291 imum is at the poles (Faulk et al., 2017). Current work (Hill et al., 2019; Singh, 2019)
 1292 is exploring this poleward limit of monsoons using constraints relating the Hadley cir-
 1293 culation regime to the curvature of the subcloud equivalent potential temperature.

¹² Although it is important to remember that the MSE distribution is itself set partially by the circula-
 tion, and interactions between the MSE and circulation must be considered.

1294 Analysis of observations has demonstrated that the South Asian, Australian and
 1295 African monsoons show behavior similar to that described by the above theoretical work.
 1296 In these monsoons, the peak precipitation is located just equatorward of the peak in sub-
 1297 cloud MSE (Nie et al., 2010) and the convergence zones migrate in line with the EFE
 1298 (Adam et al., 2016a; Boos & Korty, 2016). In monsoons where the ascending branch mi-
 1299 grates far from the Equator, such as the South Asian and Southern African monsoons,
 1300 the summertime overturning circulation becomes aligned with angular momentum con-
 1301 tours, suggesting a strongly thermally driven cross-equatorial flow regime (e.g., Bordoni
 1302 & Schneider, 2008; J. M. Walker & Bordoni, 2016). In addition, Figs. 14 & 15 suggest
 1303 the threshold distinguishing an eddy-driven ('ITCZ') from an angular momentum con-
 1304 serving ('monsoon') overturning regime is $\sim 10^\circ$ latitude, which is qualitatively simi-
 1305 lar to that seen in aquaplanet simulations. Consistent with modeling results in which
 1306 rotation rate is varied, the observed overturning circulations are confined to be within
 1307 $\sim 25^\circ$ of the Equator (Faulk et al., 2017).

1308 Based on the aquaplanet frameworks, we suggest the regional systems might be clas-
 1309 sified into either an ITCZ or monsoon circulation regime based on the following crite-
 1310 ria: the latitude at which precipitation falls; the occurrence of wind reversal; and the pres-
 1311 ence of multiple preferred latitudes for precipitation, which gives some indication of where
 1312 abrupt onset of precipitation might occur when the convergence zone shifts between these
 1313 locations. With these criteria in mind, Table 2 summarizes which systems the authors
 1314 feel fit the dynamics-based categories of monsoon, ITCZ or a hybrid with characteris-
 1315 tics of both regimes. In South America and East Asia orography results in dynamics that
 1316 does not seem to fit these descriptions. Note that the East Asian region encompasses both
 1317 the the tropical South China Sea monsoon and the orographically controlled Meiyu-Baiu
 1318 front (Section 3.1), and so is not included in the table.

1319 Awareness of these mechanisms can help motivate work investigating sources of in-
 1320 terannual variability, and the response to external forcings, with one clear goal being a
 1321 better mechanistic understanding of model projections forced by future warming scenar-
 1322 ios. On this front, some success has already been achieved. For example, interannual vari-
 1323 ability in monsoon precipitation has been found to be correlated to variability in sub-
 1324 cloud MSE (Hurley & Boos, 2013). Migrations of the zonal mean convergence zone un-
 1325 der historical forcings have been examined in relation to migrations of the EFE (Dono-
 1326 hoe et al., 2013). The weak changes to the Asian monsoon in simulations of future cli-
 1327 mate appear to be explained by opposing responses to increased CO_2 levels and surface
 1328 warming (Shaw & Voigt, 2015). Further exploration of the observations, informed by the-
 1329 ory, could prove fruitful for improved understanding of model biases, or for identifying
 1330 sources of seasonal predictability.

1331 5.2 Challenges

1332 The theoretical frameworks discussed in Section 2 each have significant known lim-
 1333 itations. The EFE framework appears most directly predictive. However, even in an aqua-
 1334 planet, uncertainties in changes in GMS and column fluxes, for example due to cloud feed-
 1335 backs, limit the predictive power of energetic diagnostics, such as the EFE and the cross-
 1336 equatorial energy transport, to the understanding of tropical and subtropical precipita-
 1337 tion changes (e.g., Biasutti & Voigt, 2020). The momentum framework is conceptually
 1338 useful for understanding seasonal changes in the Hadley cell dynamics (Bordoni & Schnei-
 1339 der, 2008; Geen et al., 2018), but implications for the response of monsoons and ITCZs
 1340 to variability on different time scales remain to be explored.

1341 Despite these limitations, constraints on the zonal and time mean convergence zone
 1342 and overturning circulation are beginning to emerge from theory and have now been suc-
 1343 cessfully applied to aquaplanets and to some features of the observations. This repre-
 1344 sents a significant step in our understanding of the tropical circulation. However, asym-

1345 metries that arise from land-sea contrast and orography introduce a zoo of additional
 1346 complications that these simple theories do not account for, and some care must there-
 1347 fore be taken in applying aquaplanet theories to reality. For example, while the mon-
 1348 soon circulation in an aquaplanet is characterized by an angular momentum conserving
 1349 Hadley circulation, stationary waves can be important when zonal asymmetries are in-
 1350 cluded in the boundary conditions (Shaw, 2014). However, as we show here in Fig. 13,
 1351 in individual monsoon sectors (South Asia, Africa and Australia) advection of momen-
 1352 tum by the mean circulation appears to be non-negligible, suggesting that even in the
 1353 presence of zonal asymmetries some monsoons do approach an angular momentum con-
 1354 serving regime.

1355 As discussed in Section 4, the pattern of precipitation in the South American mon-
 1356 soon and the intensity of the East Asian monsoon in particular are strongly influenced
 1357 by orography. The interaction of the westerly jet with the orography of Tibet generates
 1358 a stationary wave downstream over East Asia that gives rise to the Meiyu-Baiu front and
 1359 governs the duration of the stages of the East Asian summer ‘monsoon’. In South Amer-
 1360 ica, the Andes divert the tropical easterly and subtropical westerly flow, resulting in strong
 1361 equatorward descending flow to the west of the mountains, and poleward ascending flow
 1362 to the east. In austral summer, the South American Low-Level jet develops to the east
 1363 of the Andes and extends the South American monsoon flow southward. This results in
 1364 precipitation that is displaced far from the Equator, but without the formation of an an-
 1365 gular momentum conserving Hadley cell of the kind seen in aquaplanets. The descend-
 1366 ing flow to the west of the Andes suppresses precipitation year-round off the coast of South
 1367 and Central America, over the East Pacific and helps to push the convergence zone north
 1368 of the Equator year round. Overall, we conclude that aquaplanet theories do not appear
 1369 applicable to the systems seen in the Americas or East Asia.

1370 Last, transients make a non-negligible contribution to precipitation in the regional
 1371 monsoons and ITCZs. These phenomena are not accounted for in the theoretical frame-
 1372 work reviewed in Section 2. Whether they feedback onto the large-scale circulation, or
 1373 are simply organized by it, remains to be determined.

1374 5.3 Outlook

1375 Based on the challenges above we suggest the following focus areas for future re-
 1376 search, including both idealized modeling and study of the new experiments available
 1377 in the Coupled Model Intercomparison Project Phase 6 (CMIP6).

1378 *5.3.1 Address limitations of theory and connect frameworks within aqua-* 1379 *planets*

1380 The issues discussed above limit the application of theory to problems such as cli-
 1381 mate change. One focus of future idealized modeling work should be to try to resolve
 1382 known issues with theory that arise even in aquaplanets. For example TRACMIP has
 1383 proved useful in exploring elements of theory that do and do not make successful pre-
 1384 dictions across aquaplanet simulations with different climate models (Biasutti & Voigt,
 1385 2020; Harrop, Lu, & Leung, 2019; Voigt et al., 2016). Radiation-locking simulations could
 1386 tease apart the importance of cloud feedbacks (Byrne & Zanna, 2020, in press). The EFE
 1387 and momentum frameworks both consider the large-scale overturning circulation, but
 1388 are generally applied separately. A first step to connecting these is to examine both the
 1389 MSE and momentum budgets in parallel when studying tropical convergence zones. It
 1390 would also be interesting to examine whether dynamics of the overturning circulation
 1391 cell has implications for the cell’s response to forcings. For example, might the under-
 1392 lying dynamics of the cell determine the strength of the precipitation response to forc-
 1393 ing? Will the response to forcing a system with more ITCZ-like characteristics, e.g., the

1394 Australian or West African monsoons, be different to that of the South Asian or South-
1395 ern African monsoons?

1396 **5.3.2 Build beyond the aquaplanets**

1397 While aquaplanets are a valuable tool for studying the circulation in a simple con-
1398 text, it is clear from Section 4 that the application of theory developed in these settings
1399 is limited. New terms enter both the momentum and energy budgets when zonal asym-
1400 metries are included, and zonal mean changes in inter-hemispheric energy imbalances
1401 can be achieved via regional changes.

1402 Hierarchical modeling work, where complexity is introduced in a progressive way,
1403 is a clear path forward to begin to specialize theory to individual monsoon systems, as
1404 well as identifying commonalities between systems. Initial steps on this hierarchy are al-
1405 ready being taken, by introducing heating (Shaw, 2014) or continents into idealized mod-
1406 els (e.g., TRACMIP, and Chiang et al., 2020; Geen et al., 2018; Hui & Bordoni, submit-
1407 ted.; W. Zhou & Xie, 2018), or removing orography from more complete models (Bald-
1408 win, Vecchi, & Bordoni, 2019; Boos & Kuang, 2010; Wei & Bordoni, 2016). Idealized mod-
1409 eling frameworks such as Isca (Vallis et al., 2018) have been developed with such prob-
1410 lems in mind, allowing boundary conditions (e.g., land and orography) and physical pa-
1411 rameterizations (e.g., convection, radiation and land hydrology) to be trivially modified.
1412 The Global Monsoon Model Intercomparison Project (GMMIP) is ongoing under CMIP6,
1413 and includes plans for simulations in which features of orography are removed and/or
1414 surface fluxes are modified (T. Zhou et al., 2016).

1415 In terms of developing theory further, the additional terms entering the budgets
1416 make this challenging, though some regional approximations to the EFE have been de-
1417 rived (Adam et al., 2016a; Boos & Korty, 2016). The definition of the local Hadley and
1418 Walker cells are useful for visualising the regional characteristics of the overturning cir-
1419 culation (Schwendike et al., 2014). Decomposition of the momentum and energy bud-
1420 gets into rotational and divergent components in this way, and consideration of the both
1421 zonal and meridional balances, may help in extending theoretical frameworks further,
1422 if simple balances can be identified. It is worth noting that these budgets are difficult
1423 to compute and close offline; we recommend that where possible all terms be computed
1424 online and saved as output.

1425 **5.3.3 Investigate the dynamics of variability and transients**

1426 As well as exploring how theory can be extended to regional scales, we suggest look-
1427 ing at possible connections to shorter temporal scales. For example, on what timescales
1428 does CQE cease to hold? Can changes in the leading order momentum balance explain
1429 variability on shorter timescales? Can theory provide new insights into the processes re-
1430 sponsible for variability on interdecadal, interannual or intraseasonal timescales? Does
1431 the nature of the transient convective systems in which rain falls influence the large-scale
1432 circulation?

1433 In some cases, theory of monsoon circulations might prove to be commensurate with
1434 observations that suggest a more causal role for the transients. For example, as discussed
1435 in Section 4, monsoon onset over South Asia and the South China Sea has been suggested
1436 to relate to the arrival of the moist phase of a transient Intraseasonal Oscillation (ISO),
1437 with active and break phases throughout the season then arising due to further ISOs and
1438 shifts in the convergence zone (e.g., Lee et al., 2013; Webster et al., 1998). Aquaplanet
1439 based modeling work has instead led to development of a zonal- and climatological-mean
1440 view of monsoon onset as a regime change of the Hadley circulation (see Section 2.1 and
1441 Bordoni & Schneider, 2008; Schneider & Bordoni, 2008). These ideas appear tantaliz-
1442 ingly reconcilable; for example the arrival of an ISO might act as the trigger for the regime

1443 change of the circulation, or perhaps active and break phases of the Indian monsoon might
 1444 be connected to intraseasonal changes in the strength of the Hadley cell. The MSE bud-
 1445 get has been used to investigate the propagation of the MJO (Andersen & Kuang, 2012;
 1446 Jiang et al., 2018; Sobel & Maloney, 2013), and may provide a way to bridge these two
 1447 perspectives.

1448 On interannual timescales, enhanced upper-level tropical easterlies accompany more
 1449 intense precipitation over West Africa via enhancement of upper-level divergence and
 1450 meridional overturning (Nicholson, 2009). This variability in the meridional overturn-
 1451 ing again occurs in a sense consistent with the aquaplanet regimes, although in this case
 1452 the circulation has significant zonal asymmetry. Modulation of the monsoons by anom-
 1453 alous upper-level flow may help in understanding teleconnections influencing regional mon-
 1454 soons, although more work is needed to explore the mechanisms involved and to ascer-
 1455 tain the direction of causality between anomalous upper- and lower-level circulations and
 1456 precipitation.

1457 *5.3.4 Look at how theory can be tested in CMIP6*

1458 Perhaps the greatest challenge for theory and modeling is to determine how the mon-
 1459 soon systems will change in future climates. The current consensus from models is that
 1460 the precipitation in the global monsoon is likely to increase under anthropogenic forc-
 1461 ings, though the monsoon circulation is likely to weaken (Christensen et al., 2013). How-
 1462 ever, there is a significant spread in model projections (e.g., Seth et al., 2019, and re-
 1463 ferences therein), and models show varying degrees of skill in capturing the present-day
 1464 climatology of the monsoon and its variability (e.g. Jourdain et al., 2013; Roehrig, Bouniol,
 1465 Guichard, Hourdin, & Redelsperger, 2013; Sperber et al., 2013). Future changes in re-
 1466 gional tropical precipitation are strongly influenced by changes in the circulation, which
 1467 are not well constrained (Chadwick, Boutle, & Martin, 2013).

1468 As discussed in Section 3.2, future predictability depends on direct and indirect re-
 1469 sponses to radiative forcing, which may oppose one another (Shaw & Voigt, 2015). Phase
 1470 3 of the Cloud Feedback Model Intercomparison Project is built into CMIP6 (Webb et
 1471 al., 2017). This includes both simulations studying the radiative effects of clouds, and
 1472 also ‘timeslice’ simulations in which models are forced with SSTs from the climatology
 1473 of either pre-industrial control or abrupt-4xCO₂ runs. In a hierarchy of simulations, physics
 1474 schemes for radiation, sea ice and plant physiology are progressively permitted to respond
 1475 to CO₂ forcing, building up the components of the full model response (cf. Chadwick,
 1476 Douville, & Skinner, 2017). Applying theoretical ideas in these simulations may help to
 1477 identify how the dynamics of the monsoons is influenced by the various forcings and feed-
 1478 backs that build up the response to climate change. Although current theories for the
 1479 ITCZ and monsoon circulations are more diagnostic than predictive, developing and ap-
 1480 plying these to understanding model bias and climate changes is a clear priority.

1481 **Glossary**

1482 **AMIP** Atmospheric Model Intercomparison Project. A project comparing the behav-
 1483 iors of atmospheric general circulation models forced by realistic sea surface tem-
 1484 peratures and sea ice.

1485 **BSISO** Boreal Summer Intraseasonal Oscillation. Describes the dominant modes of trop-
 1486 ical intraseasonal variability over Asia during boreal summer.

1487 **CMIP6** The Coupled Model Intercomparison Project, Phase 6. An intercomparison
 1488 of the results of state-of-the-art climate models under a range of consistent exper-
 1489 imental protocols.

1490 **CQE** Convective Quasi-Equilibrium. A theoretical framework for the tropical atmosphere
 1491 that assumes the atmospheric lapse rate is maintained close to a moist adiabat

- 1492 due to the occurrence of frequent, intense moist convection. See discussion in Sec-
 1493 tion 2.1.
- 1494 **Dansgaard–Oeschger (D–O) Cycles** Millennial-scale oscillations during the last glacial
 1495 period that are nearly global in extent and feature an abrupt transition.
- 1496 **Earth System model** A comprehensive model of the Earth System, simulating the
 1497 fluid motions and thermodynamics of the atmosphere and ocean, as well as inter-
 1498 actions with ice, the land surface and vegetation, and ocean biogeochemistry.
- 1499 **EFE** Energy Flux Equator. The latitude at which the vertically integrated MSE flux
 1500 by the atmospheric circulation is zero.
- 1501 **EFPM** Energy Flux Prime Meridian. Defined as the longitudes at which the zonally
 1502 divergent column integrated MSE flux vanishes and has positive zonal gradient.
- 1503 **ENSO** The El Niño-Southern Oscillation. A recurring climate pattern involving changes
 1504 to the temperature of the waters in the Pacific Ocean. El Niño (La Niña) phases
 1505 are associated with warmer (cooler) than usual SSTs in the central and eastern
 1506 tropical Pacific Ocean.
- 1507 **GCM** Global Circulation Model. A numerical model for the circulation of the atmo-
 1508 sphere and/or ocean.
- 1509 **GMS** Gross Moist Stability. A measure of how efficiently the large scale circulation ex-
 1510 ports MSE. Various definitions are used in the literature, here we define GMS by
 1511 Eq. 14.
- 1512 **Heinrich event** A natural phenomenon featuring the collapse of Northern Hemisphere
 1513 ice shelves and consequently the release of large numbers of icebergs.
- 1514 **Idealized model** A model in which only some elements of the Earth System are in-
 1515 cluded to allow testing of theories in a more conceptually simple and computa-
 1516 tionally affordable framework.
- 1517 **ISO** Intra-seasonal Oscillation
- 1518 **ITCZ** Intertropical Convergence Zone. The location where the trade winds of the North-
 1519 ern and Southern Hemispheres converge, coincident with the ascending branch of
 1520 the Hadley circulation. Precipitation and the strength of the overturning circula-
 1521 tion are driven primarily by eddy momentum fluxes and precipitation is located
 1522 with $\sim 10^\circ$ of the Equator.
- 1523 **ITCZ** The zonal and annual mean convergence zone, which is located at 1.7°N if es-
 1524 timated by the precipitation centroid; (Donohoe et al., 2013), or $\sim 6^\circ\text{N}$ if judged
 1525 by the precipitation maximum; e.g., (Gruber et al., 2000).
- 1526 **Monsoon** The rainy summer season of a tropical or subtropical region, in which pre-
 1527 cipitation associated with the convergence zone extends far from the Equator, the
 1528 lower-level prevailing wind changes direction or strength, and the overturning cir-
 1529 culation approaches the angular momentum conserving (eddy-less) limit. Precip-
 1530 itation and the strength of the overturning circulation are primarily controlled by
 1531 the energy budget.
- 1532 **MJO** Madden-Julian Oscillation
- 1533 **MSE** Moist static energy, defined in Eq. 9.
- 1534 **RCE** Radiative-convective equilibrium. Describes the balance between the radiative cool-
 1535 ing of the atmosphere and the heating via latent heat release resulting from con-
 1536 vection.
- 1537 **Sea breeze** A wind that blows from a large body of water onto a landmass due to dif-
 1538 ferences in surface temperature, and consequently air pressure, between the land
 1539 and water.
- 1540 **SACZ** South Atlantic Convergence Zone. The band of convergence observed extend-
 1541 ing across southeast Brazil and over the southwest Atlantic, e.g., Fig. 1e.
- 1542 **SPCZ** South Pacific Convergence Zone. The band convergence observed over the south-
 1543 west Pacific, e.g., Fig. 1e.
- 1544 **SST** Sea Surface Temperature

1545 **Acknowledgments**

1546 RG was supported by the UK-China Research and Innovation Partnership Fund, through
 1547 the Met Office Climate Science for Service Partnership (CSSP) China, as part of the New-
 1548 ton Fund. SB and KLH acknowledge support from the Caltech Terrestrial Hazard Ob-
 1549 servation and Reporting (THOR) center and the Caltech GPS Discovery Fund. DSB was
 1550 funded by the Tamaki Foundation. Datasets for this research are available in these in-
 1551 text data citation references: Japan Meteorological Agency/Japan (2013); Mesoscale At-
 1552 mospheric Processes Branch/Laboratory for Atmospheres/Earth Sciences Division/Science
 1553 and Exploration Directorate/Goddard Space Flight Center/NASA, and Earth System
 1554 Science Interdisciplinary Center/University of Maryland (2018); Huffman, G. J. and D.
 1555 T. Bolvin and R. F. Adler (2016). We thank Dennis Hartmann, John Chiang, Mike Wal-
 1556 lence, Fabio Bellacanzone and three anonymous reviewers for their thoughtful and help-
 1557 ful comments on the manuscript.

1558 **References**

- 1559 Adam, O., Bischoff, T., & Schneider, T. (2016a). Seasonal and interannual
 1560 variations of the energy flux equator and ITCZ. Part II: Zonally vary-
 1561 ing shifts of the ITCZ. *Journal of Climate*, *29*(20), 7281–7293. doi:
 1562 10.1175/JCLI-D-15-0710.1
- 1563 Adam, O., Bischoff, T., & Schneider, T. (2016b). Seasonal and interannual varia-
 1564 tions of the energy flux equator and ITCZ. Part I: Zonally averaged ITCZ po-
 1565 sition. *Journal of Climate*, *29*(9), 3219–3230. doi: 10.1175/JCLI-D-15-0512.1
- 1566 Adames, Á. F., & Wallace, J. M. (2017). On the tropical atmospheric signature of El
 1567 Niño. *Journal of the Atmospheric Sciences*, *74*(6), 1923–1939.
- 1568 Adams, D. K., & Comrie, A. C. (1997). The North American Monsoon. *Bulletin*
 1569 *of the American Meteorological Society*, *78*(10), 2197–2214. doi: 10.1175/1520
 1570 -0477(1997)078<2197:TNAM>2.0.CO;2
- 1571 An, Z., Guoxiong, W., Jianping, L., Youbin, S., Yimin, L., Weijian, Z., . . . Juan,
 1572 F. (2015). Global Monsoon Dynamics and Climate Change. *Annual*
 1573 *Review of Earth and Planetary Sciences*, *43*(1), 29–77. doi: 10.1146/
 1574 annurev-earth-060313-054623
- 1575 Ananthakrishnan, R., & Soman, M. K. (1988). The Onset of the Southwest Mon-
 1576 soon over Kerala: 1901-1980. *Journal of Climatology*, *8*, 283–296. doi: 10
 1577 .1002/joc.3370080305
- 1578 Andersen, J. A., & Kuang, Z. (2012). Moist Static Energy Budget of MJO-like Dis-
 1579 turbances in the Atmosphere of a Zonally Symmetric Aquaplanet. *Journal of*
 1580 *Climate*, *25*(8), 2782-2804. Retrieved from <https://doi.org/10.1175/JCLI-D-11-00168.1> doi: 10.1175/JCLI-D-11-00168.1
- 1582 Annamalai, H., & Slingo, J. M. (2001). Active/break cycles: Diagnosis of the in-
 1583 traseasonal variability of the Asian Summer Monsoon. *Climate Dynamics*,
 1584 *18*(1), 85–102. Retrieved from <https://doi.org/10.1007/s003820100161>
 1585 doi: 10.1007/s003820100161
- 1586 Arakawa, A., & Schubert, W. H. (1974). Interaction of a Cumulus Cloud Ensemble
 1587 with the Large-Scale Environment, Part I. *J. Atmos. Sci.*, *31*, 674–701. doi: 10
 1588 .1175/1520-0469(1974)031%3C0674:IOACCE%3E2.0.CO;2
- 1589 Arbuszewski, J. A., Demenocal, P. B., Cléroux, C., Bradtmiller, L., & Mix, A.
 1590 (2013). Meridional shifts of the Atlantic Intertropical Convergence Zone
 1591 since the Last Glacial Maximum. *Nature Geoscience*, *6*(11), 959–962. doi:
 1592 10.1038/ngeo1961
- 1593 Atwood, A. R., Donohoe, A., Battisti, D. S., Liu, X., & Pausata, F. S. R. (2020).
 1594 Robust longitudinally-variable responses of the ITCZ to a myriad of climate
 1595 forcings. *Geophys. Res. Lett.*, *in press*.
- 1596 Baldwin, J. W., Vecchi, G. A., & Bordoni, S. (2019). The direct and ocean-mediated
 1597 influence of Asian orography on tropical precipitation and cyclones. *Climate*

- 1598 *Dynamics*, 1–20. Retrieved from [http://dx.doi.org/10.1007/s00382-019-](http://dx.doi.org/10.1007/s00382-019-04615-5)
 1599 <http://link.springer.com/10.1007/s00382-019-04615-5> doi: 10
 1600 .1007/s00382-019-04615-5
- 1601 Barlow, M., Nigam, S., & Berbery, E. H. (1998). Evolution of the North American
 1602 Monsoon System. *Journal of Climate*, *11*(9), 2238–2257. doi: 10.1175/1520
 1603 -0442(1998)011(2238:EOTNAM)2.0.CO;2
- 1604 Battisti, D. S., Ding, Q., & Roe, G. H. (2014). Coherent pan-Asian climatic and iso-
 1605 topic response to orbital forcing of tropical insolation. *Journal of Geophysical*
 1606 *Research*, *119*(21), 11,997–12,020. doi: 10.1002/2014JD021960
- 1607 Becker, E., Schmitz, G., & Geprags, R. (1997). The feedback of midlatitude waves
 1608 onto the Hadley cell in a simple general circulation model. *Tellus A*, *49*, 182–
 1609 199.
- 1610 Berger, A. L. (1978). Long-Term Variations of Caloric Insolation Resulting from the
 1611 Earth’s Orbital Elements. *Quaternary Research*, *9*(2), 139–167. doi: 10.1016/
 1612 0033-5894(78)90064-9
- 1613 Biasutti, M., & Voigt, A. (2020). Seasonal and CO₂-Induced Shifts of the ITCZ:
 1614 Testing Energetic Controls in Idealized Simulations with Comprehensive Mod-
 1615 els. *Journal of Climate*, *33*(7), 2853–2870.
- 1616 Biasutti, M., Voigt, A., Boos, W. R., Braconnot, P., Hargreaves, J. C., Harrison,
 1617 S. P., . . . Xie, S.-P. (2018). Global energetics and local physics as drivers of
 1618 past, present and future monsoons. *Nature Geoscience*, *11*(6), 392–400. doi:
 1619 10.1038/s41561-018-0137-1
- 1620 Bischoff, T., & Schneider, T. (2014). Energetic constraints on the position of the In-
 1621 tertropical Convergence Zone. *Journal of Climate*, *27*(13), 4937–4951. doi: 10
 1622 .1175/JCLI-D-13-00650.1
- 1623 Bischoff, T., & Schneider, T. (2016). The equatorial energy balance, ITCZ position,
 1624 and double-ITCZ bifurcations. *Journal of Climate*, *29*(8), 2997–3013. doi: 10
 1625 .1175/JCLI-D-15-0328.1
- 1626 Boos, W. R., & Korty, R. L. (2016). Regional energy budget control of the In-
 1627 tertropical Convergence Zone and application to mid-Holocene rainfall. *Nature*
 1628 *Geoscience*, *9*(12), 892–897. doi: 10.1038/ngeo2833
- 1629 Boos, W. R., & Kuang, Z. (2010). Dominant control of the South Asian monsoon by
 1630 orographic insulation versus plateau heating. *Nature*, *463*(7278), 218–222. doi:
 1631 10.1038/nature08707
- 1632 Boos, W. R., & Kuang, Z. (2013). Sensitivity of the South Asian monsoon to el-
 1633 evated and non-elevated heating. *Scientific Reports*, *3*, 3–6. doi: 10.1038/
 1634 srep01192
- 1635 Bordoni, S., Ciesielski, P. E., Johnson, R. H., McNoldy, B. D., & Stevens, B.
 1636 (2004). The low-level circulation of the North American Monsoon as re-
 1637 vealed by QuikSCAT. *Geophysical Research Letters*, *31*, L10109. doi:
 1638 10.1029/2004GL020009
- 1639 Bordoni, S., & Schneider, T. (2008). Monsoons as eddy-mediated regime transitions
 1640 of the tropical overturning circulation. *Nature Geoscience*, *1*(8), 515–519. doi:
 1641 10.1038/ngeo248
- 1642 Bordoni, S., & Schneider, T. (2010). Regime Transitions of Steady and Time-
 1643 Dependent Hadley Circulations: Comparison of Axisymmetric and Eddy-
 1644 Permitting Simulations. *Journal of the Atmospheric Sciences*, *67*(5), 1643–
 1645 1654. doi: 10.1175/2009JAS3294.1
- 1646 Broccoli, A. J., Dahl, K. A., & Stouffer, R. J. (2006). Response of the ITCZ to
 1647 Northern Hemisphere cooling. *Geophysical Research Letters*, *33*(1), 1–4. doi:
 1648 10.1029/2005GL024546
- 1649 Burpee, R. W. (1972). The origin and structure of easterly waves in the lower tropo-
 1650 sphere of North Africa. *Journal of the Atmospheric Sciences*, *29*(1), 77–90.
- 1651 Burpee, R. W. (1974). Characteristics of North African easterly waves during the
 1652 summers of 1968 and 1969. *Journal of the Atmospheric Sciences*, *31*(6), 1556–

- 1570.
- 1653 Byerle, L. A., & Paegle, J. (2002). Description of the Seasonal Cycle of Low-Level
1654 Flows Flanking the Andes and their Interannual Variability. *Meteorologica*, *27*,
1655 71–88.
- 1656 Byrne, M. P., & Zanna, L. (2020, in press). Radiative effects of clouds and water va-
1657 por on an axisymmetric monsoon. *Journal of Climate*.
- 1658 Campetella, C. M., & Vera, C. S. (2002). The influence of the Andes mountains on
1659 the South American low-level flow. *Geophysical Research Letters*, *29*(17), 7:1–
1660 4. doi: 10.1029/2002gl015451
- 1661 Chadwick, R., Boutle, I., & Martin, G. (2013). Spatial patterns of precipitation
1662 change in CMIP5: Why the rich do not get richer in the tropics. *Journal of*
1663 *Climate*, *26*(11), 3803–3822.
- 1664 Chadwick, R., Douville, H., & Skinner, C. B. (2017). Timeslice experiments for
1665 understanding regional climate projections: applications to the tropical hydro-
1666 logical cycle and European winter circulation. *Climate Dynamics*, *49*(9-10),
1667 3011–3029.
- 1668 Chang, P., & Philander, S. G. (1994). A coupled ocean–atmosphere instability of
1669 relevance to the seasonal cycle. *Journal of the Atmospheric Sciences*, *51*(24),
1670 3627–3648.
- 1671 Charney, J. G., & Drazin, P. G. (1961). Propagation of planetary-scale disturbances
1672 from the lower into the upper atmosphere. *Journal of Geophysical Research*,
1673 *66*(1), 83–109. Retrieved from [https://agupubs.onlinelibrary.wiley.com/](https://agupubs.onlinelibrary.wiley.com/doi/abs/10.1029/JZ066i001p00083)
1674 [doi/abs/10.1029/JZ066i001p00083](https://doi.org/10.1029/JZ066i001p00083) doi: 10.1029/JZ066i001p00083
- 1675 Chen, J., & Bordoni, S. (2014). Orographic Effects of the Tibetan Plateau on the
1676 East Asian Summer Monsoon: An Energetic Perspective. *Journal of Climate*,
1677 *27*(8), 3052–3072. doi: 10.1175/JCLI-D-13-00479.1
- 1678 Cheng, H., Edwards, R. L., Broecker, W. S., Denton, G. H., Kong, X., Wang, Y., ...
1679 Wang, X. (2009). Ice Age Terminations. *Science*, *326*(5950), 248–252. doi:
1680 10.1126/science.1177840
- 1681 Cheng, H., Sinha, A., Cruz, F. W., Wang, X., Edwards, R. L., d’Horta, F. M., ...
1682 Auler, A. S. (2013). Climate change patterns in Amazonia and biodiversity.
1683 *Nature Communications*, *4*(1411).
- 1684 Cheng, H., Sinha, A., Wang, X., Cruz, F. W., & Edwards, R. L. (2012). The Global
1685 Paleomonsoon as seen through speleothem records from Asia and the Ameri-
1686 cas. *Climate Dynamics*, *39*, 1045–1062. doi: 10.1007/s00382-012-1363-7
- 1687 Cheng, Y.-M., Thorncroft, C. D., & Kiladis, G. N. (2019). Two contrasting African
1688 easterly wave behaviors. *Journal of the Atmospheric Sciences*, *76*(6), 1753–
1689 1768.
- 1690 Chiang, J. C. H., & Bitz, C. M. (2005). Influence of high latitude ice cover on the
1691 marine Intertropical Convergence Zone. *Climate Dynamics*, *25*(5), 477–496.
1692 doi: 10.1007/s00382-005-0040-5
- 1693 Chiang, J. C. H., Fung, I. Y., Wu, C.-H., Cai, Y., Edman, Jacob, P., Liu, Y., ...
1694 Labrousse, C. A. (2015). Role of seasonal transitions and westerly jets in
1695 East Asian paleoclimate. *Quaternary Science Reviews*, *108*, 111–129. doi:
1696 10.1016/j.quascirev.2014.11.009
- 1697 Chiang, J. C. H., Kong, W., Wu, C. H., & Battisti, D. (2020). Origins of East Asian
1698 Summer Monsoon Seasonality. *Journal of Climate*. Retrieved from [https://](https://doi.org/10.1175/JCLI-D-19-0888.1)
1699 doi.org/10.1175/JCLI-D-19-0888.1 doi: 10.1175/JCLI-D-19-0888.1
- 1700 Chiang, J. C. H., Swenson, L. M., & Kong, W. (2017). Role of seasonal transitions
1701 and the westerlies in the interannual variability of the East Asian summer
1702 monsoon precipitation. *Geophysical Research Letters*, *44*(8), 3788–3795. doi:
1703 10.1002/2017GL072739
- 1704 Chiang, J. C. H., Zebiak, S. E., & Cane, M. A. (2001). Relative roles of elevated
1705 heating and surface temperature gradients in driving anomalous surface winds
1706 over tropical oceans. *Journal of the Atmospheric Sciences*, *58*(11), 1371–1394.
1707

- 1708 Chou, C., & Neelin, J. D. (2001). Mechanisms limiting the southward extent of
 1709 the South American summer monsoon. *Geophysical Research Letters*, *28*(12),
 1710 2433–2436. doi: 10.1029/2000GL012138
- 1711 Chou, C., & Neelin, J. D. (2003). Mechanisms limiting the northward extent of the
 1712 northern summer monsoons over North America, Asia, and Africa. *Journal of*
 1713 *Climate*, *16*(3), 406–425. doi: 10.1175/1520-0442(2003)016<0406:MLTNEO>2.0
 1714 .CO;2
- 1715 Christensen, J., Krishna Kumar, K., Aldrian, E., An, S.-I., Cavalcanti, I., de Cas-
 1716 tro, M., ... Zhou, T. (2013). Climate phenomena and their relevance
 1717 for future regional climate change [Book Section]. In T. Stocker et al.
 1718 (Eds.), *Climate Change 2013: The Physical Science Basis. Contribution of*
 1719 *Working Group I to the Fifth Assessment Report of the Intergovernmen-*
 1720 *tal Panel on Climate Change* (pp. 1217–1308). Cambridge, United King-
 1721 dom and New York, NY, USA: Cambridge University Press. Retrieved from
 1722 www.climatechange2013.org doi: 10.1017/CBO9781107415324.028
- 1723 Cook, K. H. (2000). The South Indian Convergence Zone and Interannual Rainfall
 1724 Variability over Southern Africa. *Journal of Climate*, *13*(21), 3789–3804. doi:
 1725 10.1175/1520-0442(2000)013<3789:TSICZA>2.0.CO;2
- 1726 D’Agostino, R., Bader, J., Bordoni, S., Ferreira, D., & Jungclauss, J. (2019). North-
 1727 ern Hemisphere Monsoon Response to Mid-Holocene Orbital Forcing and
 1728 Greenhouse Gas-Induced Global Warming. *Geophysical Research Letters*, 1–11.
 1729 doi: 10.1029/2018GL081589
- 1730 Dansgaard, W., Johnsen, S. J., Clausen, H. B., Dahl-Jensen, D., Gundestrup, N.,
 1731 Hammer, C., ... others (1993). Evidence for general instability of past climate
 1732 from a 250-kyr ice-core record. *Nature*, *364*(6434), 218–220.
- 1733 Deplazes, G., Lckge, A., Peterson, L. C., Timmermann, A., Hamann, Y., Hughen,
 1734 K. A., ... Haug, G. H. (2013). Links between tropical rainfall and North
 1735 Atlantic climate during the last glacial period. *Nature Geosci*, *6*, 213–217. doi:
 1736 10.1038/ngeo1712
- 1737 Diaz, M., & Boos, W. R. (2019a). Barotropic growth of monsoon depressions. *Quar-*
 1738 *terly Journal of the Royal Meteorological Society*, *145*(719), 824–844.
- 1739 Diaz, M., & Boos, W. R. (2019b). Monsoon depression amplification by moist
 1740 barotropic instability in a vertically sheared environment. *Quarterly Journal of*
 1741 *the Royal Meteorological Society*, *145*(723), 2666–2684. doi: 10.1002/qj.3585
- 1742 Ding, Y., & Chan, J. C. L. (2005). The East Asian summer monsoon: An
 1743 overview. *Meteorology and Atmospheric Physics*, *89*(1), 117–142. doi:
 1744 10.1007/s00703-005-0125-z
- 1745 Dokken, T. M., Nisancioglu, K. H., Li, C., Battisti, D. S., & Kissel, C. (2013).
 1746 Dansgaard-Oeschger cycles: Interactions between ocean and sea ice intrinsic to
 1747 the Nordic seas. *Paleoceanography*, *28*(3), 491–502.
- 1748 Donohoe, A., Marshall, J., Ferreira, D., & Mcgee, D. (2013). The relationship be-
 1749 tween ITCZ location and cross-equatorial atmospheric heat transport: From
 1750 the seasonal cycle to the last glacial maximum. *Journal of Climate*, *26*(11),
 1751 3597–3618. doi: 10.1175/JCLI-D-12-00467.1
- 1752 Duffy, M. L., O’Gorman, P. A., & Back, L. E. (2020). Importance of laplacian
 1753 of low-level warming for the response of precipitation to climate change over
 1754 tropical oceans. *Journal of Climate*, *33*(10), 4403–4417.
- 1755 Egger, J., Weickmann, K., & Hoinka, K.-P. (2007). Angular momentum in the
 1756 global atmospheric circulation. *Reviews of Geophysics*, *45*(4). Retrieved
 1757 from [https://agupubs.onlinelibrary.wiley.com/doi/abs/10.1029/](https://agupubs.onlinelibrary.wiley.com/doi/abs/10.1029/2006RG000213)
 1758 [2006RG000213](https://agupubs.onlinelibrary.wiley.com/doi/abs/10.1029/2006RG000213) doi: 10.1029/2006RG000213
- 1759 Ellis, A. W., Saffell, E. M., & Hawkins, T. W. (2004). A method for defining mon-
 1760 soon onset and demise in the Southwestern USA. *International Journal of Cli-*
 1761 *matology*, *24*(2), 247–265. doi: 10.1002/joc.996
- 1762 Eltahir, E. A., & Gong, C. (1996). Dynamics of Wet and Dry Years in West Africa.

- 1763 *Journal of Climate*, 9, 1030–1042. doi: 10.1175/1520-0442(1996)009%3C1030:
1764 DOWADY%3E2.0.CO;2
- 1765 Emanuel, K. A. (1983a). The Lagrangian parcel dynamics of moist symmetric insta-
1766 bility. *Journal of the Atmospheric Sciences*, 40, 2368–2376.
- 1767 Emanuel, K. A. (1983b). On assessing local conditional symmetric instability from
1768 atmospheric soundings. *Monthly weather review*, 111, 2016–2033.
- 1769 Emanuel, K. A. (1988). Observational evidence of slantwise convective adjustment.
1770 *Monthly weather review*, 116(9), 1805–1816.
- 1771 Emanuel, K. A. (1995). On Thermally Direct Circulations in Moist Atmo-
1772 spheres. *Journal of the Atmospheric Sciences*, 52(9), 1529–1534. doi:
1773 10.1175/1520-0469(1995)052<1529:OTDCIM>2.0.CO;2
- 1774 Emanuel, K. A., Neelin, J. D., & Bretherton, C. S. (1994). On large-scale circula-
1775 tions in convecting atmospheres. *Quarterly Journal of the Royal Meteorological*
1776 *Society*, 120(519), 1111–1143. doi: 10.1002/qj.49712051902
- 1777 Eroglu, D., McRobie, F. H., Ozken, I., Stemler, T., Wyrwoll, K. H., Breitenbach,
1778 S. F., . . . Kurths, J. (2016). See-saw relationship of the Holocene East
1779 Asian-Australian summer monsoon. *Nature Communications*, 7, 1–7. doi:
1780 10.1038/ncomms12929
- 1781 Faulk, S., Mitchell, J., & Bordoni, S. (2017). Effects of Rotation Rate and Seasonal
1782 Forcing on the ITCZ Extent in Planetary Atmospheres. *Journal of the Atmo-*
1783 *spheric Sciences*, 74(3), 665–678. doi: 10.1175/JAS-D-16-0014.1
- 1784 Frierson, D. M., Hwang, Y. T., Fućkar, N. S., Seager, R., Kang, S. M., Donohoe, A.,
1785 . . . Battisti, D. S. (2013). Contribution of ocean overturning circulation to
1786 tropical rainfall peak in the Northern Hemisphere. *Nature Geoscience*, 6(11),
1787 940–944. doi: 10.1038/ngeo1987
- 1788 Frierson, D. M. W. (2007). The Dynamics of Idealized Convection Schemes and
1789 Their Effect on the Zonally Averaged Tropical Circulation. *Journal of the At-*
1790 *mospheric Sciences*, 64(6), 1959–1976. doi: 10.1175/JAS3935.1
- 1791 Frierson, D. M. W., & Hwang, Y. T. (2012). Extratropical influence on ITCZ shifts
1792 in slab ocean simulations of global warming. *Journal of Climate*, 25(2), 720–
1793 733. doi: 10.1175/JCLI-D-11-00116.1
- 1794 Fućkar, N. S., Xie, S.-P., Farneti, R., Maroon, E. A., & Frierson, D. M. (2013). In-
1795 fluence of the extratropical ocean circulation on the intertropical convergence
1796 zone in an idealized coupled general circulation model. *Journal of Climate*,
1797 26(13), 4612–4629. doi: 10.1175/JCLI-D-12-00294.1
- 1798 Gadgil, S. (2018). The monsoon system: Land-sea breeze or the ITCZ? *Journal of*
1799 *Earth System Science*, 127(1), 1–29. doi: 10.1007/s12040-017-0916-x
- 1800 Geen, R., Lambert, F. H., & Vallis, G. K. (2018). Regime Change Behavior Dur-
1801 ing Asian Monsoon Onset. *Journal of Climate*, 31, 3327–3348. Retrieved
1802 from <http://journals.ametsoc.org/doi/10.1175/JCLI-D-17-0118.1> doi:
1803 10.1175/JCLI-D-17-0118.1
- 1804 Geen, R., Lambert, F. H., & Vallis, G. K. (2019). Processes and Timescales in On-
1805 set and Withdrawal of ‘Aquaplanet Monsoons’. *J. Atmos. Sci.*, 76, 2357–2373.
1806 doi: 10.1175/JAS-D-18-0214.1
- 1807 Godbole, R. V. (1977). The composite structure of the monsoon depression. *Tellus*,
1808 29(1), 25–40.
- 1809 Goswami, B. N., & Ajaya Mohan, R. S. (2001). Intraseasonal Oscillations and In-
1810 terannual Variability of the Indian Summer Monsoon. *Journal of Climate*, 14,
1811 1180–1198. doi: 10.1175/1520-0442(2001)014<1180:IOAIVO>2.0.CO;2
- 1812 Green, B., & Marshall, J. (2017). Coupling of Trade Winds with Ocean Circulation
1813 Damps ITCZ Shifts. *Journal of Climate*, 30(12), 4395–4411. Retrieved from
1814 <https://doi.org/10.1175/JCLI-D-16-0818.1> doi: 10.1175/JCLI-D-16-0818
1815 .1
- 1816 Gruber, A., Su, X., Kanamitsu, M., & Schemm, J. (2000). The Compari-
1817 son of Two Merged Rain Gauge-Satellite Precipitation Datasets. *Bul-*

- 1818 *letin of the American Meteorological Society*, 81(11), 2631-2644. doi:
1819 10.1175/1520-0477(2000)081<2631:TCOTMR>2.3.CO;2
- 1820 Hagos, S. M., & Cook, K. H. (2007). Dynamics of the West African monsoon jump.
1821 *Journal of Climate*, 20(21), 5264–5284. doi: 10.1175/2007JCLI1533.1
- 1822 Halley, E. (1686). An Historical Account of the Trade Winds, and Monsoons,
1823 Observable in the Seas between and Near the Tropicks, with an Attempt to
1824 Assign the Phisical Cause of the Said Winds, By E. Halley. *Philosophical*
1825 *Transactions of the Royal Society of London*, 16(179-191), 153–168. doi:
1826 10.1098/rstl.1686.0026
- 1827 Harrop, B. E., Lu, J., & Leung, L. R. (2019). Sub-cloud moist entropy curvature as
1828 a predictor for changes in the seasonal cycle of tropical precipitation. *Climate*
1829 *Dynamics*, 53(5-6), 3463–3479.
- 1830 Hartmann, D. L., & Michelsen, M. L. (1989). Intraseasonal periodicities in Indian
1831 rainfall. *Journal of the Atmospheric Sciences*, 46(18), 2838–2862.
- 1832 Hawcroft, M., Haywood, J. M., Collins, M., Jones, A., Jones, A. C., & Stephens, G.
1833 (2017). Southern Ocean albedo, inter-hemispheric energy transports and the
1834 double ITCZ: Global impacts of biases in a coupled model. *Climate Dynamics*,
1835 48(7-8), 2279–2295.
- 1836 Heinrich, H. (1988). Origin and consequences of cyclic ice rafting in the north-
1837 east Atlantic Ocean during the past 130,000 years. *Quaternary research*, 29(2),
1838 142–152.
- 1839 Held, I. M. (2005). The gap between simulation and understanding in climate
1840 modeling. *Bulletin of the American Meteorological Society*, 86(11), 1609-
1841 1614. Retrieved from <https://doi.org/10.1175/BAMS-86-11-1609> doi:
1842 10.1175/BAMS-86-11-1609
- 1843 Hemming, S. R. (2004). Heinrich events: Massive late Pleistocene detritus layers
1844 of the North Atlantic and their global climate imprint. *Reviews of Geophysics*,
1845 42(1).
- 1846 Hendon, H. H., & Liebmann, B. (1990). A Composite Study of Onset of the Aus-
1847 tralian Summer Monsoon. *Journal of Atmospheric Sciences*, 47(18), 2227–
1848 2240. doi: 10.1175/1520-0469(1990)047<2227:ACS000>2.0.CO;2
- 1849 Hide, R. (1969). Dynamics of the Atmospheres of the Major Planets with an Ap-
1850 pendix on the Viscous Boundary Layer at the Rigid Bounding Surface of an
1851 Electrically-Conducting Rotation Fluid in the Presence of a Magnetic Field.
1852 *J. Atmos. Sci.*, 26, 841–853. doi: 10.1175/1520-0469(1969)026%3C0841:
1853 DOTAOT%3E2.0.CO;2
- 1854 Hilgenbrink, C. C., & Hartmann, D. L. (2018). The response of Hadley circulation
1855 extent to an idealized representation of poleward ocean heat transport in an
1856 aquaplanet GCM. *Journal of Climate*, 31, 9753–9770.
- 1857 Hill, S. A. (2019). Theories for Past and Future Monsoon Rainfall Changes. *Current*
1858 *Climate Change Reports*, 5, 160–171.
- 1859 Hill, S. A., Bordoni, S., & Mitchell, J. L. (2019). Hadley cell emergence and extent
1860 in axisymmetric, nearly inviscid, planetary atmospheres. *J. Atmos. Sci.*
- 1861 Hill, S. A., Ming, Y., & Held, I. M. (2015). Mechanisms of forced tropical meridional
1862 energy flux change. *Journal of Climate*, 28, 1725–1742. doi: 10.1175/JCLI-D
1863 -14-00165.1
- 1864 Hill, S. A., Ming, Y., Held, I. M., & Zhao, M. (2017). A moist static energy budget-
1865 based analysis of the Sahel rainfall response to uniform oceanic warming. *Jour-
1866 nal of Climate*, 30(15), 5637–5660. doi: 10.1175/JCLI-D-16-0785.1
- 1867 Hill, S. A., Ming, Y., & Zhao, M. (2018). Robust Responses of the Hydrological Cy-
1868 cle to Global Warming. *Journal of Climate*, 1931, 9793–9814. doi: 10.1175/
1869 JCLI-D-18-0238.1
- 1870 Holton, J. R., Wallace, J. M., & Young, J. (1971). On boundary layer dynamics and
1871 the ITCZ. *Journal of the Atmospheric Sciences*, 28(2), 275–280.
- 1872 Houze Jr, R. A. (2018). 100 years of research on mesoscale convective systems. *Me-*

- 1873 *eteorological Monographs*, 59, 17–1.
- 1874 Huffman, G. J., Adler, R. F., Morrissey, M. M., Bolvin, D. T., Curtis, S., Joyce, R.,
1875 ... Susskind, J. (2001). Global Precipitation at One-Degree Daily Resolution
1876 from Multisatellite Observations. *Journal of Hydrometeorology*, 2, 36–50.
- 1877 Huffman, G. J. and D. T. Bolvin and R. F. Adler. (2016). *GPCP Version 1.2 One-*
1878 *Degree Daily Precipitation Data Set*. Boulder CO: Research Data Archive
1879 at the National Center for Atmospheric Research, Computational and Infor-
1880 mation Systems Laboratory. Retrieved from [https://doi.org/10.5065/](https://doi.org/10.5065/D6D50K46)
1881 [D6D50K46](https://doi.org/10.5065/D6D50K46)
- 1882 Hui, K., & Bordoni, S. (submitted.). Influence of Continental Geometry on the On-
1883 set and Spatial Distribution of Monsoonal Precipitation. *J. Atmos. Sci.*.
- 1884 Hunt, K. M., Turner, A. G., Inness, P. M., Parker, D. E., & Levine, R. C. (2016).
1885 On the structure and dynamics of Indian monsoon depressions. *Monthly*
1886 *Weather Review*, 144(9), 3391–3416.
- 1887 Hurley, J. V., & Boos, W. R. (2013). Interannual variability of monsoon precipita-
1888 tion and local subcloud equivalent potential temperature. *Journal of Climate*,
1889 26(23), 9507–9527. doi: 10.1175/JCLI-D-12-00229.1
- 1890 Hurley, J. V., & Boos, W. R. (2015). A global climatology of monsoon low-pressure
1891 systems. *Quarterly Journal of the Royal Meteorological Society*, 141(689),
1892 1049–1064. doi: 10.1002/qj.2447
- 1893 Japan Meteorological Agency/Japan. (2013). *JRA-55: Japanese 55-year Reanalysis,*
1894 *Monthly Means and Variances*. Boulder CO: Research Data Archive at the
1895 National Center for Atmospheric Research, Computational and Information
1896 Systems Laboratory. Retrieved from <https://doi.org/10.5065/D60G3H5B>
- 1897 Jeevanjee, N., Hassanzadeh, P., Hill, S., & Sheshadri, A. (2017). A perspective
1898 on climate model hierarchies. *Journal of Advances in Modeling Earth Systems*,
1899 9(4), 1760–1771. doi: 10.1002/2017MS001038
- 1900 Jiang, X., Adames, . F., Zhao, M., Waliser, D., & Maloney, E. (2018). A unified
1901 moisture mode framework for seasonality of the Madden-Julian oscillation.
1902 *Journal of Climate*, 31(11), 4215–4224. Retrieved from [https://doi.org/](https://doi.org/10.1175/JCLI-D-17-0671.1)
1903 [10.1175/JCLI-D-17-0671.1](https://doi.org/10.1175/JCLI-D-17-0671.1) doi: 10.1175/JCLI-D-17-0671.1
- 1904 Jourdain, N. C., Gupta, A. S., Taschetto, A. S., Ummenhofer, C. C., Moise, A. F., &
1905 Ashok, K. (2013). The Indo-Australian monsoon and its relationship to ENSO
1906 and IOD in reanalysis data and the CMIP3/CMIP5 simulations. *Climate*
1907 *Dynamics*, 41(11), 3073–3102. Retrieved from [https://doi.org/10.1007/](https://doi.org/10.1007/s00382-013-1676-1)
1908 [s00382-013-1676-1](https://doi.org/10.1007/s00382-013-1676-1) doi: 10.1007/s00382-013-1676-1
- 1909 Jouzel, J., Masson-Delmotte, V., Cattani, O., Dreyfus, G., Falourd, S., Hoffmann,
1910 G., ... Wolff, E. W. (2007). Orbital and Millennial Antarctic Climate
1911 Variability over the Past 800,000 Years. *Science*, 317(5839), 793–796. doi:
1912 [10.1126/science.1141038](https://doi.org/10.1126/science.1141038)
- 1913 Kang, S. M. (2020). Extratropical Influence on the Tropical Rainfall Distribution.
1914 *Current Climate Change Reports*, 6, 24–36.
- 1915 Kang, S. M., Frierson, D. M. W., & Held, I. M. (2009). The Tropical Response
1916 to Extratropical Thermal Forcing in an Idealized GCM: The Importance of
1917 Radiative Feedbacks and Convective Parameterization. *Journal of the Atmo-*
1918 *spheric Sciences*, 66(9), 2812–2827. doi: 10.1175/2009jas2924.1
- 1919 Kang, S. M., & Held, I. M. (2012). Tropical precipitation, SSTs and the surface
1920 energy budget: A zonally symmetric perspective. *Climate Dynamics*, 38(9-10),
1921 1917–1924. doi: 10.1007/s00382-011-1048-7
- 1922 Kang, S. M., Held, I. M., Frierson, D. M., & Zhao, M. (2008). The response of the
1923 ITCZ to extratropical thermal forcing: Idealized slab-ocean experiments with a
1924 GCM. *Journal of Climate*, 21(14), 3521–3532. doi: 10.1175/2007JCLI2146.1
- 1925 Kang, S. M., Shin, Y., & Xie, S.-P. (2018). Extratropical forcing and tropical rainfall
1926 distribution: Energetics framework and ocean Ekman advection. *npj Climate*
1927 *and Atmospheric Science*, 1(1), 1–10.

- 1928 Kanner, L. C., Burns, S. J., Cheng, H., & Edwards, R. L. (2012). High-Latitude
1929 Forcing of the South American Summer Monsoon During the Last Glacial. *Sci-*
1930 *ence*, *335*(6068), 570–573. doi: 10.1126/science.1213397
- 1931 Kay, J. E., Wall, C., Yettella, V., Medeiros, B., Hannay, C., Caldwell, P., & Bitz,
1932 C. (2016). Global climate impacts of fixing the Southern Ocean shortwave
1933 radiation bias in the Community Earth System Model (CESM). *Journal of*
1934 *Climate*, *29*(12), 4617–4636.
- 1935 Kerns, B., & Chen, S. S. (2020). A 20-year climatology of Madden-Julian Oscillation
1936 convection: Large-scale precipitation tracking from TRMM-GPM rainfall. *In*
1937 *press, J. Geophys. Res. Atmos.*
- 1938 Kiladis, G. N., Thorncroft, C. D., & Hall, N. M. J. (2006). Three-Dimensional Struc-
1939 ture and Dynamics of African Easterly Waves. Part I: Observations. *Journal of*
1940 *the Atmospheric Sciences*, *63*(9), 2212–2230. doi: 10.1175/JAS3741.1
- 1941 Kiladis, G. N., Wheeler, M. C., Haertel, P. T., Straub, K. H., & Roundy, P. E.
1942 (2009). Convectively coupled equatorial waves. *Reviews of Geophysics*,
1943 *47*(RG2003).
- 1944 Kobayashi, S., Ota, Y., Harada, Y., Ebata, A., Moriya, M., Onoda, H., . . . Taka-
1945 hashi, K. (2015). The JRA-55 Reanalysis: General Specifications and
1946 Basic Characteristics. *J. Meteorol. Soc. Jpn.*, *93*(1), 5–48. doi: 10.2151/
1947 jmsj.2015-001
- 1948 Kodama, Y. (1992). Large-Scale Common Features of Subtropical Precipitation
1949 Zones (the Baiu Frontal Zone, the SPCZ, and the SACZ). Part I: Character-
1950 istics of Subtropical Frontal Zones. *Journal of the Meteorological Society of*
1951 *Japan*, *70*(4), 813–836. doi: 10.2151/jmsj1965.70.4.813
- 1952 Kong, W., & Chiang, J. C. H. (2020). Interaction of the Westerlies with the Tibetan
1953 Plateau in Determining the Mei-Yu Termination. *Journal of Climate*, *33*(1),
1954 339–363. doi: 10.1175/JCLI-D-19-0319.1
- 1955 Kong, W., Swenson, L. M., & Chiang, J. C. H. (2017). Seasonal transitions and the
1956 westerly jet in the Holocene East Asian summer monsoon. *Journal of Climate*,
1957 *30*(9), 3343–3365. doi: 10.1175/JCLI-D-16-0087.1
- 1958 Kothawale, D., & Kumar, K. R. (2002). Tropospheric temperature variation over In-
1959 dia and links with the Indian summer monsoon: 1971–2000. *Mausam*, *53*, 289–
1960 308.
- 1961 Lea, D. W., Pak, D. K., Peterson, L. C., & Hughen, K. A. (2003). Temperatures
1962 over the Last Glacial Termination Synchronicity of Tropical and High-Latitude
1963 Atlantic Temperatures over the Last Glacial Termination. *Science*, *301*, 1361–
1964 1364. doi: 10.1126/science.1088470
- 1965 Lebel, T. (2003). Seasonal cycle and interannual variability of the Sahelian rainfall
1966 at hydrological scales. *Journal of Geophysical Research*, *108*(D8), 8389. doi: 10
1967 .1029/2001JD001580,
- 1968 Lee, J.-Y., Wang, B., Wheeler, M. C., Fu, X., Waliser, D. E., & Kang, I.-S. (2013).
1969 Real-time multivariate indices for the boreal summer intraseasonal oscillation
1970 over the Asian summer monsoon region. *Climate Dynamics*, *40*(1), 493–
1971 509. Retrieved from <https://doi.org/10.1007/s00382-012-1544-4> doi:
1972 10.1007/s00382-012-1544-4
- 1973 Lenters, J. D., & Cook, K. H. (1997). On the Origin of the Bolivian High and Related
1974 Circulation Features of the South American Climate. *Journal of the At-*
1975 *mospheric Sciences*, *54*, 656–678. doi: 10.1175/1520-0469(1997)054%3C0656:
1976 OTOOTB%3E2.0.CO;2
- 1977 Levine, X. J., & Schneider, T. (2011). Response of the Hadley Circulation to
1978 Climate Change in an Aquaplanet GCM Coupled to a Simple Representa-
1979 tion of Ocean Heat Transport. *Journal of the Atmospheric Sciences*, *68*(4),
1980 769–783. Retrieved from <https://doi.org/10.1175/2010JAS3553.1> doi:
1981 10.1175/2010JAS3553.1
- 1982 Levins, R. (1966). The strategy of model building in population biology. *American*

- 1983 *Scientist*, 54(4), 421–431.
- 1984 Levy, G., & Battisti, D. S. (1995). The symmetric stability and the low level equator-
1985 rial flow. *Global Atmosphere-Ocean System*, 3(4), 341–354.
- 1986 Liebmann, B., & Hendon, H. H. (1990). Synoptic-scale disturbances near the equator.
1987 *Journal of the Atmospheric Sciences*, 47(12), 1463–1479.
- 1988 Lindzen, R. S., & Hou, A. Y. (1988). Hadley Circulations for Zonally Averaged
1989 Heating Centred off the Equator. *J. Atmos. Sci.*, 45(17), 2416–2427.
- 1990 Lindzen, R. S., & Nigam, S. (1987). On the role of sea surface temperature gradients
1991 in forcing low-level winds and convergence in the tropics. *Journal of the Atmo-*
1992 *spheric Sciences*, 44(17), 2418–2436.
- 1993 Linho, L. H., Huang, X., & Lau, N. C. (2008). Winter-to-spring transition in east
1994 Asia: A planetary-scale perspective of the south China spring rain onset. *Jour-*
1995 *nal of Climate*, 21(13), 3081–3096. doi: 10.1175/2007JCLI1611.1
- 1996 Liu, X., & Battisti, D. S. (2015). The influence of orbital forcing of tropical in-
1997 solation on the climate and isotopic composition of precipitation in South
1998 America. *Journal of Climate*, 28(12), 4841–4862.
- 1999 Liu, X., Battisti, D. S., & Donohoe, A. (2017). Tropical precipitation and cross-
2000 equatorial ocean heat transport during the mid-Holocene. *Journal of Climate*,
2001 30(10), 3529–3547. doi: 10.1175/JCLI-D-16-0502.1
- 2002 Madden, R. A., & Julian, P. R. (1971). Detection of a 40–50 day oscillation in the
2003 zonal wind in the tropical Pacific. *Journal of the Atmospheric Sciences*, 28(5),
2004 702–708.
- 2005 Madden, R. A., & Julian, P. R. (1972). Description of global-scale circulation cells
2006 in the tropics with a 40–50 day period. *Journal of the Atmospheric Sciences*,
2007 29(6), 1109–1123.
- 2008 Maher, P., Gerber, E. P., Medeiros, B., Merlis, T. M., Sherwood, S., Sheshadri, A.,
2009 ... ZuritaGotor, P. (2019). Model Hierarchies for Understanding Atmo-
2010 spheric Circulation. *Reviews of Geophysics*, 2018RG000607. Retrieved from
2011 <https://onlinelibrary.wiley.com/doi/abs/10.1029/2018RG000607> doi:
2012 10.1029/2018RG000607
- 2013 Mao, J., & Wu, G. (2007). Interannual variability in the onset of the summer mon-
2014 soon over the Eastern Bay of Bengal. *Theoretical and Applied Climatology*,
2015 89(3-4), 155–170. doi: 10.1007/s00704-006-0265-1
- 2016 Marengo, J. A., Liebmann, B., Grimm, A. M., Misra, V., Silva Dias, P. L., Cav-
2017 alcanti, I. F., ... Alves, L. M. (2012). Recent developments on the South
2018 American monsoon system. *International Journal of Climatology*, 32(1), 1–21.
2019 doi: 10.1002/joc.2254
- 2020 Maroon, E. A., Frierson, D. M., & Battisti, D. S. (2015). The tropical precipitation
2021 response to Andes topography and ocean heat fluxes in an aquaplanet model.
2022 *Journal of Climate*, 28(1), 381–398. doi: 10.1175/JCLI-D-14-00188.1
- 2023 Marshall, J., Donohoe, A., Ferreira, D., & McGee, D. (2014). The ocean’s role in
2024 setting the mean position of the Inter-Tropical Convergence Zone. *Climate Dy-*
2025 *namics*, 42(7-8), 1967–1979. doi: 10.1007/s00382-013-1767-z
- 2026 Martin, G. M., Chevuturi, A., Comer, R. E., Dunstone, N. J., Scaife, A. A., &
2027 Zhang, D. (2019). Predictability of South China Sea Summer Mon-
2028 soon Onset. *Advances in Atmospheric Sciences*, 36(3), 253–260. doi:
2029 10.1007/s00376-018-8100-z
- 2030 Matsuno, T. (1966). Quasi-Geostrophic Motions in the Equatorial Area. *J. Meteor.*
2031 *Soc. Japan*, 44(1), 25–43. doi: 10.2151/jmsj1965.44.1.25
- 2032 McGee, D., Donohoe, A., Marshall, J., & Ferreira, D. (2014). Changes in ITCZ
2033 location and cross-equatorial heat transport at the Last Glacial Maximum,
2034 Heinrich Stadial 1, and the mid-Holocene. *Earth and Planetary Science Let-*
2035 *ters*, 390, 69–79. doi: 10.1016/j.epsl.2013.12.043
- 2036 Merlis, T. M., Schneider, T., Bordoni, S., & Eisenman, I. (2013). Hadley cir-
2037 culation response to orbital precession. Part I: Aquaplanets. *Journal of Climate*,

- 2038 26, 740–753. doi: 10.1175/JCLI-D-11-00716.1
- 2039 Mesoscale Atmospheric Processes Branch/Laboratory for Atmospheres/Earth Sci-
- 2040 ences Division/Science and Exploration Directorate/Goddard Space Flight
- 2041 Center/NASA, and Earth System Science Interdisciplinary Center/University
- 2042 of Maryland. (2018). *GPCP Version 2.3 Monthly Analysis Product*. Boul-
- 2043 der CO: Research Data Archive at the National Center for Atmospheric Re-
- 2044 search, Computational and Information Systems Laboratory. Retrieved from
- 2045 <https://doi.org/10.5065/D6SN07QX>
- 2046 Mitchell, T. P., & Wallace, J. M. (1992). The Annual Cycle in Equatorial Convec-
- 2047 tion and Sea Surface Temperature. *Journal of Climate*, 5(10), 1140–1156. doi:
- 2048 10.1175/1520-0442(1992)005<1140:TACIEC>2.0.CO;2
- 2049 Molnar, P., Boos, W. R., & Battisti, D. S. (2010). Orographic controls on cli-
- 2050 mate and paleoclimate of Asia: thermal and mechanical roles for the Tibetan
- 2051 Plateau. *Annual Review of Earth and Planetary Sciences*, 38(1), 77–102. doi:
- 2052 10.1146/annurev-earth-040809-152456
- 2053 Mooley, D. A. (1973). Some aspects of Indian monsoon depression and associated
- 2054 rainfall. *Monthly Weather Review*, 101, 271–280.
- 2055 Mulitza, S., Prange, M., Stuut, J.-B., Zabel, M., von Dobebeck, T., Itambi, A. C.,
- 2056 ... Wefer, G. (2008). Sahel megadroughts triggered by glacial slow-
- 2057 downs of Atlantic meridional overturning. *Paleoceanography*, 23(4). doi:
- 2058 10.1029/2008PA001637
- 2059 Nicholson, S. E. (2009). On the factors modulating the intensity of the tropical rain-
- 2060 belt over West Africa. *International Journal of Climatology*, 29(5), 673–689.
- 2061 Nicholson, S. E., Barilon, A. I., Challa, M., & Baum, J. (2007). Wave Activity on
- 2062 the Tropical Easterly Jet. *Journal of the Atmospheric Sciences*, 64(7), 2756–
- 2063 2763. doi: 10.1175/JAS3946.1
- 2064 Nie, J., Boos, W. R., & Kuang, Z. (2010). Observational evaluation of a convective
- 2065 quasi-equilibrium view of monsoons. *Journal of Climate*, 23(16), 4416–4428.
- 2066 doi: 10.1175/2010JCLI3505.1
- 2067 Parthasarathy, B., Munot, A. A., & Kothawale, D. R. (1994). All-India monthly and
- 2068 seasonal rainfall series: 1871–1993. *Theoretical and Applied Climatology*, 49(4),
- 2069 217–224. doi: 10.1007/BF00867461
- 2070 Pausata, F. S., Battisti, D. S., Nisancioglu, K. H., & Bitz, C. M. (2011). Chinese
- 2071 stalagmite $\delta^{18}\text{O}$ controlled by changes in the Indian monsoon during a simu-
- 2072 lated Heinrich event. *Nature Geoscience*, 4(7), 474.
- 2073 Philander, S., Gu, D., Lambert, G., Li, T., Halpern, D., Lau, N., & Pacanowski, R.
- 2074 (1996). Why the ITCZ is Mostly North of the Equator. *Journal of Climate*,
- 2075 9(12), 2958–2972.
- 2076 Plumb, R. A., & Hou, A. Y. (1992). The response of a zonally symmetric atmo-
- 2077 sphere to subtropical thermal forcing - Threshold behavior. *Journal of the*
- 2078 *Atmospheric Sciences*, 49(19), 1790–1799. doi: 10.1175/1520-0469(1992)
- 2079 049<1790:TROAZS>2.0.CO;2
- 2080 Privé, N. C., & Plumb, R. A. (2007a). Monsoon Dynamics with Interactive Forc-
- 2081 ing. Part I: Axisymmetric Studies. *Journal of the Atmospheric Sciences*, 64(5),
- 2082 1417–1430. doi: 10.1175/JAS3916.1
- 2083 Privé, N. C., & Plumb, R. A. (2007b). Monsoon Dynamics with Interactive Forc-
- 2084 ing. Part II: Impact of Eddies and Asymmetric Geometries. *Journal of the At-*
- 2085 *mospheric Sciences*, 64(5), 1431–1442. doi: 10.1175/JAS3917.1
- 2086 Rao, V. B., Cavalcanti, I. F. A., & Hada, K. (1996). Annual variation of rain-
- 2087 fall over Brazil and water vapor characteristics over South America. *Jour-*
- 2088 *nal of Geophysical Research: Atmospheres*, 101(D21), 26539–26551. doi:
- 2089 10.1029/96JD01936
- 2090 Reed, R. J., Norquist, D. C., & Recker, E. E. (1977). The structure and properties
- 2091 of African wave disturbances as observed during Phase III of GATE. *Monthly*
- 2092 *Weather Review*, 105(3), 317–333.

- 2093 Roberts, W. H., Valdes, P. J., & Singarayer, J. S. (2017). Can energy fluxes be used
2094 to interpret glacial/interglacial precipitation changes in the tropics? *Geophysical*
2095 *Research Letters*, *44*(12), 6373–6382. doi: 10.1002/2017GL073103
- 2096 Rodwell, M. J., & Hoskins, B. J. (2001). Subtropical anticyclones and summer mon-
2097 soons. *Journal of Climate*, *14*(15), 3192–3211. doi: 10.1175/1520-0442(2001)
2098 014(3192:SAASM)2.0.CO;2
- 2099 Roehrig, R., Bouniol, D., Guichard, F., Hourdin, F., & Redelsperger, J.-L. (2013).
2100 The Present and Future of the West African Monsoon: A Process-Oriented
2101 Assessment of CMIP5 Simulations along the AMMA Transect. *Journal of*
2102 *Climate*, *26*(17), 6471–6505. Retrieved from [https://doi.org/10.1175/
2103 JCLI-D-12-00505.1](https://doi.org/10.1175/JCLI-D-12-00505.1) doi: 10.1175/JCLI-D-12-00505.1
- 2104 Roundy, P. E., & Frank, W. M. (2004). A climatology of waves in the equatorial re-
2105 gion. *Journal of the Atmospheric Sciences*, *61*(17), 2105–2132.
- 2106 Sampe, T., & Xie, S.-P. (2010). Large-scale dynamics of the Meiyu-Baiu rainband:
2107 Environmental forcing by the westerly jet. *Journal of Climate*, *23*(1), 113–134.
2108 doi: 10.1175/2009JCLI3128.1
- 2109 Schneider, T. (2017). Feedback of Atmosphere-Ocean Coupling on Shifts of the
2110 Intertropical Convergence Zone. *Geophysical Research Letters*, *44*(22), 11,644-
2111 11,653. Retrieved from [https://agupubs.onlinelibrary.wiley.com/doi/
2112 abs/10.1002/2017GL075817](https://agupubs.onlinelibrary.wiley.com/doi/abs/10.1002/2017GL075817) doi: 10.1002/2017GL075817
- 2113 Schneider, T., Bischoff, T., & Haug, G. H. (2014). Migrations and dynamics of
2114 the Intertropical Convergence Zone. *Nature*, *513*(7516), 45–53. doi: 10.1038/
2115 nature13636
- 2116 Schneider, T., & Bordoni, S. (2008). Eddy-Mediated Regime Transitions in
2117 the Seasonal Cycle of a Hadley Circulation and Implications for Monsoon
2118 Dynamics. *Journal of the Atmospheric Sciences*, *65*(1), 915–934. doi:
2119 10.1175/2007JAS2415.1
- 2120 Schneider, T., O’Gorman, P., & Levine, X. (2010). Water vapor and the dynamics of
2121 climate changes. *Reviews of Geophysics*(48), 1–22. doi: 10.1029/2009RG000302
2122 .1.INTRODUCTION
- 2123 Schumacher, C., & Houze Jr, R. A. (2003). Stratiform rain in the tropics as seen by
2124 the TRMM precipitation radar. *Journal of Climate*, *16*(11), 1739–1756.
- 2125 Schwendike, J., Govekar, P., Reeder, M. J., Wardle, R., Berry, G. J., & Jakob, C.
2126 (2014). Local partitioning of the overturning circulation in the tropics and
2127 the connection to the Hadley and Walker circulations. *Journal of Geophysical*
2128 *Research*, *119*(3), 1322–1339. doi: 10.1002/2013JD020742
- 2129 Seo, J., Kang, S. M., & Merlis, T. M. (2017). A model intercomparison of the trop-
2130 ical precipitation response to a CO₂ doubling in aquaplanet simulations. *Geo-*
2131 *physical Research Letters*, *44*(2), 993-1000. Retrieved from [https://agupubs
2132 .onlinelibrary.wiley.com/doi/abs/10.1002/2016GL072347](https://agupubs.onlinelibrary.wiley.com/doi/abs/10.1002/2016GL072347) doi: 10.1002/
2133 2016GL072347
- 2134 Seth, A., Giannini, A., Rojas, M., Rauscher, S. A., Bordoni, S., Singh, D., & Ca-
2135 margo, S. J. (2019, Jun 01). Monsoon responses to climate changes—
2136 connecting past, present and future. *Current Climate Change Reports*, *5*(2),
2137 63–79. Retrieved from <https://doi.org/10.1007/s40641-019-00125-y> doi:
2138 10.1007/s40641-019-00125-y
- 2139 Shaw, T. A. (2014). On the Role of Planetary-Scale Waves in the Abrupt Seasonal
2140 Transition of the Northern Hemisphere General Circulation. *Journal of the At-*
2141 *mospheric Sciences*, *71*(5), 1724–1746. doi: 10.1175/JAS-D-13-0137.1
- 2142 Shaw, T. A., & Voigt, A. (2015). Tug of war on summertime circulation between
2143 radiative forcing and sea surface warming. *Nature Geoscience*, *8*(7), 560–566.
2144 doi: 10.1038/ngeo2449
- 2145 Shekhar, R., & Boos, W. R. (2016). Improving energy-based estimates of monsoon
2146 location in the presence of proximal deserts. *Journal of Climate*, *29*(13), 4741–
2147 4761. doi: 10.1175/JCLI-D-15-0747.1

- 2148 Shekhar, R., & Boos, W. R. (2017). Weakening and shifting of the Saharan shallow
 2149 meridional circulation during wet years of the West African monsoon. *Journal*
 2150 *of Climate*, *30*(18), 7399–7422.
- 2151 Shi, X., Lohmann, G., Sidorenko, D., & Yang, H. (2020). Early-Holocene simu-
 2152 lations using different forcings and resolutions in AWI-ESM. *The Holocene*,
 2153 *30*(7), 996–1015. doi: 10.1177/0959683620908634
- 2154 Sikka, D. (1978). Some aspects of the life history, structure and movement of mon-
 2155 soon depressions. In *Monsoon dynamics* (pp. 1501–1529). Springer.
- 2156 Sikka, D. R., & Gadgil, S. (1980). On the Maximum Cloud Zone and the
 2157 ITCZ over Indian, Longitudes during the Southwest Monsoon. *Monthly*
 2158 *Weather Review*, *108*(11), 1840–1853. Retrieved from [https://doi.org/](https://doi.org/10.1175/1520-0493(1980)108<1840:OTMCZA>2.0.CO;2)
 2159 [10.1175/1520-0493\(1980\)108<1840:OTMCZA>2.0.CO;2](https://doi.org/10.1175/1520-0493(1980)108<1840:OTMCZA>2.0.CO;2) doi: 10.1175/
 2160 [10.1175/1520-0493\(1980\)108<1840:OTMCZA>2.0.CO;2](https://doi.org/10.1175/1520-0493(1980)108<1840:OTMCZA>2.0.CO;2)
- 2161 Simpson, G. (1921). The South-West monsoon. *Quarterly Journal of the Royal Me-*
 2162 *teorological Society*, *47*(199), 151–171.
- 2163 Singh, M. S. (2019). Limits on the extent of the solstitial Hadley Cell: The role of
 2164 planetary rotation. *Journal of Atmospheric Sciences*.
- 2165 Smyth, J. E., Hill, S. A., & Ming, Y. (2018). Simulated Responses of the West
 2166 African Monsoon and Zonal-Mean Tropical Precipitation to Early Holocene
 2167 Orbital Forcing. *Geophysical Research Letters*(Figure 1), 49–57. doi:
 2168 [10.1029/2018GL080494](https://doi.org/10.1029/2018GL080494)
- 2169 Sobel, A., & Maloney, E. (2013). Moisture Modes and the Eastward Propagation
 2170 of the MJO. *Journal of the Atmospheric Sciences*, *70*(1), 187–192. Retrieved
 2171 from <https://doi.org/10.1175/JAS-D-12-0189.1> doi: 10.1175/JAS-D-12-
 2172 -0189.1
- 2173 Sperber, K. R., Annamalai, H., Kang, I.-S., Kitoh, A., Moise, A., Turner, A., ...
 2174 Zhou, T. (2013). The Asian summer monsoon: An intercomparison of CMIP5
 2175 vs. CMIP3 simulations of the late 20th century. *Climate Dynamics*, *41*(9),
 2176 2711–2744. Retrieved from <https://doi.org/10.1007/s00382-012-1607-6>
 2177 doi: 10.1007/s00382-012-1607-6
- 2178 Stevens, D. E. (1983). On symmetric stability and instability of zonal mean flows
 2179 near the equator. *Journal of the Atmospheric Sciences*, *40*(4), 882–893.
- 2180 Sultan, B., & Janicot, S. (2003). The West African monsoon dynamics. Part II: The
 2181 preonset and onset of the summer monsoon. *Journal of climate*, *16*(21), 3407–
 2182 3427. doi: 10.1175/1520-0442(2003)016<3407:TWAMDP>2.0.CO;2
- 2183 Svensson, A., Andersen, K. K., Bigler, M., Clausen, H. B., Dahl-Jensen, D., Davies,
 2184 S. M., ... Vinther, B. M. (2008). A 60 000 year Greenland stratigraphic ice
 2185 core chronology. *Climate of the Past*, *4*(1), 47–57. doi: 10.5194/cp-4-47-2008
- 2186 Takahashi, K. (2005). The annual cycle of heat content in the Peru current region.
 2187 *Journal of Climate*, *18*(23), 4937–4954. doi: 10.1175/JCLI3572.1
- 2188 Takahashi, K., & Battisti, D. S. (2007). Processes Controlling the Mean Tropical
 2189 Pacific Precipitation Pattern. Part I: The Andes and the Eastern Pacific ITCZ.
 2190 *Journal of Climate*, *20*(14), 3434–3451. doi: 10.1175/jcli4198.1
- 2191 Tomas, R. A., & Webster, P. J. (1997). The role of inertial instability in determin-
 2192 ing the location and strength of near-equatorial convection. *Quarterly Journal*
 2193 *of the Royal Meteorological Society*, *123*(542), 1445–1482.
- 2194 Trenberth, K. E., Stepaniak, D. P., & Caron, J. M. (2000). The global mon-
 2195 soon as seen through the divergent atmospheric circulation. *Journal of*
 2196 *Climate*, *13*(22), 3969–3993. doi: 10.1175/1520-0442(2000)013<3969:
 2197 TGMAS>2.0.CO;2
- 2198 Uppala, S. M., Kållberg, P., Simmons, A., Andrae, U., Bechtold, V. D. C., Fiorino,
 2199 M., ... others (2005). The ERA-40 re-analysis. *Q. J. R. Meteorol. Soc.*, *131*,
 2200 2961–3012.
- 2201 Vallis, G., Colyer, G., Geen, R., Gerber, E., Jucker, M., Maher, P., ... Thomson, S.
 2202 (2018). Isca, v1.0: A framework for the global modelling of the atmospheres

- of Earth and other planets at varying levels of complexity. *Geoscientific Model Development*, *11*, 843–859. doi: 10.5194/gmd-11-843-2018
- Voigt, A., Biasutti, M., Scheff, J., Bader, J., Bordoni, S., Codron, F., . . . Zeppetello, L. R. V. (2016). The Tropical Rain belts with an Annual Cycle and Continent Model Intercomparison Project: TRACMIP. *JAMES*, *8*(4), 1868–1891.
- Walker, C. C., & Schneider, T. (2006). Eddy Influences on Hadley Circulations: Simulations with an Idealized GCM. *Journal of the Atmospheric Sciences*, *63*(12), 3333–3350. Retrieved from <http://journals.ametsoc.org/doi/abs/10.1175/JAS3821.1> doi: 10.1175/JAS3821.1
- Walker, J. M., & Bordoni, S. (2016). Onset and withdrawal of the large-scale South Asian monsoon: A dynamical definition using change point detection. *Geophysical Research Letters*, *43*(22), 11,815–11,822. doi: 10.1002/2016GL071026
- Walker, J. M., Bordoni, S., & Schneider, T. (2015). Interannual variability in the large-scale dynamics of the South Asian summer monsoon. *Journal of Climate*, *28*(9), 3731–3750. doi: 10.1175/JCLI-D-14-00612.1
- Wang, B., & Ding, Q. (2008). Global monsoon: Dominant mode of annual variation in the tropics. *Dynamics of Atmospheres and Oceans*, *44*(3), 165 - 183. doi: <https://doi.org/10.1016/j.dynatmoce.2007.05.002>
- Wang, B., Ding, Q., & Joseph, P. V. (2009). Objective definition of the Indian summer monsoon onset. *Journal of Climate*, *22*(12), 3303–3316. doi: 10.1175/2008JCLI2675.1
- Wang, B., & LinHo. (2002). Rainy Season of the Asian-Pacific Summer Monsoon. *Journal of Climate*, *15*, 386–398. doi: 10.1175/1520-0442(2002)015%3C0386:RSOTAP%3E2.0.CO;2
- Wang, B., LinHo, Zhang, Y., & Lu, M. M. (2004). Definition of South China Sea monsoon onset and commencement of the East Asian summer monsoon. *Journal of Climate*, *17*(4), 699–710. doi: 10.1175/2932.1
- Wang, B., Liu, J., Kim, H. J., Webster, P. J., & Yim, S. Y. (2012). Recent change of the global monsoon precipitation (1979-2008). *Climate Dynamics*, *39*(5), 1123–1135. doi: 10.1007/s00382-011-1266-z
- Wang, B., & Wang, Y. (1999). Dynamics of the ITCZ–Equatorial Cold Tongue Complex and Causes of the Latitudinal Climate Asymmetry. *Journal of Climate*, *12*(6), 1830–1847.
- Wang, B., & Xie, X. (1997). A model for the boreal summer intraseasonal oscillation. *Journal of the Atmospheric Sciences*, *54*(1), 72-86. doi: 10.1175/1520-0469(1997)054<0072:AMFTBS>2.0.CO;2
- Wang, P. X., Wang, B., Cheng, H., Fasullo, J., Guo, Z. T., Kiefer, T., & Liu, Z. Y. (2014). The global monsoon across timescales: Coherent variability of regional monsoons. *Climate of the Past*, *10*(6), 2007–2052. doi: 10.5194/cp-10-2007-2014
- Wang, X., Auler, A. S., Edwards, R. L., Cheng, H., Cristalli, P. S., Smart, P. L., . . . Shen, C.-C. (2004). Wet periods in northeastern Brazil over the past 210 kyr linked to distant climate anomalies. *Nature*, *432*, 740 - 743.
- Wang, X., Auler, A. S., Edwards, R. L., Cheng, H., Ito, E., & Solheid, M. (2006). Interhemispheric anti-phasing of rainfall during the last glacial period. *Quaternary Science Reviews*, *25*(23), 3391 - 3403. (Critical Quaternary Stratigraphy) doi: <https://doi.org/10.1016/j.quascirev.2006.02.009>
- Wang, X., Auler, A. S., Edwards, R. L., Cheng, H., Ito, E., Wang, Y., . . . Solheid, M. (2007). Millennial-scale precipitation changes in southern Brazil over the past 90,000 years. *Geophysical Research Letters*, *34*(23). doi: 10.1029/2007GL031149
- Webb, M. J., Andrews, T., Bodas-Salcedo, A., Bony, S., Bretherton, C. S., Chadwick, R., . . . others (2017). The cloud feedback model intercomparison project (CFMIP) contribution to CMIP6. *Geoscientific Model Development*, *2017*, 359–384.

- 2258 Webster, P. J., Magaña, V. O., Palmer, T. N., Shukla, J., Tomas, R. A., Yanai, M.,
2259 & Yasunari, T. (1998). Monsoons: Processes, predictability, and the prospects
2260 for prediction. *Journal of Geophysical Research: Oceans*, *103*(C7), 14451–
2261 14510. Retrieved from <http://doi.wiley.com/10.1029/97JC02719> doi:
2262 10.1029/97JC02719
- 2263 Wei, H.-H., & Bordoni, S. (2016). On the Role of the African Topography in
2264 the South Asian Monsoon. *Journal of the Atmospheric Sciences*, *73*(8),
2265 3197–3212. Retrieved from [http://journals.ametsoc.org/doi/10.1175/
2266 JAS-D-15-0182.1](http://journals.ametsoc.org/doi/10.1175/JAS-D-15-0182.1) doi: 10.1175/JAS-D-15-0182.1
- 2267 Wei, H.-H., & Bordoni, S. (2018). Energetic Constraints on the ITCZ Position in
2268 Idealized Simulations With a Seasonal Cycle. *Journal of Advances in Modeling
2269 Earth Systems*, *10*(7), 1708–1725. doi: 10.1029/2018MS001313
- 2270 Wei, H.-H., & Bordoni, S. (2020). Energetic Constraints on the ITCZ position
2271 in the Observed Seasonal Cycle from MERRA-2 Reanalysis. Retrieved from
2272 <https://resolver.caltech.edu/CaltechAUTHORS:20200625-123438067>
- 2273 Weldeab, S. (2012). Bipolar modulation of millennial-scale West African mon-
2274 soon variability during the last glacial (75,000–25,000 years ago). *Qua-
2275 ternary Science Reviews*, *40*, 21 - 29. doi: [https://doi.org/10.1016/
2276 j.quascirev.2012.02.014](https://doi.org/10.1016/j.quascirev.2012.02.014)
- 2277 Wheeler, M., & Kiladis, G. N. (1999). Convectively coupled equatorial waves:
2278 Analysis of clouds and temperature in the wavenumber-frequency do-
2279 main. *Journal of the Atmospheric Sciences*, *56*(3), 374–399. doi: 10.1175/
2280 1520-0469(1999)056<0374:CCEWAO>2.0.CO;2
- 2281 White, R., Battisti, D., & Skok, G. (2017). Tracking precipitation events in time
2282 and space in gridded observational data. *Geophysical Research Letters*, *44*(16),
2283 8637–8646.
- 2284 Wu, M.-L. C., Reale, O., Schubert, S. D., Suarez, M. J., & Thorncroft, C. D. (2012).
2285 African easterly jet: Barotropic instability, waves, and cyclogenesis. *Journal of
2286 Climate*, *25*(5), 1489–1510.
- 2287 Wu, R., & Wang, B. (2001). Multi-stage onset of the summer monsoon over the
2288 western North Pacific. *Climate Dynamics*, *17*(4), 277–289. doi: 10.1007/
2289 s003820000118
- 2290 Xiang, B., Zhao, M., Ming, Y., Yu, W., & Kang, S. M. (2018). Contrasting impacts
2291 of radiative forcing in the Southern Ocean versus southern tropics on ITCZ po-
2292 sition and energy transport in one GFDL climate model. *Journal of Climate*,
2293 *31*(14), 5609–5628. doi: 10.1175/JCLI-D-17-0566.1
- 2294 Xie, S.-P., & Philander, S. G. H. (1994). A coupled ocean-atmosphere model of rel-
2295 evance to the ITCZ in the eastern Pacific. *Tellus*, *46A*, 340–350. doi: 10.3402/
2296 tellusa.v46i4.15484
- 2297 Yang, G.-Y., Methven, J., Woolnough, S., Hodges, K., & Hoskins, B. (2018). Link-
2298 ing African easterly wave activity with equatorial waves and the influence of
2299 Rossby waves from the Southern Hemisphere. *Journal of the Atmospheric
2300 Sciences*, *75*(6), 1783–1809.
- 2301 Yim, S.-Y., Wang, B., Liu, J., & Wu, Z. (2014). A comparison of regional monsoon
2302 variability using monsoon indices. *Climate Dynamics*, *43*, 1423–1437.
- 2303 Zhai, J., & Boos, W. R. (2017). The drying tendency of shallow meridional cir-
2304 culations in monsoons. *Quarterly Journal of the Royal Meteorological Society*,
2305 *143*(708), 2655–2664. doi: 10.1002/qj.3091
- 2306 Zhang, C. (2005). Madden-Julian oscillation. *Reviews of Geophysics*, *43*(2).
- 2307 Zhang, C., Nolan, D. S., Thorncroft, C. D., & Nguyen, H. (2008). Shallow merid-
2308 ional circulations in the tropical atmosphere. *Journal of Climate*, *21*(14),
2309 3453–3470. doi: 10.1175/2007JCLI1870.1
- 2310 Zhang, G., & Wang, Z. (2013). Interannual variability of the Atlantic Hadley circu-
2311 lation in boreal summer and its impacts on tropical cyclone activity. *Journal of
2312 Climate*, *26*(21), 8529–8544. doi: 10.1175/JCLI-D-12-00802.1

- 2313 Zhang, R., & Delworth, T. L. (2005). Simulated tropical response to a substan-
2314 tial weakening of the Atlantic thermohaline circulation. *Journal of Climate*,
2315 *18*(12), 1853–1860. doi: 10.1175/JCLI3460.1
- 2316 Zhang, S., & Wang, B. (2008). Global summer monsoon rainy seasons. *International*
2317 *Journal of Climatology*, *28*, 1563–1578. doi: 10.1002/joc.1659
- 2318 Zhou, T., Turner, A. G., Kinter, J. L., Wang, B., Qian, Y., Chen, X., ... He, B.
2319 (2016). GMMIP (v1.0) contribution to CMIP6: Global Monsoons Model Inter-
2320 comparisonProject. *Geoscientific Model Development*, *9*(10), 3589–3604. doi:
2321 10.5194/gmd-9-3589-2016
- 2322 Zhou, W., & Xie, S.-P. (2018). A Hierarchy of Idealized Monsoons in an Interme-
2323 diate GCM. *Journal of Climate*, *31*, 9021–9036. Retrieved from [http://](http://journals.ametsoc.org/doi/10.1175/JCLI-D-18-0084.1)
2324 [journals.ametsoc.org/doi/10.1175/JCLI-](http://journals.ametsoc.org/doi/10.1175/JCLI-D-18-0084.1)
2325 [D-18-0084.1](http://journals.ametsoc.org/doi/10.1175/JCLI-D-18-0084.1) doi: 10.1175/JCLI-
2326 [D-18-0084.1](http://journals.ametsoc.org/doi/10.1175/JCLI-D-18-0084.1)
- 2327 Ziegler, M., Simon, M. H., Hall, I. R., Barker, S., Stringer, C., & Zahn, R. (2014).
2328 Development of Middle Stone Age innovation linked to rapid climate change.
Nature Communications, *4*(1905).